Worcester Polytechnic Institute
Digital WPI

Major Qualifying Projects (All Years)   Major Qualifying Projects

October 2008

Multiple Target Tracking

Alexander Volfson
Worcester Polytechnic Institute

Kathleen Haas
Worcester Polytechnic Institute

Matthew J. Connor
Worcester Polytechnic Institute

Follow this and additional works at: https://digitalcommons.wpi.edu/mqp-all

Multiple Target Tracking

A Major Qualifying Project Report
submitted to the Faculty of the
WORCESTER POLYTECHNIC INSTITUTE
in partial fulfillment of the requirements for the
Degree of Bachelor of Science by:

_____
Matthew Connor

_____
Kathleen Haas

_____
Alexander Volfson

Submitted:
October 14, 2008

Approved:

_____
Professor Jonathan Abraham, Major Advisor

_____
Professor Edward Clancy, Major Advisor

Abstract

Often, a radar measures targets by their distance, or range, from the radar. A method for viewing these measurements is a Range Time plot, which plots the ranges of targets vs. time. When radar tracks objects whose Range Time tracks cross, it is sometimes uncertain which track belongs to which target. The crossings themselves are called "odd" if the tracks cross straight through each other, forming an 'X', or are called "even" if the tracks approach each other and then diverge.

It was studied how often these different crossings occur due to objects separating in space. An analysis of the situation where an object splits into n objects led to the conclusion that all crossings were odd. If these n splits occur sequentially, however, even crossings were possible, but turned out to be extremely rare in a Monte Carlo simulation. Statistics about the odd crossings of this simulation were aggregated for their frequency, crossing angle, and crossing time.

In addition, it was examined how well targets could be tracked through an individual crossing. An algorithm was devised to track targets through crossings using only data from Range Time plots, i.e. data about the targets' ranges over time. The performance of this algorithm was tested with a large set of Monte Carlo simulations. Another, smaller set, of Monte Carlo simulations were generated, and those for which this algorithm could not give an answer with certainty were re-analyzed by a human in a series of blinded tests, using data from a Range Doppler plot, i.e. data about the targets' range and radial velocity over time. It was determined that the performance of both tests increased as the targets' relative radial velocities and track times increased.

Statement of Authorship

During her summer internship at MIT Lincoln Laboratory, Kathleen developed a test for evenness and oddness of Range Time track crossings for point scatterer targets, and evaluated its performance as a function of track crossing angle and length of track time. For this project, Kathleen extended the test to include dumbbell-shaped targets and evaluated its performance as a function of track crossing angle, length of track time, rate of tumble, and direction of radar line of sight.

Matthew adapted a Doppler imaging algorithm written by Fannie Rogal, an MIT Lincoln Laboratory employee, during his summer internship at MIT Lincoln Laboratory. Matthew modified the code to test the minimum range separation required to discriminate two targets traveling at the same radial velocity, as a function of both targets' rates of spin, rates and angles of precession, target lengths, and radar line of sight. For this project, the code was modified to accept predetermined ballistic scenarios that led to Range Time track crossings. The script created time lapsed Range Doppler plots of the targets which were visually discriminated by a human.

Alexander analyzed track crossing situations for a variety of crossing statistics. He algebraically derived crossing times for both the starburst and periodically separating situations. For the latter situation, he developed a Monte Carlo simulation in order to gather these statistics.

Acknowledgements

Executive Summary

Background

Air and missile defense and radar have developed hand in hand since their appearance on the world stage during World War II. A measure of the ability of radar to track many objects through the sky while associating their trajectories correctly is extremely important to many radar missions. The goal is to track multiple targets while avoiding confusing them with each other.

Radar can determine an object's location, keep a record of past locations, and can give an estimate as to where this object, or target, will be. Radar measures a target by emitting an electromagnetic signal and measuring the reflection off of the target. By measuring the round trip time and Doppler frequency shift, this method measures distance and velocity very well, but measures angle very poorly. Sometimes rather than keep track of every aspect of a target's trajectory, radar will instead use a simplified representation based on only one or two observables that are measured very accurately and precisely – range and Doppler frequency shifts.

A Range Time plot is a method for illustrating target data from radar. This plot represents the target by its range. Over time, many measurements are recorded, creating a time lapsed track of where the target has been. Targets of interest may have Range Time tracks which cross those of other targets even though the targets are separated in three dimensional space. Since the tracks in question may be curved, as shown in Figure 1.1.1, it is not immediately apparent whether tracks actually crossed or merely came very close to each other and then separated. This uncertainty may confuse track association algorithms, degrading our ability to correctly track targets.
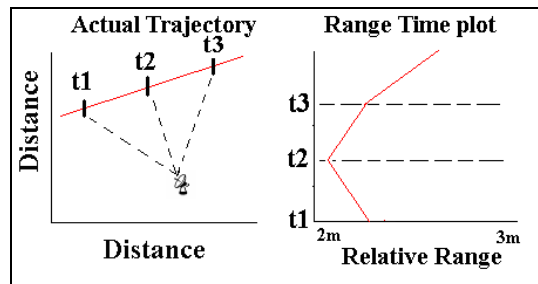
Figure 1.1.1

a. (left) A two dimensional target trajectory. Vertical hashes show two dimensional target locations at times t1, t2, and t3. Lines through these locations are an aid to the eye only. Radar location is depicted in the lower right, along with distances between the radar and each target location (dashed lines).

b. (right) The Range Time plot which arises from Figure 1A

A second observable upon which a plot can be based is a target's Doppler frequency shift in the signal returned to the radar. A Range Doppler plot graphs range against these Doppler measurements. Returns are again plotted chronologically as they are received. An example of a two dimensional target trajectory and the corresponding Range Doppler plot is shown in Figure 1.1.2.

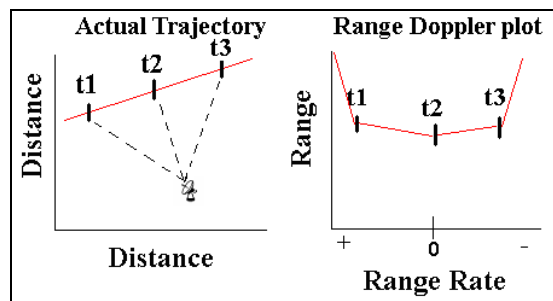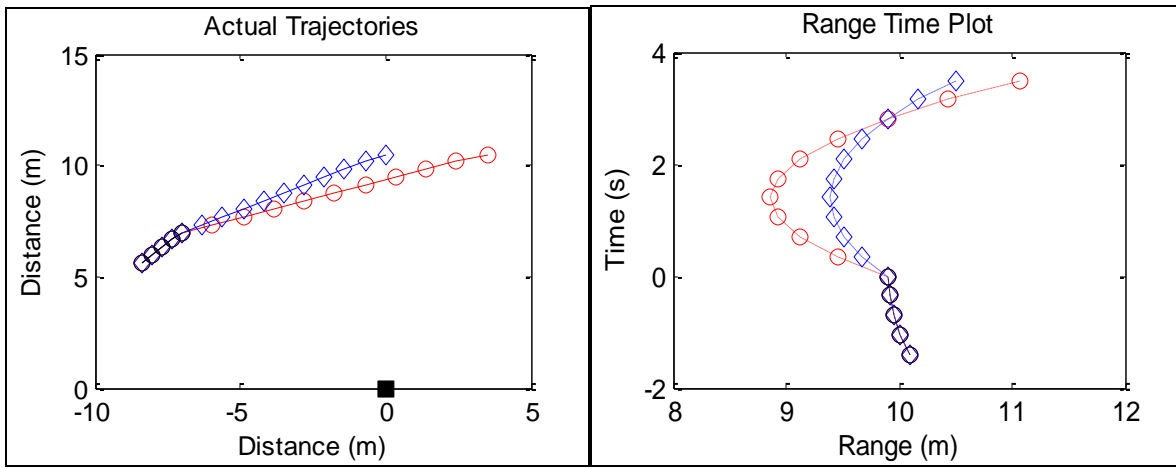**Figure 1.1.2**

a. (left) A two dimensional target trajectory. Vertical hashes show two dimensional target locations at times t1, t2, and t3. Lines through these locations are an aid to the eye only. Radar location is depicted in the lower right, along with distances between the radar and each target location (dashed lines).

b. (right) The Range Doppler plot which arises from Figure 1A

Many real life situations lead to crossings on a Range Time plot, such as a single central target periodically separating smaller targets, a single target breaking into many targets (also known as a starburst), or the periodically separating smaller targets individually starbursting. These splitting targets, even though separated by kilometers in cross range to the radar, can appear to be in the same place on a Range Time plot when they are equidistant from the radar. An example of a two dimensional target trajectory where the trajectories do not cross, but their ranges do is shown in Figure 3.

Figure 1.1.3

a.) (left) A two dimensional real-life trajectory representation of one target (left) splitting into two (red circle and blue diamond). Constant velocity trajectory is assumed. Notice that the split objects never touch each other.

b.) (right) The Range Time plot resulting from measuring range to the targets from the radar. The split objects have different speeds, but the angle between the difference in velocities and the radar line of sight is obtuse; thus a Range Time crossing is perceived at t = 3 s.

Problem Statement

The intent of this project is to evaluate how well radar can successfully distinguish tracks of multiple objects as the objects' ranges approach each other, as well as to estimate the likely frequency of these range time crossings for splitting and starbursting targets.

It is assumed that the targets are tracked for short periods of time and are not subject to the effects of gravity, drag, and lift, this causes the targets to travel on constant velocity straight

line trajectories.. The targets are modeled as a discrete point, a dumbbell (a coupled pair of discrete points separated by a constant distance), and a cone.

Track Crossings of Point Targets:

The first step is to analyze the likelihood of track crossings occuring due to different separation situations of discrete point targets. The type of each crossing is also important. Crossings can be "even", where the tracks of two targets appear to cross on a Range Time plot because these tracks either come close together and then diverge, or cross twice in a short amount of time. Crossings can also be "odd," where the tracks cross straight through each other.

Since the targets are assumed to move with a constant velocity, the times of Range Time track crossings were analytically derived. For starbursts (one object splitting into many) it was proven that no even crossings were possible. This broad result means that tracking objects through a starburst is only dependent on the radar being able to determine whether a starburst occurred.

The situation where an object periodically separates objects which do not alter the trajectory of the original target was also considered. Again, the track crossing times were derived algebraically. In this situation, both even and odd crossings were possible. These trajectories were simulated for a variety of different ejection time periods, number of objects ejected, and radar error. It was found that even crossings were highly unlikely, thus, only odd crossings were analyzed for crossing angle and other statistics. From this analysis, the frequency of crossings was found to grow linearly until all objects had separated and then tapered off approximately exponentially.

Crossing Discrimination of Dumbbell and Cone Targets:

The second step was to estimate the probability of correctly tracking two objects through a Range Time plot crossing as a function of the viewing angle of the specific radar, rotational dynamics, and radial velocities of the targets relative to each other. An algorithm was devised to test a Range Time plot to estimate whether the crossing was odd or even. Overall, given reasonable distributions of parameters from which independent random values were selected to create simulations, roughly 70% of the crossings were correctly identified as either odd or even. It was found that the probability of successful tracking increased significantly as the amount of

time tracked and the angle between the crossing tracks increased, as the angle between the radar line of sight (RLOS) and a target's z-inertial axis became close to 0, 180, and 360 degrees, and as the rate of tumble decreased.

In a separate experiment, more simulations of Range Time plots were generated, and the test for Range Time plots estimated whether the crossing was even, the crossing was odd, or the test was uncertain. Crossings for which the Range Time algorithm was unsure were analyzed a second time by a visual discrimination using a Range Doppler plot. The visual discrimination was a blinded test by a human that estimated whether the crossing was even, the crossing was odd, or the viewer was uncertain. The intent was to examine if a Range Doppler plot could provide additional discriminatory information and increase the probability of successfully tracking these targets over the time of confusion. This information will lead to a recommendation of when sensor fusion, switching from radar designed for ranging to one designed for velocity measurements, would be advantageous. It was found that, given the assumptions and models previously described, sensor fusion was favorable. Of the cases which were passed to the Range Doppler simulation, approximately 85% were correctly identified. The single most influential parameter that led to an increase in probability of correct identification was the difference in the two targets' radial velocities in a Range Doppler plot. A decrease in spin rate, an increase in the track time, certain viewing angles, and a decrease in rate of precession also increased the probability of correctly identifying the crossing.

These statistics, combined with data about the probability of successful tracking through a single crossing, will lead to a more comprehensive understanding about the probability of successfully tracking targets through many crossings, and the advantages of sensor fusion on the larger scale.

Table of Contents

1 Introduction

Air and missile defense and radar have developed hand in hand since their appearance on the world stage during World War II. As with the evolution of many defense elements, a progression in one area has brought about a parallel improvement in its counter technology. It was with the advent of the German V class rockets, during World War II, that the development of both early warning and tracking radar as the mainstays of ballistic missile defense was prompted. A measure of the ability of radar to track many objects through the sky while associating their trajectories correctly is of grave importance to many radar missions.

1.1 Project Area

One of the core applications for radar in missile defense is target tracking. Radar can determine an object's location, can keep a record of past locations, and can give an estimate as to where this object, or target, will be. Sometimes rather than keep track of every aspect of a target's trajectory, radar will instead use a simplified representation based on only one or two observables. Radar may be accurate to the 10's of centimeters in range, but may only have an angular accuracy in fractions of a degree. This angular accuracy equates to a cross range accuracy on the order of kilometers. This accuracy in range is one reason for the popularity of what is known as a Range Time plot for target tracking. Another reason for this wide spread usage of Range Time plots is the potential to resolve individual portions of the target that are at different ranges. The Range Time plot is based on range, or the distance to the target from the radar. Range tracking was one of the first tracking methods ever used by radar operators and is still one of the most accurate. [Skolnik 2001]

A Range Time plot is a method for viewing range target data about targets which are relatively closely spaced. Instead of keeping track of target elevation, azimuth (cross-range) as well as range, only a single range measurement and the time at which that measurement was taken are stored. This method of tracking represents the target by its range, the observable which radar measures most accurately. Over time, many measurements are recorded; creating a time lapsed track of where the target has been. Figure 1.1.1 shows an example of a three dimensional space time situation and the resulting Range Time plot. Figure 1.1.1b shows the effect of the transformation from reality to a Range Time plot. Here, although the target itself is on a straight,

constant-velocity ballistic trajectory, the Range Time plot is curved due to the location of the radar. In reality, radar data transforms information about four dimensional space-time trajectories into two dimensional range-time pairs. When plotting these data, effects of this transformation can lead to the straight trajectories of targets appearing curved on a Range Time plot.
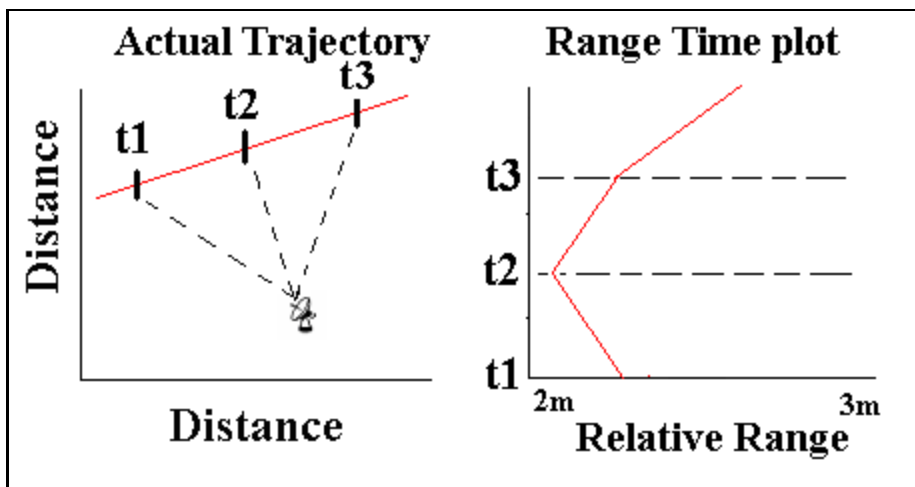
Figure 1.1.1 -
a.) (left) Depicts the x-y (planar model) location of a constant velocity target, measurements are taken at each of the three discrete points (t1, t2, t3) with the radar located at the bottom.
b.) (right) Shows the corresponding Range Time plot for a.), dashed lines correspond to measurement intervals. Because the range is from the target to radar, the actual constant velocity track (straight line) becomes a curved in Range Time.

Targets of interest may have Range Time tracks which cross those of other targets. Since the tracks in question may be curved, it is not immediately apparent whether tracks in question actually crossed or merely came very close to each other and then separated making it difficult to correctly associate the target and its track, which is the underlying goal. Real life situations that lead to these crossings on a Range Time plot are the focus of our project because they may confuse track association algorithms.

A second observable upon which a plot can be based is the velocity of a target. It is possible to compute this observable directly from the range data, but, by measuring the Doppler frequency shift in the signal returned to the radar, this aspect of the target can be measured much

more accurately. The resulting measurement is used to calculate radial velocity, the component of a target's velocity in the direction of the radar.

A Range Doppler plot graphs range against these Doppler measurements. Returns are again plotted chronologically as they are received, but there is no direct indication of this time information given in the plot itself. Most prior radar work based on Doppler frequency shifts has been in the form of target imaging, detection, and identification. Doppler tracking is not a new idea but one that has had limited time and resources devoted to it within the context of this problem. [Weiner] An example of a Range Doppler plot, for a precessing target approaching the radar at 2 m/s, is given in Figure 1.1.2. In this case, the target is resolved in Doppler as well as in range. Note that the target moves about 40 meters in the 20s tracking time
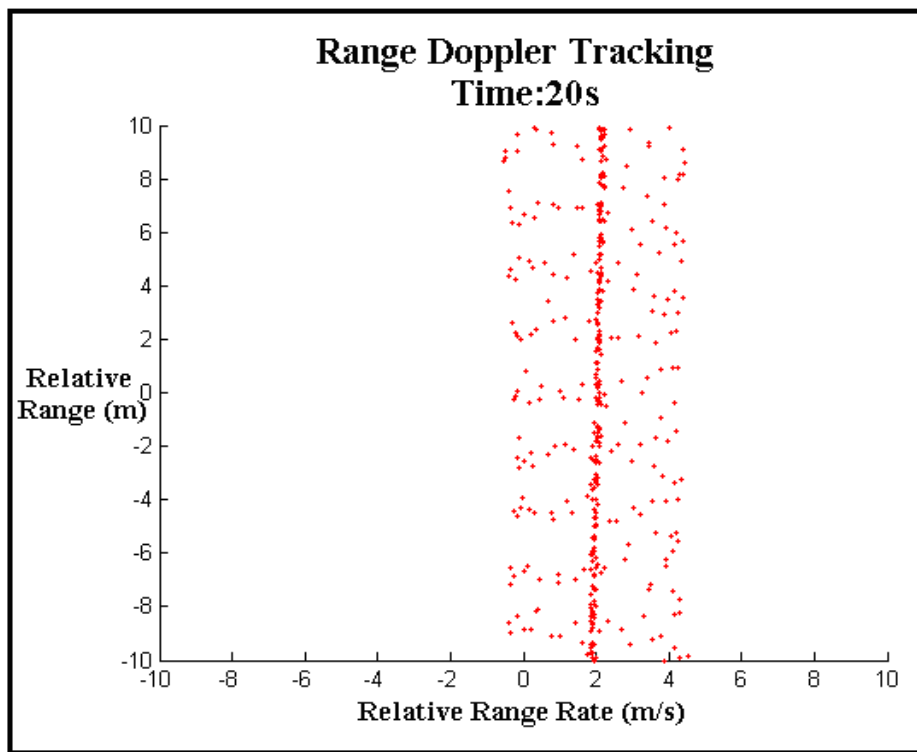
Figure 1.1.2 – Example of a range Doppler plot for a precessing target with a relative range rate of 2m/s.

For this project, the targets of interest are those whose paths cross on a Range Time plot. There are many real life situations of interest that lead to these crossings on a Range Time plot

such as: a single central target periodically separating smaller targets; a single target breaking into many targets (also known as a starburst); or multiple targets separating into smaller targets. This may cause confusion because while radar measures velocity and range very accurately, it measures angle relatively poorly. These splitting targets, even though separated by kilometers in cross range, will appear to be in the same place when they are equidistant from the radar and viewed on a Range Time plot. In these separation incidents, only a single target may be the one of interest surrounded by other targets, which can confuse the radar.

This collocation of targets in range and time is the project's focus. Over extended time intervals many of these crossings can occur when tracking in a Range Time plot, especially when there are many targets, and their many tracks are crossing repeatedly. These crossings can lead to a degradation of tracking ability, equating to a loss of a priori information, such as target identification and target origin. The introduction of this uncertainty is also detrimental to target destination estimation.

1.2 Project Goal

The intent of this project is to evaluate how well radar can successfully distinguish tracks of multiple objects as the objects' ranges approach each other as well as analyze the frequency of occurrence of these range time crossings. As targets' ranges become closer, their tracks as observed by radar and described in a Range Time plot appear to cross. The first step is to calculate the probability of successfully tracking objects through a Range Time plot crossing as a function of various factors, including the viewing angle of the specific radar, rotational dynamics of the target, track time and crossing angle. Once this information is obtained, trajectories created using sets of parameters that lead to a low probability of successful tracking will be examined. These trajectories will be observed a second time using a Range Doppler plot to determine whether additional information can be gained from the Doppler shift of the object's radar return. The intent is that once a Range Time plot identifies sets of parameters that lead to tracks which are not easily distinguished, a Range Doppler plot will increase the probability of successfully tracking these targets over the time of confusion. This information will lead to a recommendation of when sensor fusion, switching from radar designed for ranging to those designed for velocity measurements, would be advantageous.

Beyond evaluation of the probability of correctly describing an individual crossing, an examination of how often track crossings occur due to different separation situations was also performed. These statistics, combined with data about the probability of successful tracking through a single crossing, will lead to a more comprehensive understanding about the probability of successfully tracking targets through many crossings, and the advantages of sensor fusion on the larger scale.

2 Background

Our project is based on methods for plotting information provided by radar and patterns that arise within those plots. Fundamental to these plots are not only the plotting techniques but the operation of radar itself. The following sections provide an overview of the most significant concepts related to how radar and ballistic missile defense developed, as well as how radar systems operate, retrieve target observables, and plot these observables in a meaningful way.

2.1 BMD History

Since World War II, ballistic missiles have been more a psychological and morale weapon than one of firepower. Neither the original German V-2s, nor the Iraqi Scuds from the Gulf War that evolved from the V-2s, were disastrously lethal. They were more a show of technological prowess. When the first ballistic missiles were launched in 1944, there was an early assessment of the lack of effectiveness in the Allied forces' ability to intercept German V-2s post launch. Still, defense attempts at the time relied on radars to provide the alert for artillery to try and intercept missiles. Allied defense efforts were focused on striking the missile manufacturing facilities and launch pads. This strategy, which appeared simple initially, turned out to be very difficult and resulted in little success. Even now, the ease of moving, hiding, and setting decoys for ballistic missiles and their launch pads has made pre-launch destruction challenging and unproductive. "Although a large device, 46 feet in length and weighing about 27,000 pounds at lift off, it [ballistic missiles] proved mobile and elusive. Technical difficulties delayed the V-2's, not the bombing." [Werrel 2000]

In the late 1940's and early 1950's, United States Army Air Forces were the leaders in ballistic missile defense. The initial stages of development focused on short range and medium range theater level missile defense, but in the mid 1950's focus began to shift to long range nuclear armed intercontinental ballistic missile (ICBM) threats. This development was a major stepping stone, not only for long range defense tactics, but also for sensor fusion, the combining of data from multiple radars. At this time, the Army began the development of missiles, computing technology, and site radars that had to tie into communications with the United States Air Force, which was developing the Ballistic Missile Early Warning System long range radars.

At the same time, many of the current technical questions and doubts about the program began to arise. Among these doubts was not only the massive cost these defense initiatives would incur, but also feasibility questions: Could these defense technologies defend against a substantial full scale attack? Would the defense be left blind due to equipment malfunction during the first nuclear detonations? Were radars and interceptors sensitive enough to properly discriminate threats from decoys?

Changes in the 1960's were both technological and political in nature. The systematic improvement in defense was focused at target discrimination and tracking techniques. Two approaches were used. The first leveraged the advent of high acceleration short range defense missiles by locating them near possible ICBM end points with sensors that used differences in the trajectories of targets and decoys due to the atmosphere to discriminate in the final stages. The second method used a new technology known as phased array radars. Phased array radars were unique in that they did not rely on mechanical steering to view in different directions, but instead used much quicker and more efficient electronic steering. This fundamental alteration in one of the baseline technologies allowed for the detection and continual tracking of multiple targets instead of only a few. "[M]ost single beam dishes have only a few tracking channels (one to four) [independent tracking channels are where a radar stores the track information for an individual target]. A phased array may have very many (several hundred)." [Toomay 1989]

As technology advanced, questions began to arise about the social implications of ballistic missile defense. Nuclear weapons at the time were under the control of major world powers and their proliferation was heavily stalemated by the threat of mutually assured destruction (MAD). Fundamentally, mutually assured destruction was the idea that since there was much more firepower than defense capability, any launch by a world power meant not only the destruction of their enemy but of themselves due to second strike capabilities. As the leaders of the United States began to question the validity of missile defense, events began to force the hand on developing a stronger missile defense. Russia denied offers for a treaty putting upper bounds on defense in 1967 and China simultaneously announced successful hydrogen bomb testing.

With newfound motivation to develop ballistic missile defense, the question became what to defend. "…[T]he secretary of defense announced that the US would deploy a 'light'

ABM [antiballistic missile] system to protect the US from a Chinese attack." [Werrel 2000] The system was also designed to protect our offensive missile silos and defend against accidental ICBM launches. Just a few years later, Nixon came into office and at last entered into a treaty with Russia that effectively capped strategic defense capabilities for each nation with a maximum of two anti-ballistic missile sites. The treaties sought to limit threats by reentering the stalemate of MAD, citing full scale national defense as unreliable against a full fledged nuclear attack as a motivation.

The next large scale shift in the U.S.'s defense policy came with President Reagan's Strategic Defense Initiative (SDI) in 1983. It called for an end to the balance of mutual fear that had been the base of nuclear deterrence for decades. SDI sought to put defense into the hands of America's technological prowess, where before it was based in both fear of retaliation and honest obedience to arms treaties. The new focus became the ability to defend against full scale massive nuclear attacks, and moved from the detonation of defensive warheads to independently engaging non-nuclear interceptors. The shape of national missile defense remained constant for a few years until the collapse of the Soviet Union in the late 1980's and early 1990's.

This brief history culminates with the current state of missile defense focus which has existed since the start of the Gulf War in 1990. This is a defense focused not on a large scale nuclear war, but with rogue states and militant groups with small caches of weapons. This concern arose due in large part to the collapse of the Soviet Union and a dispersion of weapons to states such as Iran and North Korea. The past ten to fifteen years has seen an expansion in focus from theater level defense, consisting of shorter range non-nuclear tactical missiles (such as the Iraqi Scuds), to national missile defense stemming from concerns over increases in the range capabilities of ballistic missiles and the hostile countries which possess them. One technological issue which has been consistent throughout national missile defense developments has been the challenge of tracking and identifying large quantities of targets.

2.2 Radar History

The technological basis for radar began in 1831 when Michael Faraday discovered electrical induction. Electrical induction was the first realistic basis for the previously unproven theoretical idea of invisible electromagnetic waves. Induction is the concept that a changing

current created an electric field which would in turn create a new electric current in a surface upon which it is incident.

Faraday's experiment involved wrapping two parallel wires around an iron ring with one of them connected to a battery. When the battery was turned on or off, a current would register briefly in the second closed circuit wire due to the current starting or stopping in the first wire. Although Faraday envisioned many of the ideas and principles behind electromagnetic wave theory, it was Scottish physicist James Clark Maxwell who developed the mathematical basis that governed these fields. Maxwell's field theory, published in 1864, was a culmination of the work of Andre Ampere, Carl F. Gauss, and Faraday. Maxwell's theory reduced electromagnetism to four equations and made it possible to calculate the speed of these waves, which turned out to be the speed of light.

The first person to experimentally verify Maxwell's equations and to show that radio waves could be reflected by objects was the German physicist Heinrich Hertz in 1887. Hertz used a spark generator to create electromagnetic waves and studied how they induced an electromagnetic force in a wire separated by a distance. Hertz did not see an application for this technology, however, and it was Christian Hulsmeyer who first applied and patented, in 1904 England, radar technology which could be used to identify and find the range of ships which could not be seen. The technology, though praised, was not exploited and all but forgotten.

Radar's next big step came in 1922 when A. Hoyt Taylor and Leo C. Young of the U.S. Naval Research Laboratory (USNRL) noticed anomalies in radio signals being transmitted bank to bank across a river. A ship passing between the two terminals of the radio caused a disturbance in the signal. This is the principle behind continuous wave bistatic radar. Continuous wave bistatic radars constantly transmit a signal which requires the transmitter and receiver be independent antennas. The idea proved to be of limited practical use but was the foundation for many future improvements in radar to come.

The first successful pulsed radar was implemented in 1934 again by the USNRL. Pulsed radars usually use one antenna for transmit and receive. It transmits a signal for an interval then uses the same antenna as a receiver after the pulse ends. The first sea radar was not deployed until 1940 at which time England, France, Germany, the Soviet Union and several other nations had their own programs well underway. England had the first operational radar system in 1938.

On a side note, on December 7, 1941, the United States had a fully functional 100 MHz frequency radar in place at Pearl Harbor. It was not the radar which failed to warn of the attack that day, but a lack in trained personnel to interpret the radar's output.

The next big improvement in radar, after the advent of the pulse, came in 1940 when the British and Japanese each independently developed the high-power microwave magnetron which generated enough power to reach higher frequencies, decrease aperture (antenna) size and mobilize radar. Due to their extensive involvement in World War II, England shared the magnetron technology with the U.S. for development efforts at the MIT Radiation Laboratory, which evolved into Lincoln Laboratory, and Bell Telephone Laboratories. Some of the biggest exploitations which showcased the effectiveness of radar, for both sides, in WWII were advanced air attack warning in all weather and lighting conditions and the ability for naval engagement under the cover of darkness. Eventually, radar became important not only in offensive and defensive military tactics, but also in many civilian fields such as aviation and weather monitoring and prediction.

2.3 Radar Overview

Radar is a system, consisting of a transmitter, a receiver and an electromagnetic signal. "The signal can be described by a carrier sine wave at frequency f_c with modulation of one or more of its parameters – amplitude, phase, and frequency." [Levanon 1988] The radar measurement process begins when an electromagnetic wave is emitted by the antenna. The signal propagates outward through space, at some point reflecting off an object, known as the target. Ideally, this reflection is isotropic, in all directions equally, but is subject to many factors in reality. The act of the signal reflecting off an object of interest is referred to as scattering, and the part of an object which causes this reflection is referred to as a scatterer. This reflection creates a weaker return signal because only a portion of the reflected energy travels in the direction of the receiver. Once the return signal is received by the antenna, it is then compared to the transmitted signal, and the differences reveal information about the scattering incident.

While the body of even an uncomplicated real object will contain multiple scatterers, a simulated object of interest may be a single scatterer. A few examples of physical features which could be scatterers are tips of conical objects, joins on a body, exposed nuts and bolts, propellers

or intakes and engines. These are each parts of a body which reflect the transmitted signal, and cause the changes in the signal evident at the receiver.

2.3.1 Target Range

The most basic information derived from the return signal is the range to the target. Range is the distance between some predetermined point, usually the radar, and the object of interest. Target ranging is accomplished by keeping track of elapsed time from the moment of initial signal emission to the registering of the reflected signal at the receiver as shown in Figure 2.3.1.
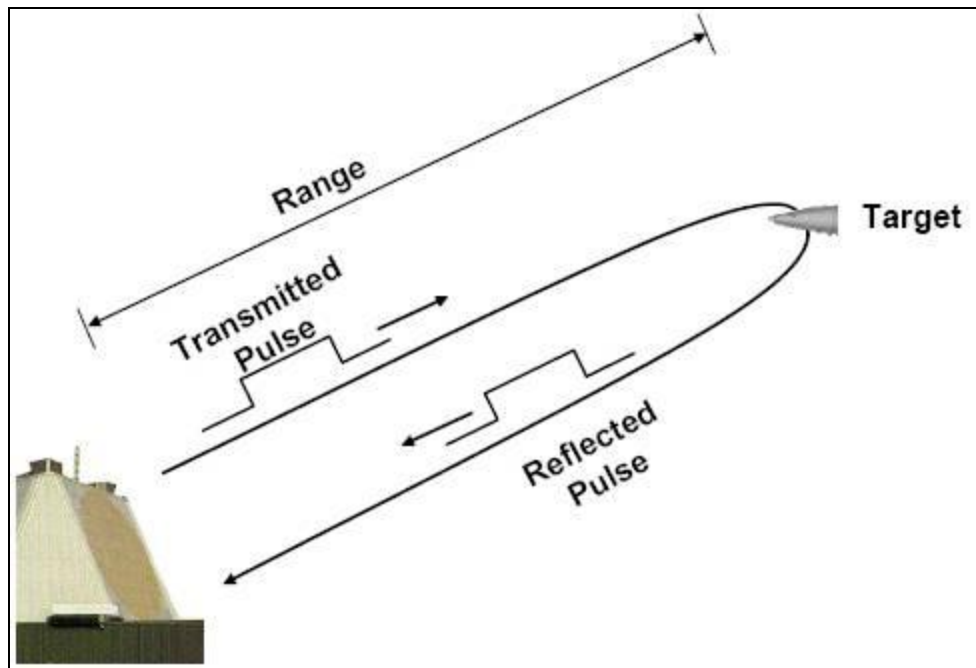
Figure 2.3.1 - How target ranging is achieved by using half of a signals round trip time. (Modified from Noiseux slide 17, Lecture 2, Introduction to Radar Systems 2006)

In a vacuum, electromagnetic waves travel at the speed of light c, which is a good approximation for their speed in targeting applications. Both the initial signal and the reflected signal are assumed to propagate at this rate.

$$c \approx 3 \times 10^{8} m/s$$

Equation 1 (Speed of Light)

The round trip distance that the signal traveled is then the product of the speed of light, c, and the round trip time, Δt. The range to the object R, then, is half of this product:

$$R = \frac{c\Delta t}{2}$$

Equation 2 (Target Range)

Skolnik [2001] gives a good approximation of the range-time relationship as 1 μsec roundtrip ≈ 150 m. Target range is one of the aspects radar measures best, the basis of much of our project work, and the basis for much of radar applications in general.

2.3.2 Radar Equation

There are a variety of characteristics which contribute to the effectiveness and advantages of a particular radar system. Usually a system is engineered with a specific goal in mind, and there is some observable of a target which the system designers seek the radar to be more adept at quantifying. Radar signal waveform, peak power, antenna size and shape and hardware design are just a few of the factors which need to be considered. Many of these attributes are dependent on one another; altering one to better measure a certain radar observable can lead to a detrimental effect in the ability to measure another observable. The most fundamental mathematical relationship underlying a radar system is the radar range equation. This equation is the basis for the relation of many of these aforementioned characteristics. The equation is usually referred to simply as the radar equation because of its general application and ability to be solved for any one of its parameters.

The radar equation is the culmination of several simpler formulae. This section develops the final equation in the natural progression from signal transmission to return signal reception. Different authors evolve this equation in their own way; the method presented here follows

Toomay [1989]. The five equations that are defined are labeled in an illustration in Figure 2.3.2 for chronological clarification.
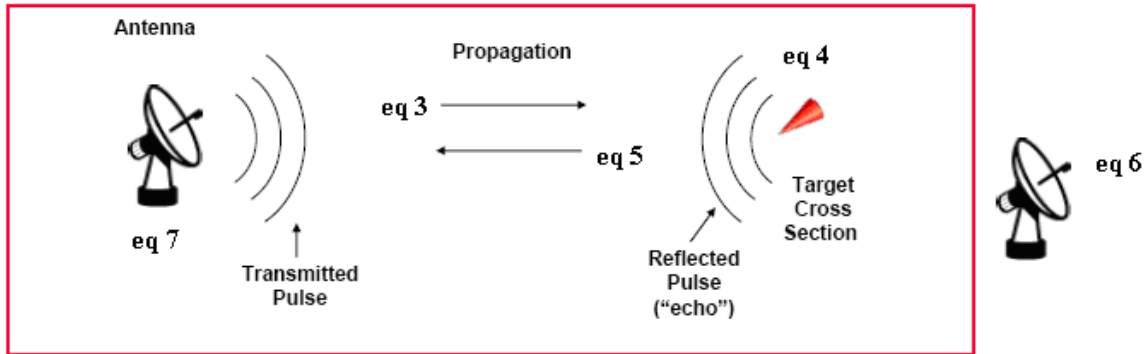
Figure 2.3.2 – Equation 3 expresses the power density at a distance of the emitted signal, Equation 4 expresses the reflected power density, equation 5 expresses the amount of signal which arrives on the receiving antenna, equation 6 expresses the relationship between antenna area and gain, and equation 7 expresses the final form of the radar equation as measured in the receiver. (Modified from Noiseux slide 8, Lecture 2, Introduction to Radar Systems 2006)

The first formula describes the transmitted energy density, E_{D1} that exists at a range R, defined as energy per unit area. In this formula, $4\pi R^2$ relates the power transmitted by the radar to an isotropic sphere, the electromagnetic energy propagates equally in all directions. G_T is the gain in a specific direction due to the transmit antenna. $G_T/(4\pi R^2)$ is the ratio of the focus of the antenna signal. P_T and τ are the peak transmitted power and the duration of that transmission, respectively.

$$E_{D1} = \frac{P_T \cdot \tau \cdot G_T}{4\pi R^2}$$

Equation 3 (Power Density)

The next term introduced in developing the final equation is σ, which represents what is known as the radar cross section (RCS), the reflected size of the object on which the radar beam

is focused. RCS is a scaling factor in the radar equation but is not directly related to the physical size of a target. RCS depends on the target's unique scattering characteristics. Factoring RCS into the previous equation leads to the energy reradiated by the target.

$$E_{D2} = \frac{P_T \cdot \tau \cdot G_T \cdot \sigma}{4\pi R^2}$$

Equation 4 (Power Density & RCS)

This reradiating principle is further related back to the amount of the signal S which falls on the receiving antenna located at the same point as the transmit antenna. Often, it is the same antenna just performing a different function, referred to as monostatic radar. Monostatic radar is the most common form, as opposed to the more historical bistatic radars where the transmitter and receiver are not collocated. The $4\pi R^2$ in the previous equations becomes $(4\pi)^2 R^4$ with the added term A_R in the numerator. The term A_R is the effective area of the receiving antenna and is the numerator in a ratio relating to the second $4\pi R^2$ representing the isotropic radiation due to an object's radar cross section. These additional factors lead to equation 5:

$$S = \frac{P_T \cdot \tau \cdot G_T \cdot A_R \cdot \sigma}{(4\pi)^2 R^4}$$

Equation 5 (Received Signal)

The final components in the radar equation are the terms related to the noise in the receiver of the system. The noise term N is the denominator in the signal to noise ratio, often abbreviated as SNR, on the left hand side of the final equation. This signal to noise ratio is one of the most important terms in radar. The term relates to where detection thresholds are set and where target false alarms are dismissed. Maximizing this ratio is where most development and design efforts are focused. Examples of sources of noise are other electromagnetic sources in the area, vehicles, other radars, and the transmitter. Other noise factors are related to the front end amplification, such as thermal noise temperature T_S, Boltzmann's constant K, the receiver bandwidth B_S, and L_S which represent losses within the system itself. One last element which

needs to be developed for the final equation is a relation between antenna gain, its effective area, and signal wavelength λ.

$$A_R = G_R \lambda^2 / 4\pi$$

Equation 6 (Gain and Effective Aperture Relation)

Substituting A_R and the noise constants into the previously developed formula leads to the final form of the radar range equation.

$$\frac{S}{N} = \frac{P_T \cdot G^2 \cdot \lambda^2 \cdot \sigma}{(4\pi)^3 R^4 K T_S B_S L_S}$$

Equation 7 (Final Radar Equation)

This last version of the radar equation is one of the many forms it may take. Additional terms may be added or substituted for different designs. For example, sometimes the transmission interval represents the integration of many pulses and is represented by the letter "t" for the amount of total time over which the integration occurs. The most important idea to take from the radar equation is the interdependency of many different aspects of radar.

2.3.3 Velocity Measurement

Target velocity is the second observable radar measures well. Radars measure a target's radial velocity, or range rate. As defined previously, range rate is not the overall velocity of an object, only the component of velocity which is in the direction of the radar itself. For example, a target traveling perpendicular to the radar's line of sight would register a range rate of zero despite a non-zero velocity. There are two independent methods for measuring the velocity of a target. One simple (indirect) way is to take the difference between two sequential measurements in range and divide by the elapsed time between measurements. This measure is called range rate. Radar operators used this less precise, though valid, method for measuring velocity for years utilizing a charcoal pencil to mark the radar output screen and make quick calculations. The second (direct) method is to measure what is known as the Doppler shift in the frequency of the transmitted radar signal. "…the Doppler frequency shift of the target return due to radial

motion can be used to make precision velocity measurements: relative motion and range separation between multiple unresolved targets can be used to create a range-Doppler map of the target space." [Kachelmeyer 1991]

Skolnik [2001] gives an excellent example of radar measurable Doppler frequency shift. He describes the escalation in pitch in a siren approaching a listener due to the compression of sound waves from the velocity of the source of the sound. This same frequency alteration occurs in the radar signal scattering off a moving object; it compresses the signal (increasing frequency) if the target is approaching the radar transmitter and dilates (decreases frequency) if the target is receding away from the transmitter. Figure 2.3.3 illustrates this concept. When the signal is received, it is compared to the one being radiated, or a stored version of the one previously transmitted. The frequency difference from the original signal gives the Doppler frequency of the scatterer.
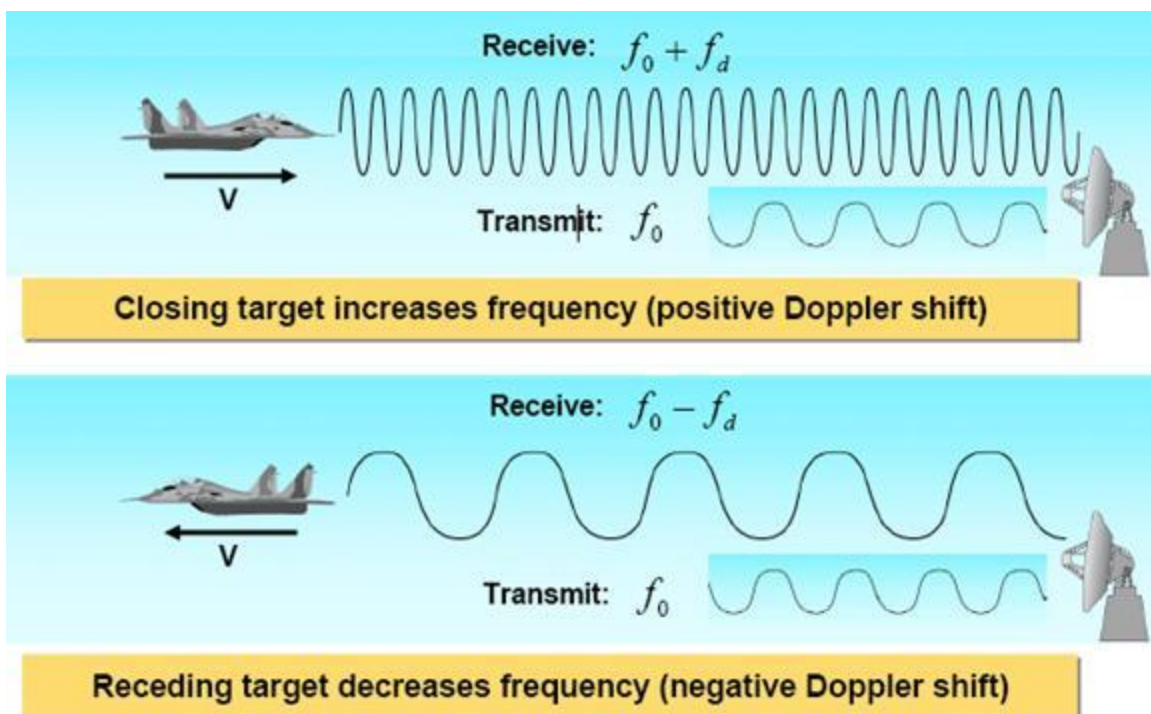

Figure 2.3.3
a.) (top)- Doppler compression, the signal frequency is increased due to target velocity being in the direction of the source of the radar signal.
b.) (bottom) - Doppler dilation, the signal frequency is decreased due to target velocity not being in the direction of the source of the radar signal.

If the target is tumbling, spinning or maneuvering, it may also have a range of different frequency shifts depending on how parts of the body are moving. "This rotational motion gives rise to a rotational Doppler spectrum in the target return…" [Kachelmeyer 1991] Scatterers on different parts of a target's body can have unique velocities due to rotational dynamics. For example, consider radar viewing a stationary cone with its base down and tip pointing straight up. If the tip rotates toward the radar and the base away, a scatterer at the tip would register a frequency increase and a scatterer at the base would register a decrease in frequency. Note that a scatterer at the point about which the cone rotated would not register a Doppler shift at all, as long as the cone is stationary. If the cone had a velocity of its own, the tip rotating towards the radar would increase this velocity and the scatterer at the base would decrease this velocity.

2.3.4 Radar Waveforms

The basic form of the electromagnetic wave is dispatched in one of two methods. The first method is known as continuous wave (CW), where the radar antenna continuously radiates the sinusoidal signal, and the return is either measured elsewhere or checked for a Doppler frequency shift caused by a scattering from a moving target. A second method is a pulse, where the signal is radiated for a period of time and then shut off, allowing time for a return to be registered. In this latter case, the return signal is compared to the original transmitted and matched up by its phase. The difference in wave forms is shown in Figure 2.3.4.
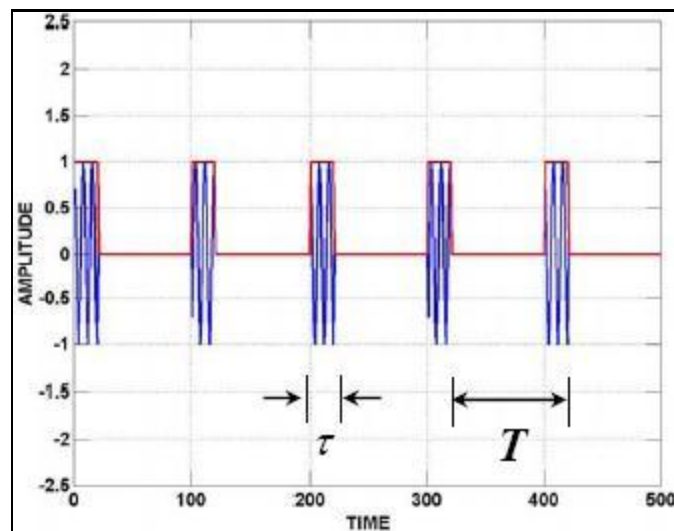
Figure 2.3.4
a.) (left) An example of a continuous wave radar signal.
b.) (right) An example of a pulsed radar signal.
**(Modified from Noiseux slide 17, Lecture 2, Introduction to Radar Systems 2006)**

This pulse creation process is then repeated, occurring at a certain repetition rate called the pulse repetition frequency or PRF. Figure 2.3.5 shows a pulse train with τ representing the

pulse duration as it did in the radar equation, and T the pulse interval, the reciprocal of which is equal to the PRF.

Figure 2.3.5 – A pulse train, T is the pulse repetition interval and τ is the pulse duration. (Modified from Kogon slide 5, Lecture 11, Introduction to Radar Systems 2006)

The PRF is a limiting factor when it comes to making an unambiguous measurement of the range to a target. Ambiguities arise when a return is received shortly after the second of two sequentially emitted pulses; it is not known whether the source is a distant object reflecting the initial pulse or a close target reflecting the second pulse. These ambiguities may be resolved by using multiple pulse repetition frequencies and only declaring a target at a range which is observed in both frequencies. "Blind speeds" is another issue that can arise in radar signal processing. This issue with Doppler processing arises if a target is traveling with a velocity at or near an integer multiple of the frequency of the signal. The shift may not be detected due to alignment in wavelengths. A method of resolving these issues is by decreasing the pulse duration. Shorter pulses have several advantages. One is leaving more time to receive a return, and another is a higher bandwidth which results in better range resolution. The concept of better resolution is shown in Figure 2.3.6 and explicitly defined in a later section.
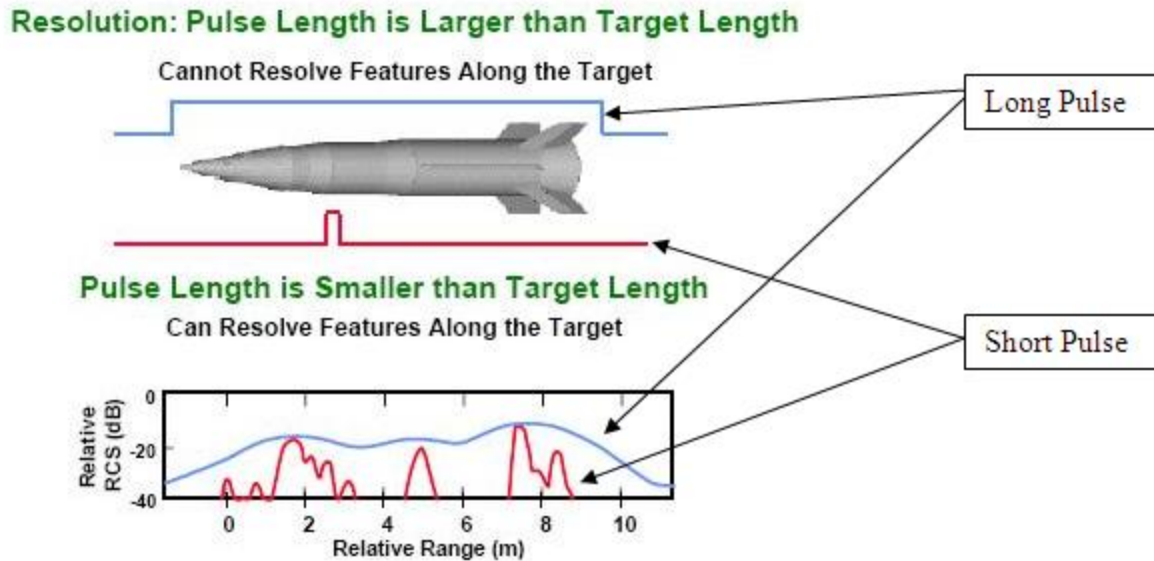
Figure 2.3.6 – Pulse duration and resolution, the blue line is a long pulse which is better for target detection and the red line is a short pulse more advantageous for resolution. (Modified from Kogon slide 7, Lecture 11, Introduction to Radar Systems 2006)

Smaller pulses allow the individual pieces of a target to be resolved in range, while a longer pulse results in better target detection as more energy falls on the object of interest. Also, better Doppler accuracy is based in longer pulse intervals. Another limitation of short pulses is a higher peak power requirement. A lot of radar principles are centered on average power, so a shorter pulse interval necessitates an increase in peak power to compensate. Peak power requirements begin to push practical limits and the size limitations for mobile radar systems.

2.3.5 Accuracy and Resolution

The difference in the notions of accuracy and resolution is one requiring clarification. Accuracy is the correctness of a calculation. Resolution is how far apart individual targets must be before they can be recognized as individual objects. If resolution is small enough, it is the ability to distinguish individual scatterings on the body. An analogy for resolution could be the thickness of a pen when drawing a picture, imagine drawing the same detailed picture once with a fine tipped pen, good resolution, and again with a dull marker, poor resolution, on the same piece of paper. Accuracy could be referred to as the variance you would get in multiple returns from a stationary target.. It is in the calculation of the accuracy of measurements in target

velocity where the advantage of using Doppler measurement is seen. The method of rate of change of range is less accurate than Doppler measurement by a factor of about seven, according to Toomay [1989].

For a tangible sense of the difference between the accuracy of range and angle, Skolnik [2001] explains that the most precise of range measuring radars to be accurate within tens of centimeters at long distances but the most accurate angle measuring radars operating within optimal parameters manage an error of 0.006˚. This fractional number may seem very small, but the issue arises when this 0.006˚ angle is extended out for hundreds or thousands of kilometers. With a little rudimentary trigonometry it can be calculated that an angular accuracy of 0.006˚ at a range of 500 km is a circular area with approximately a 50 m radius. A radar looking straight down on a person from a satellite 500 km above the earth could register the difference between the person's shoes and knees but could not accurately place that person within a circular area with a diameter of 100 m, or the length of a football field. An example of the "pancake" of radar resolution is shown in Figure 2.3.7.
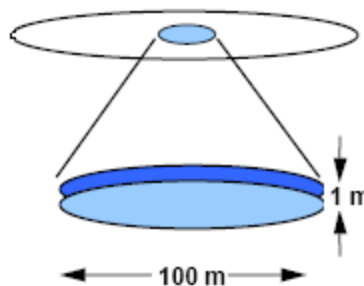
Figure 2.3.7 – The "pancake" in radar accuracy that arises due to the difference in accuracy in angle and range. (Modified from Weiner slide 14, Lecture 6, BMD Systems Analysis 2004)

2.3.6 Radar Overview Conclusion

This section completes the explanation of the base principles of radar operation, though any single topic reviewed here has entire books written about it. A fundamental understanding of these theories is essential to be able to competently work with the subject matter approached in the project itself. One of the most important justifications for the plotting techniques that are utilized within the project is presented in the last section on accuracy. This section showed that

despite the omission of certain observables, such as target angle, there is still retention of the most precise information.

2.4 Plotting Techniques

Another central topic is how a system interprets and conveys the information discerned about a target. Information derived about a target is only as useful as the clarity of its display to the operator. Many times, viewing and tracking multiple three dimensional objects moving through four dimensional space-time is too much information for practical data processing and visualization. Because of this limitation, simplified representations of target data are created. The two main methods of plotting which are the focus of this project are Range Time plots and Range Doppler plots. These plots focus on either target range or target range and velocity, which are two observables radar measures very accurately, as opposed to target angle and target size which it does not measure nearly as well.
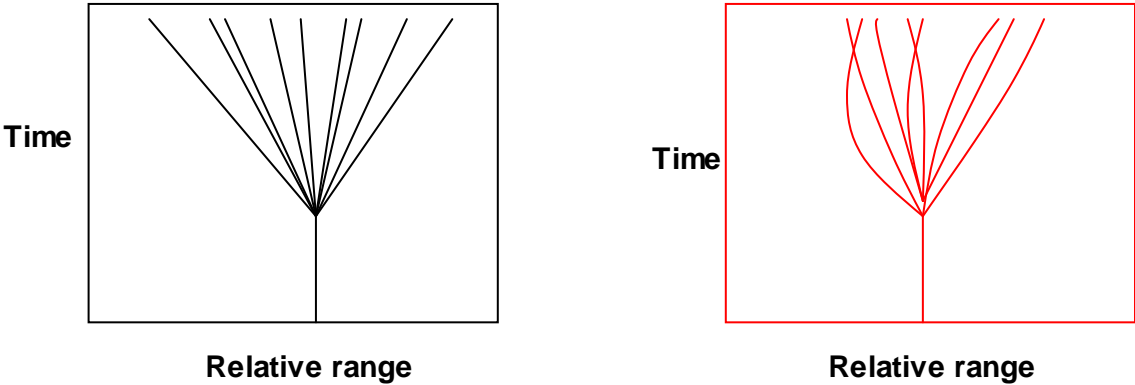
2.4.1 Range Time plots

A very widely used representation of targets is a Range Time plot. The vertical axis of the plot is time, and the horizontal is range. As time passes, marks are made for corresponding range returns, creating a time-lapsed track of the movement of objects. These ranges are found relative to the ranges of some baseline object which the radar has locked on. The tracks on a Range Time plot may imply or directly include information about point of origin, current location, and destination prediction. The tracks themselves may bear little or no resemblance to the Newtonian trajectory of a target. It is fundamental to note that at a point where two tracks cross, the two targets may only be aligned in range from the radar's perspective but be separated by large distances which are perpendicular to the radar's line of sight, such as the two splitting targets illustrated in red in Figure 2.4.1.
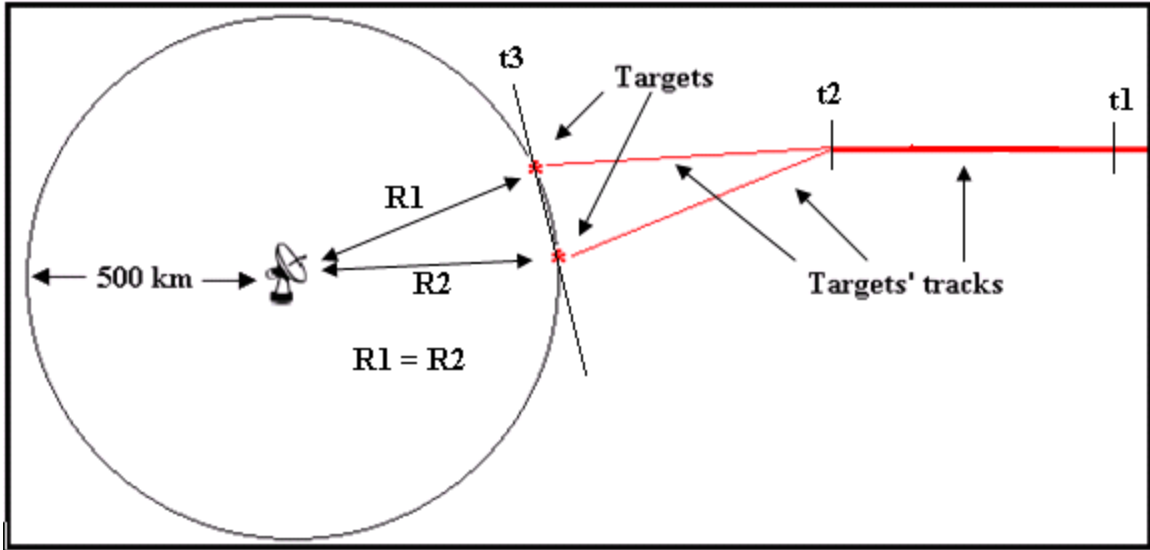
Figure 2.4.1 – One target, traveling right to left in the figure from discrete time t1 to t2. At time t2 the single target splits into two targets. And at time t3 the two non-collocated targets are equidistant from the radar.

Track crossings can come from a single target which splits apart into multiple targets. It may seem counter-intuitive at first that targets moving away from each other would result in crossings on a Range Time plot, but the crossing occurs for the same reason as before; radar loses spatial separation because it reduces three dimensional trajectories to one dimension range measurements. In Figure 2.4.2 are two examples of Range Time plots that might be generated from a single point target splitting into many targets. Because of differences in viewing geometry, these Range Time plots look quite different and contain different numbers of track crossings although they are plots of the same target.

Figure 2.4.2 – Range Time plots of a single target splitting into many, viewed from two different angles

2.4.2 Range Doppler plots

A second method of viewing targets is by a Range Doppler plot. This plotting technique again uses scatterer range as one axis but instead of time for the second, it uses the Doppler return of the scatterer at that range. Range Doppler plotting is rooted in the practice of target identification, decision making on what is and is not an object of interest. Although it has been used heavily for target imaging, cases have been made for its usage as a tool for tracking. A tumbling and/or spinning target will have returns from scatterers on its body, which can lead to an image that is similar in dimension to the object that sourced the signal returns. An example of this imaging is shown in Figure 2.4.3.
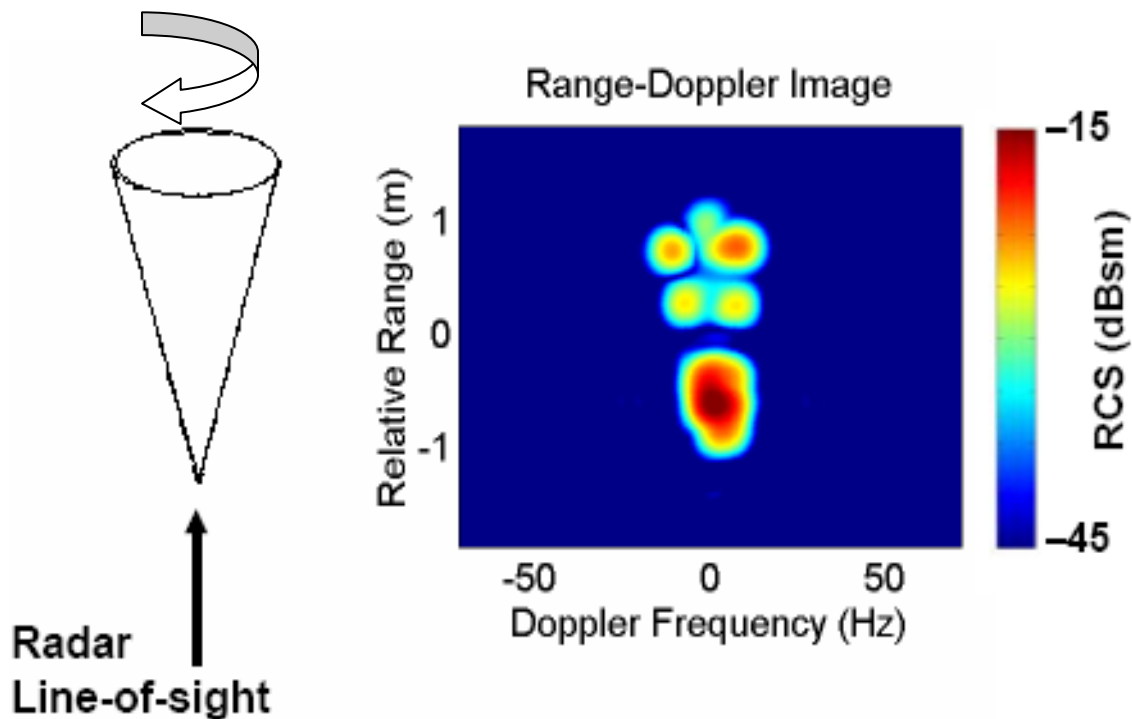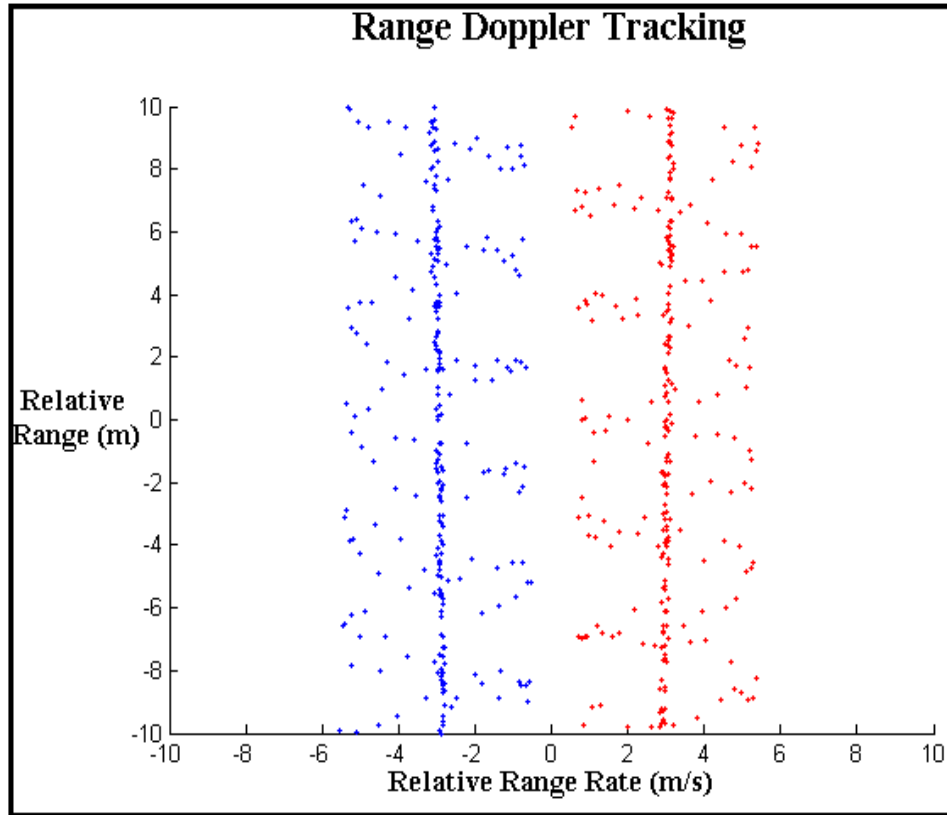

Figure 2.4.3

a.) (left) A spinning cone and the line of sight of the radar measuring it

b.) (right)The range Doppler image which arises from the measured cone

(Modified from Sheeks slide 3, Lecture 15, Introduction to Radar Systems 2004)

Figure 2.4.3 is focused on the central Doppler frequency of the target and shows the difference in the rate and direction of spin of different parts of the body. This image has a signal

intensity added that will not be present in our simulations. In this example, the right side of the cone is spinning towards the reader, increasing the frequency of the radar wave incident upon it, resulting in a positive Doppler shift. Hence the scattering from this part of the cone is plotted to the right of the zero Doppler frequency on the horizontal axis. The left side spins away from the reader, dilating the frequency and causing a negative shift and a corresponding plotting to the left of the zero Doppler frequency on the horizontal axis.

Analogous to a Range Time plot, target history can be recorded in the form of a track showing past data in Range Doppler plotting. Much like the Range Time plots, Range Doppler plots contain tracks that may bear no resemblance to the Newtonian trajectory of the targets.. As with the Range Time plot's tracks which cross, the crossing tracks of a Range Doppler plot may not reflect targets' doing so in reality. The true area of interest is whether the two plotted crossings are brought about by different situational parameters. The two targets' tracks in Figure 2.4.4 would cross on a Range Time plot, but are completely isolated in this Range Doppler plot. In this plot the two tracks do not cross or overlap because the two targets which led to the tracks have a substantial enough difference in range rate. This shows about 10 sec of data. The left target moves from top to bottom, creating the blue track, while the right target moves from bottom to top, creating the red track. The color of the tracks in Figure 2.4.4 is an aid for the reader to identify the two unique tracks. Actual Range Doppler plots do not have this information and the individual tracks may be difficult to determine from the data.

Figure 2.4.4 – Range Doppler plot of two target tracks, the targets have a significant enough difference in their velocities that the two tracks have a spatial separation. The red track is for a precessing target with a relative range rate of 2 m/s and the blue track is for a precessing target with a relative range rate of -2 m/s.

2.4.3 Plotting Conclusion

Similar to radar wave forms, different plotting techniques have unique advantages over one another. It is essential to always keep in mind that although Range Time and Range Doppler are two different plotting techniques, they are merely views of different data from the same targets viewed by radar.

3 Target Simulation

The basis for all simulation and analysis in the project is in modeling targets and the scenarios in which they exist. Practical limits were placed on both the targets and the scenario. Some limitations were ubiquitous throughout the project, other models were unique to a specific area.

3.1 Target Body

A target model can take on many different forms depending on the level of intricacy necessitated by the simulation or analysis. The simplest representation utilized in this project is a single point scatterer. Here a target is represented as a discrete point in space. It is subject only to its own trajectory and is the simplest representation of any target. The point scatterer is used for the overall analysis of rate and severity of crossing instances on Range Time plots.

Our second representation of a target is as a dumbbell, two discrete point scatterers separated by a constant length. The dumbbell will be used in the simulations of the Range Time plots. The targets simulated as dumbbells will be subject to a tumbling effect, a 90˚ angle of precession, and precession rate ω_p.

Our final representation of a target is as a cone, consisting of two point scatterers, one at the tip and one point along the circumference of the base. This model is used in the Range Doppler plots. This conical target is subject not only to precession as with the dumbbell, but also a spin about the cone's axis of symmetry. Each of these representations has a unique reason why it was the optimal choice for simulation in a specific area which is more extensively explained within the respective methods sections.

The scatterers for all three target representations are point scatterers which means that they remain locked in a single place on the body. Imagine a bolt on the side of a cylinder. As the cylinder turns, so does the bolt, which is a discrete scatterer. In our model, the scatterers are not subject to shadowing, meaning that the scatterers are never hidden by the target body, or any other object that might be between the discrete scattering point and the radar.

3.2 Scenario

Certain assumptions are made about the scenarios being simulated and analyzed. The assumptions are equally a result of the relatively short time interval which will be simulated and the conditions of the target being tracked. The targets are assumed to be in the ballistic midcourse phase of their trajectory. An illustration of the different phases of an object with a ballistic trajectory is shown in Figure 3.2.1. Targets in midcourse are subject only to gravity. Over the relatively short viewing intervals of our project even the effect of gravity can be ignored. Thus, the targets are moving in constant-velocity straight line trajectories over the simulated time intervals. Curved tracks in either of the Range Time or Range Doppler plots, then, are due to viewing geometry and not acceleration or change of direction.
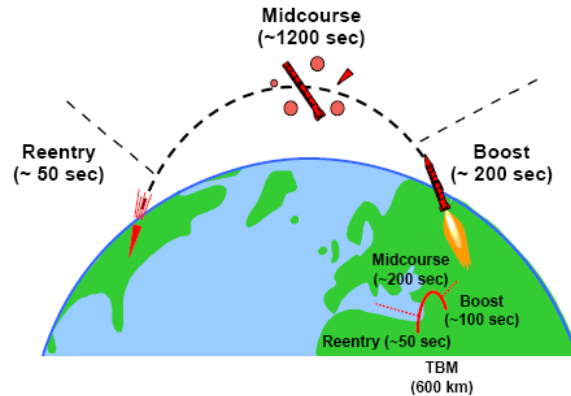
Figure 3.2.1 – Different phases of an object with a ballistic trajectory (Modified from Weiner slide 3, Lecture 4, BMD Systems Analysis 2004)

4 Track Crossings

4.1 Methodology

In order to analyze the tracks of many targets as they appear on a Range Time plot, a simple point-scatterer model was used. In this Euclidean three-space model, the positions of targets will be defined with ordered triples, (x, y, z). The x-y plane will represent the ground; however, since the effect of gravity on the targets in question is small, this assumption is merely an aid for visualization. The radar, located at the origin (0, 0, 0) will be assumed to be tracking a single target located at X_{rv} the instant before time $t = 0$. As described earlier, it will be assumed that projectiles will follow constant velocity paths through space because the effects of drag, lift, and gravity are minimal.

4.1.1 Target Track Crossings During a Starburst

One building block of target tracking is tracking through a starburst. At time $t = 0$ s, a single target breaks up into n targets, each with its own constant velocity. In such a starburst, the object can be modeled as having random separation velocities. It is assumed that both the angle of the trajectories of the separated objects to the original trajectory and the difference in velocity of the separated objects from the original is random.

At the instant of the starburst, each of n targets begins moving with a constant velocity. Since the ith target has a velocity of V_i m/s, its position at time t is then given by:

$$X_i(t) = X_{rv} + t \cdot V_i \tag{1}$$

Since the radar measures range to the target, at time $t = 0$ s, the radar is tracking one target at a range of $\|X_{rv}\|$. After the target breaks up, the range at time t of the ith target is then given by:

$$R_i(t) = \|X_i(t)\| \tag{2}$$

For the tracks of the ith and jth objects to cross on a Range Time plot, they must have the same range at some time $t > 0$, implying that:

$$R_i(t) = R_j(t) \tag{3}$$

$$\|X_i(t)\| = \|X_j(t)\| \tag{4}$$

$$\|X_{rv} + t \cdot V_i\| = \|X_{rv} + t \cdot V_j\| \tag{5}$$

Squaring both sides,

$$\|X_{rv}\|^2 + 2\langle X_{rv}, t \cdot V_i\rangle + t^2 \cdot \|V_i\|^2 = \|X_{rv}\|^2 + 2\langle X_{rv}, t \cdot V_j\rangle + t^2 \cdot \|V_j\|^2 \tag{6}$$

where $\langle a,b\rangle$ is the inner dot product of the vectors a and b. Simplifying and regrouping, one has

a quadratic in t,

$$2t \cdot \langle X_{rv}, V_i\rangle + t^2 \cdot \|V_i\|^2 = 2t \cdot \langle X_{rv}, V_j\rangle + t^2 \cdot \|V_j\|^2 \tag{7}$$

$$t^2 \left(\|V_i\|^2 - \|V_j\|^2\right) + 2t \left(\langle X_{rv}, V_i\rangle - \langle X_{rv}, V_j\rangle\right) = 0 \tag{8}$$

$$t^2 \left(\|V_i\|^2 - \|V_j\|^2\right) + 2t \cdot \langle X_{rv}, V_i - V_j\rangle = 0 \tag{9}$$

Finally, factoring out t, one has:

$$t \left(\left(\|V_i\|^2 - \|V_j\|^2\right) + 2\langle X_{rv}, V_i - V_j\rangle\right) = 0 \tag{10}$$

Thus, to get a crossing of the target's tracks, this equation must hold true. Because all targets

originate from X_{rv} there is a trivial solution at $t = 0$ s. Solving for the other solution, one has:

$$t \left(\|V_i\|^2 - \|V_j\|^2\right) + 2\langle X_{rv}, V_i - V_j\rangle = 0 \tag{11}$$

Thus, if a crossing occurs at a time after $t = 0$ s, the time at that crossing is:

$$t_{\text{crossing}} = \frac{-2\langle X_{rv}, V_i - V_j\rangle}{\|V_i\|^2 - \|V_j\|^2} \tag{12}$$

4.1.1.1 Case 1: $\|V_i\| = \|V_j\|$, Same speed

If $\|V_i\| = \|V_j\|$, then the two paths of the objects will be either completely distinct, i.e. their tracks never cross, or completely indistinguishable, i.e. their tracks overlap perfectly. If the dot product $X_{rv} \cdot (V_i - V_j)$ is also zero, then equation (11) will always be true, thus implying that the objects' tracks will cross at every point in time, overlapping perfectly. An example of this situation can be found in Figure 4.1.1.
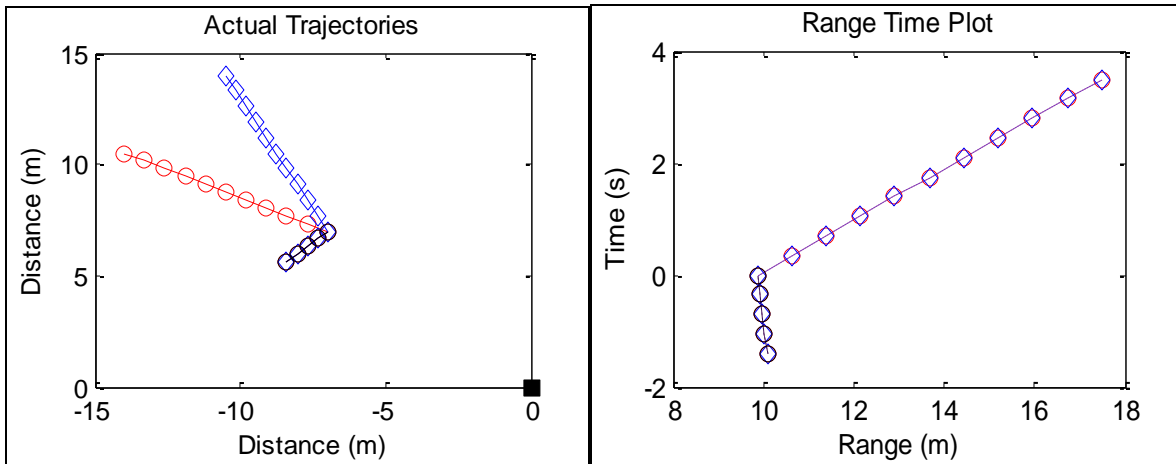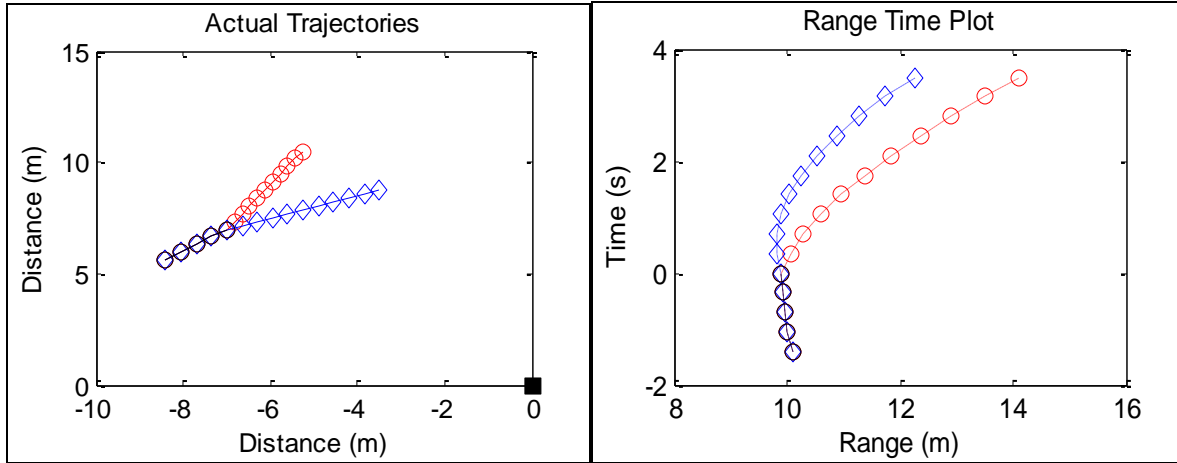

Figure 4.1.1

a.) (left) A two dimensional real-life trajectory representation of one target (bottom black circle) splitting into two (red circle and blue diamond) targets. The radar is at the bottom right. Notice that the split objects never touch after the split.

b.) (right) The Range Time plot resulting from measuring range to the targets from the radar. Despite the split objects being separated, their distance to the radar is always the same so their Range Time tracks overlap perfectly.

Perfectly overlapping target tracks occur when the dot product $\langle X_{rv}, V_i - V_j \rangle$ is zero. Thus, if the difference in the velocities of the two objects is orthogonal to the radar line of sight, the tracks left by the objects on a Range Time plot will overlap if the speeds of the two objects are the same.

Because of measurement error of the radar, there exists a range of angles which are "orthogonal enough," and a range of values which are "zero enough" to confuse the tracking

algorithm. In these cases, the perceived target split time would lag the actual target split time. Either way, as the example in Figure 4.1.2 shows, the tracks of these targets will not cross in the future.
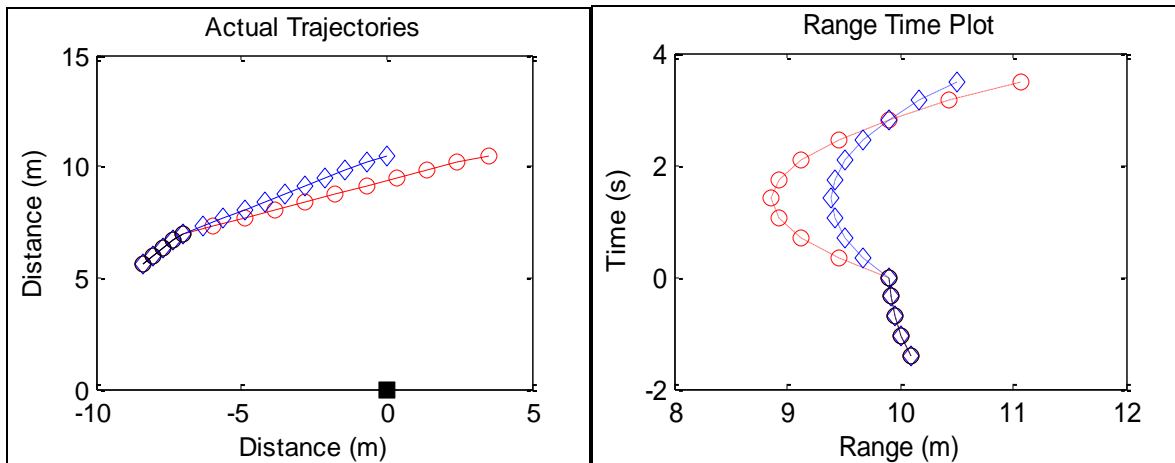

Figure 4.1.2

a.) (left) A two dimensional real-life trajectory representation of one target (bottom) splitting into two (red circle and blue diamond) targets. The radar is at the bottom right. b.) (right) The Range Time plot resulting from measuring range to the targets from the radar. Despite the split objects having the same speed (as in Figure 4.1.1), their distance to the radar is always different so their Range Time tracks never touch after $t = 0$ s.

4.1.1.2 Case 2: $\|V_i\| \neq \|V_j\|$ and $\langle X_{rv}, V_i - V_j \rangle \neq 0$

Assuming, without loss of generality, that $\|V_i\| > \|V_j\|$, then if the difference in the velocities of the two objects forms an obtuse angle with the radar line of sight, $\langle X_{rv}, V_i - V_j \rangle < 0$, a crossing will be perceived on a Range Time plot. In other words, the difference in the velocities of the two objects must be pointed away from the radar. Figure 4.1.3 has an example of what trajectory could lead to this type of crossing.
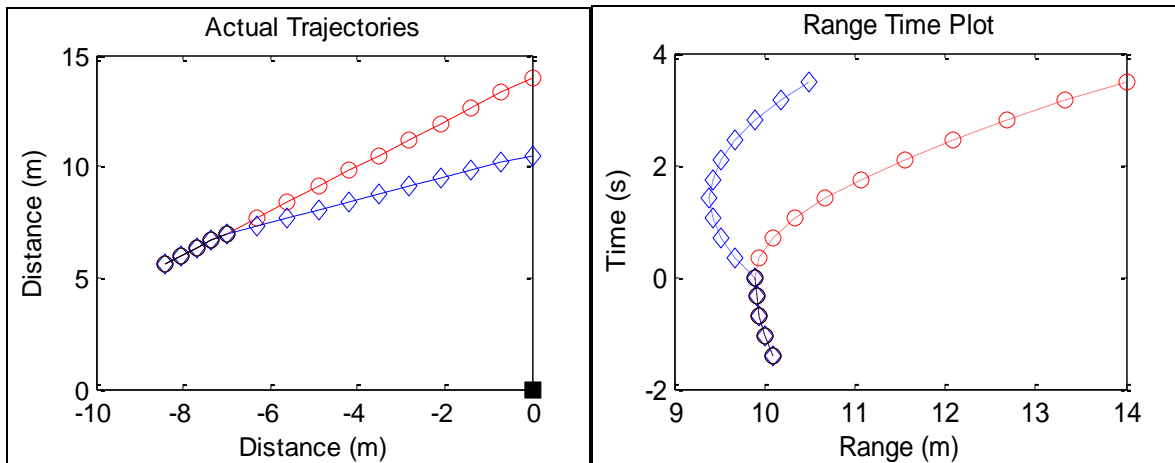
Figure 4.1.3

a.) (left) A two dimensional real-life trajectory representation of one target (bottom) splitting into two (red circle and blue diamond) targets. The radar is at the bottom right. Notice that the split objects never touch after the split.

b.) (right) The Range Time plot resulting from measuring range to the targets from the radar. The split objects have different speeds, but the angle between the difference in velocities and the radar line of sight is obtuse; thus a Range Time crossing is perceived at t = 3 s.

If the difference in the velocities of the two objects forms an acute angle with the radar line of sight, a negative time of crossing is given by equation (12). This theoretical solution only suffices to prove that no future crossing is possible because before time $t = 0$, only one target was observed. Figure 4.1.4 has an example of such a trajectory.

Figure 4.1.4

a.) (left) A two dimensional real-life trajectory representation of one target (bottom) splitting into two (red circle and blue diamond) targets. The radar is at the bottom right. The red object is moving faster than the blue one, thus the difference in velocities forms an acute angle with the radar line of sight.

b.) (right) The Range Time plot resulting from measuring range to the targets from the radar. The split objects have different speeds, but the angle between the difference in velocities and the radar line of sight is acute; thus no Range Time crossing is ever perceived.

4.1.2 A Starburst

During a starburst, many targets may result from the break up of one target. This event may result in a large number of crossings, each of which may be either "even" or "odd." An even crossing occurs if the two tracks merely come close to each other and then separate, or cross twice in quick succession. On a Range Time plot, an even crossing may be impossible to differentiate from an odd crossing, where the tracks cross straight through each other, especially when the crossing angle of the tracks is small. For each pair of targets, equation (10) proves that if a pair of targets is distinguishable, then their tracks can cross at most one time after time $t = 0$. Assuming zero radar measurement error, it is thus shown that all target crossings that result from a starburst are odd crossings.

4.1.3 Target Track Crossings During Periodic Splits

An object from which targets periodically separate is another situation which challenges target tracking capabilities. In this model, the original target will be considered an object whose trajectory is unchanged while ejecting other objects. The original object, travelling with constant velocity V_{rv} m/s ejects one object every Δt seconds beginning at time $t = 0$ s. The ith target is ejected with an additional velocity of V_i m/s after $\Delta t \cdot i$ seconds. After ejection, the position of the ith target is then given by:

$$X_i(t) = X_{rv} + t \cdot V_{rv} + (t - \Delta t \cdot i) \cdot V_i, \text{ for } t > \Delta t \cdot i \tag{13}$$

Just as before, the range to the target is:

$$R_i(t) = \left\| X_i(t) \right\| \tag{14}$$

Considering, again, the tracks of the ith and j^{th} objects on a Range Time plot, their intersection must occur at time t such that:

$$\left\| X_i(t) \right\| = \left\| X_j(t) \right\| \tag{15}$$

Expanding this:

$$\left\| X_{rv} + t \cdot V_{rv} + (t - \Delta t \cdot i) \cdot V_i \right\| = \left\| X_{rv} + t \cdot V_{rv} + (t - \Delta t \cdot j) \cdot V_j \right\| \tag{16}$$

Grouping terms by powers of t:

$$\left\| (X_{rv} - \Delta t \cdot i \cdot V_i) + t \cdot (V_{rv} + V_i) \right\| = \left\| (X_{rv} - \Delta t \cdot j \cdot V_j) + t \cdot (V_{rv} + V_j) \right\| \tag{17}$$

It is clear that equation (17) takes the same form as (5). Thus, by algebraic manipulations similar to before, equation (18), for track crossing time results:

$$at^2 + bt + c = 0, \text{ where}:$$
$$a = \left\| V_{rv} + V_i \right\|^2 - \left\| V_{rv} + V_j \right\|^2$$
$$b = 2\left(\left\langle X_{rv} - \Delta t \cdot i \cdot V_i, V_{rv} + V_i \right\rangle - \left\langle X_{rv} - \Delta t \cdot j \cdot V_j, V_{rv} + V_j \right\rangle \right)$$
$$c = \left\| X_{rv} - \Delta t \cdot i \cdot V_i \right\|^2 - \left\| X_{rv} - \Delta t \cdot j \cdot V_j \right\|^2$$

$$\tag{18}$$

A significant difference between equation (17) and equation (10) is that the quadratic in t now contains a non-zero constant term. This means that it is possible for there to be two non-zero track crossing times.

4.1.4 Track Crossings Times During Periodic Splits

The two crossing times which satisfy equation (17) are given by the quadratic equation:

$$t_{1,2} = \frac{-b \pm \sqrt{b^2 - 4ac}}{2a} \tag{19}$$

The determinant of the quadratic equation in (17), $b^2 - 4ac$, can be used to determine how many crossing times are possible. Because of radar measurement error, this determinant can give somewhat ambiguous information. Where equation (19) yields crossing times before the ejection of one or both targets, these crossing would not be realized on a Range Time plot.

4.1.4.1 Case 1: $b^2 - 4ac > 0$, two real crossing times

If the determinant of the quadratic in equation (18) is positive, the tracks of the ith and j^{th} objects may cross twice. If both crossing times, as given by equation (19), occur after the ejection of the later target, and the radar measures range without measurement error, two separate, odd crossings are always perceived. If, however, the two targets are not separated by more than the radar's measurement error between the two crossing times, the two odd crossings appear as one, merged even crossing.

If only one crossing time occurs after the ejection of the later target, and the radar measures range without measurement error, one odd crossing would be perceived. If the radar measurement error was larger than the maximum distance between the two targets before this crossing, no crossing would be perceived; the tracks would look like one target which broke off of the original object which later split into two targets.

4.1.4.2 Case 2: $b^2 - 4ac = 0$, one real crossing time

If the determinant is zero, the two tracks will have an even crossing, assuming the crossing time is after the ejection of the later target. In reality, the determinant will never be zero because this would require a priori knowledge of the radar viewing angle and infinite precision. In simulations with continuous distributions for trajectory parameters, the probability that the

determinant will be non-zero is one. Even crossings occur, however, when the determinant is close to zero. If the determinant is small, but positive, the previously described case may occur where two odd crossings are perceived as one even crossing.

4.1.4.3 Case 3: $b^2 - 4ac < 0$, no real crossing times

If the determinant is small in magnitude, but negative, the two tracks will not cross at all. Instead, the two tracks might become very close in range at the apex of the parabola in equation (18), at time $-b/2a$, and then diverge. If the difference in range is less than the radar measurement error, again, an even crossing would be perceived. If time $-b/2a$ occurs before the later target is ejected, no crossings are realizable in the Range Time plot.

4.1.4.4 Same Speed Case: $\|V_i\| = \|V_j\|$

Though not distinct from the previous cases covered, the situation were the speeds of the ith and jth objects are the same is worth considering. If the two post-ejection speeds of the ith and jth objects are the same, the value of a in equation (18) is zero. This reduces equation (18) to a linear equation in t, which gives *-c/b* as the one crossing time. As in Case 2, above, if the crossing time occurs before the ejection of the later object, this solution is meaningless. If, however, it occurs later, one odd crossing may be perceived if the radar measurement error is small enough to detect the two targets before they cross.

4.1.5 Simulating Periodic Splits

The complicated form of equation (18) does not lend itself to analytically determining the frequency, time and crossing angle of track crossings. Thus, Monte Carlo simulations were performed. By generating independent, uniform random values for the parameters of the model, target track trajectories could be modeled. Because objects generally remain in ballistic midcourse for up to twenty minutes, crossings occurring after this time were not included in the analysis. The following table of assumptions was used for generating the parameter values [Weiner, 2008].

Value	Magnitude	Direction
Δt	{1, 3, 10} seconds	NA
n	{3, 10, 30} ejected objects	NA
Radar measurement error	{1, 2, 5, 10} m	NA
X_{rv}	1,000,000 m	Elevation: Uniform on $\left[0, \dfrac{\pi}{2}\right]$ rad; Azimuth: 0 rad.
V_{rv}	7,000 m/s	Uniform Spherical Random in elevation $[0, 2\pi]$ and $[0, \pi]$ azimuth.
V_i	Uniform on [0, 10] m/s	Uniform Spherical Random in elevation $[0, 2\pi]$ and $[0, \pi]$ azimuth.

*Each random value was generated independent of all others.

One thousand randomly generated scenarios of thirty objects were run for each value of Δt. Data about the Range Time track crossings caused by the first three, ten and thirty objects were then calculated using equation (18) and (19). Radar measurement error was factored in by going through each of the nine resulting sets of crossings and "merging" pairs of odd crossings, which were due to the same two targets, into a single even crossings. This merging was performed based on the maximum separation of the object's tracks between the times of the two odd crossings; if the maximum separation was less than the radar error, an even crossing was recorded; otherwise, two odd crossings were recorded. Finally, if the minimum separation between two tracks was less than the radar measurement error, an even crossing was also recorded. This merging process was performed for all four radar errors studied.

While calculating crossing times is straight forward, finding the crossing angle is not. On a Range Time plot the difference in slopes of the tracks at a crossing, at time t_{cross}, is a result of the difference in relative radial velocities of the objects. Determining the time, t_{start}, before the

crossing suffices to define the angle, as shown in Figure 4.1.5 because while the two tracks may be separate at time t_{start}, they cross at time t_{cross}. In order to be consistent with the individual crossing model used later, which takes crossing angle as an input, t_{start} was taken to be the mean of t_{cross} and either the previous crossing time or the average ejection time [Weiner, 2008].
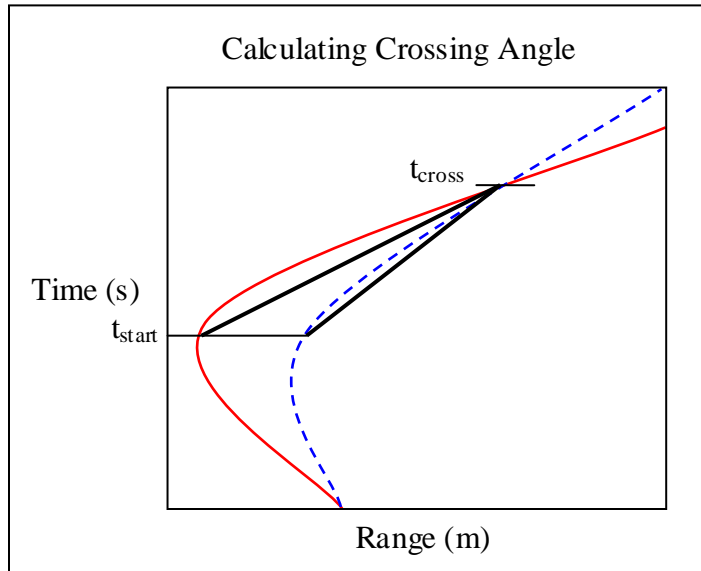
Figure 4.1.5 The red and blue tracks cross for the second time at t$_{cross}$. The crossing angle is defined by t$_{start}$, which is halfway between the two crossings.

In determining the probability of successfully tracking two targets through a crossing, the cross-free time before the crossing and the angle of the crossing are key parameters. Thus, measures of these parameters were aggregated from the data by averaging over the scenarios run. Both the average time to the first crossing (for the ith target) and the average time between target crossings were computed by averaging over the set of 1,000 scenarios for each Δt, n, and measurement error. Estimates for the distributions of crossing angles were similarly aggregated by the same parameters. Finally, the evolution of the number of crossings was computed by averaging over all of the scenarios at ten to twenty second snapshots.

4.2 Track Crossing Results

4.2.1 Starbursts

Equation (10) shows that for any pair of targets emitted by a starburst of one target into *n* targets, their Range Time tracks may cross at most one time after the starburst in an odd crossing. This fact implies crossing resulting from all pairs of targets thus emitted will be odd. Since each crossing results in an odd number of crossings, associating tracks to targets follows a simple rule. For each track which crosses another, the track which was farther away from the radar before t_{cross} is associated with the track which is closer to the radar after t_{cross}. In fact, even if there are $n > 2$ targets crossing at the same time, track association still follows this simple rule: the track furthest away from the radar before the crossing is associated with the track closest to the radar after the crossing. The tracks of the remaining *n*-1 targets maybe assigned by recursively applying this rule until all tracks have been associated. Radar measurement error would not, however, introduce even crossings, since two target tracks which are distinguishable will either cross once or never cross. A larger measurement error would only delay the perception of splits and crossings, not change their nature.

4.2.2 Periodic Splits

Having completed all of the simulations described, statistics about track crossings could be aggregated. First, the probability of a track having crossings is assessed. Next, frequency of even crossings is considered. With this broad understanding of track crossings, the distribution of crossing angles as well as the amount of time before a crossing occurs were calculated.

4.2.2.1 Crossings-Free Tracks

To begin the investigation of target track crossings, their very frequency should be first considered. As Figure 4.2.1 shows, the number of objects being ejected substantially affect the probability that the ith object's track will be free from crossings.
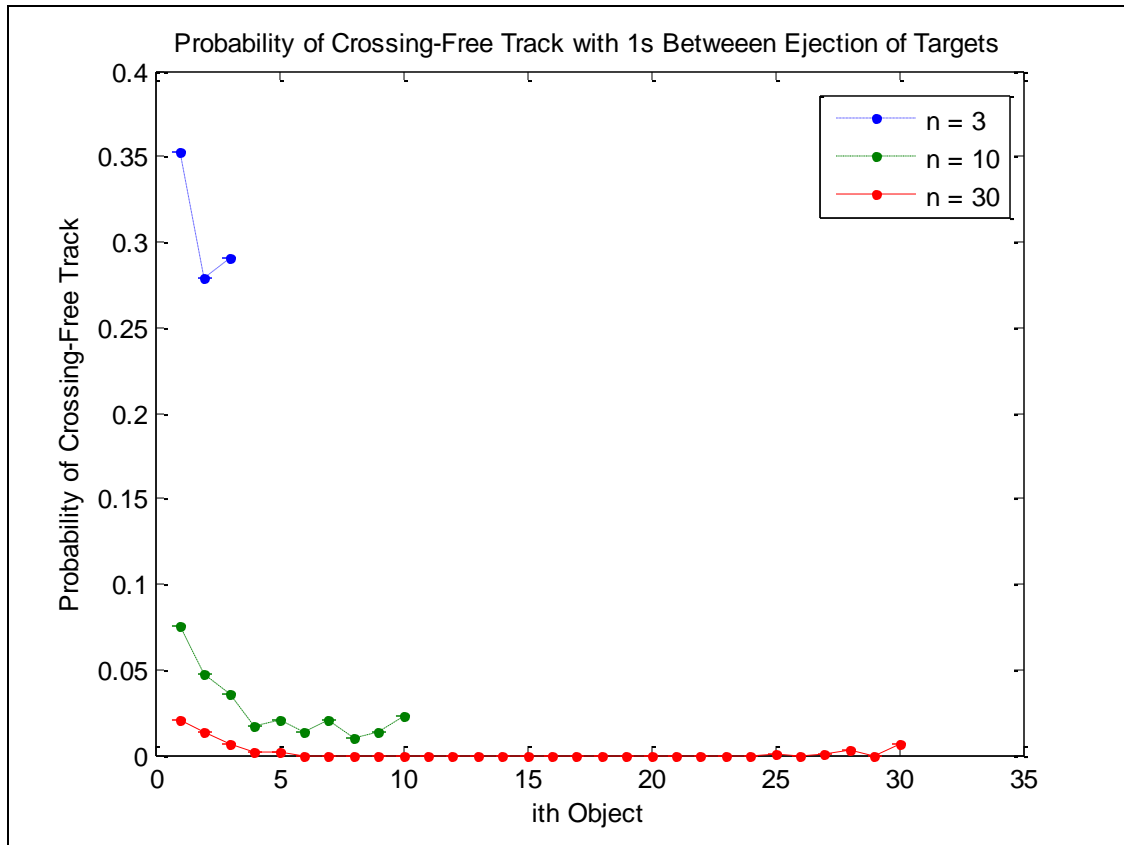
Figure 4.2.1 The probability of the ith object having no track crossings is plotted for the three different numbers of objects ejected: three, ten, and thirty. Objects ejected toward the beginning and toward the end had a slightly higher chance of being crossing-free. Overall, the ejection of less objects resulted in large increase in the probability of crossing-free tracks.

For objects ejected among three, the probability of a track free of crossings is between 0.25 and 0.35. For objects among ten this probability quickly drops to below 0.10 and for thirty objects this probability is below 0.03. Objects both toward the beginning of the ejection order and toward the end experienced higher rates of crossing-free tracks, though the effect was larger for tracks of objects ejected earlier.

This ejection order effect is illustrated even better in Figure 4.2.2, where the probability of a crossing-free track is plotted for thirty targets for each time delay between ejections. Earlier ejected objects have small probabilities of having a track free from crossings, while many of the later ones have probabilities which are ten-times less or even zero.
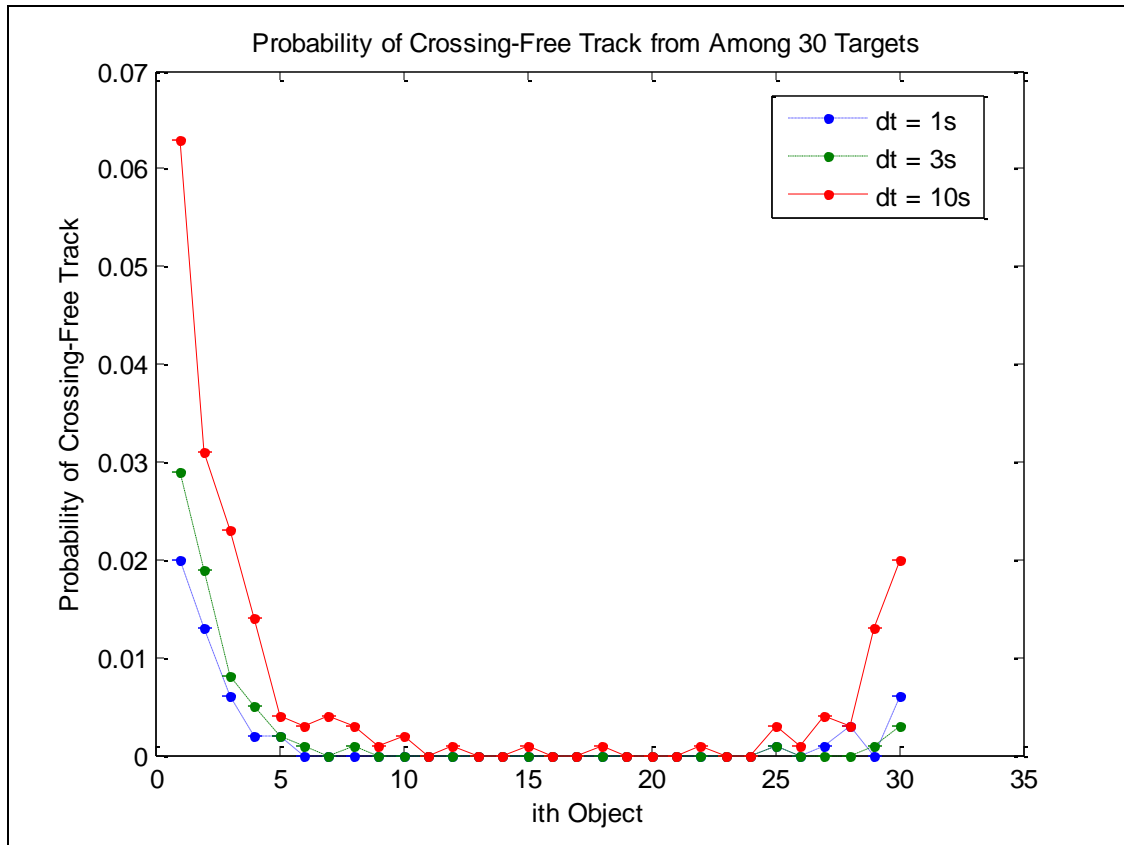
Figure 4.2.2 The probability of the ith object having no track crossings is plotted for the three time delays investigated: one, three, and ten seconds between target ejections. Objects ejected toward the beginning, among the first ten, had a substantially higher chance of being crossing-free, as did objects ejected toward the end, though to a lesser extent.

The first objects ejected have probabilities of a crossing free track of 0.06, 0.02, and 0.01 corresponding to time delays of one, three, and ten seconds. This roughly linear relation is maintained throughout the first four objects ejected. Overall, few target tracks had no crossings. Those objects whose tracks do are usually either one of the first, or one of the last to be ejected.

4.2.2.2 Even crossings

Despite the presence of objects whose tracks remain cross-free, the vast majority of tracks in the scenarios do have crossings. As previously described, crossings come in two varieties, even and odd. The relative frequencies of these crossing is also important. In the simulation that was previously described, our scenarios produced zero even crossings at the radar

measurement errors of one, two, five, and ten meters. Figure 4.2.3 shows how many of over half a million crossings would appear as even crossings at different radar measurement error levels.
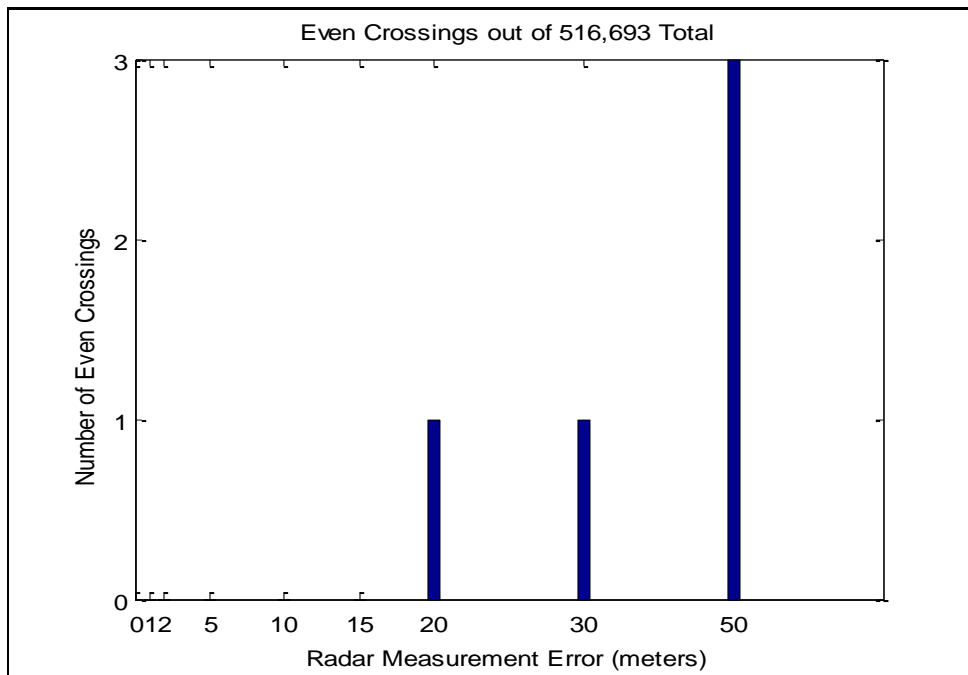
Figure 4.2.3 The number of even crossings resulting from using a given radar measurement error. Only three even crossings would result if the radar measurement error was 50 meters, corresponding to a probability of 5.8×10^{-6}. Each bin evaluates 516,693 crossings.

Even with a very poor radar measurement error of 25 m, only one even crossing would have occurred. In fact, no even crossings would appear unless the radar measurement error was larger than 18 m. Thus, using radar errors of 1, 2, 5 or 10 m did not result in any odd crossings being merged into an even crossing.

4.2.2.3 The Distribution of the Crossing Angle

Since the simulations run only yielded odd crossings, the statistics to follow will not be broken down by crossing type. Figure 4.2.4 shows the distribution of crossing angles averaged over the track crossings of thirty objects for time delays of one, three, and ten seconds between object ejections.
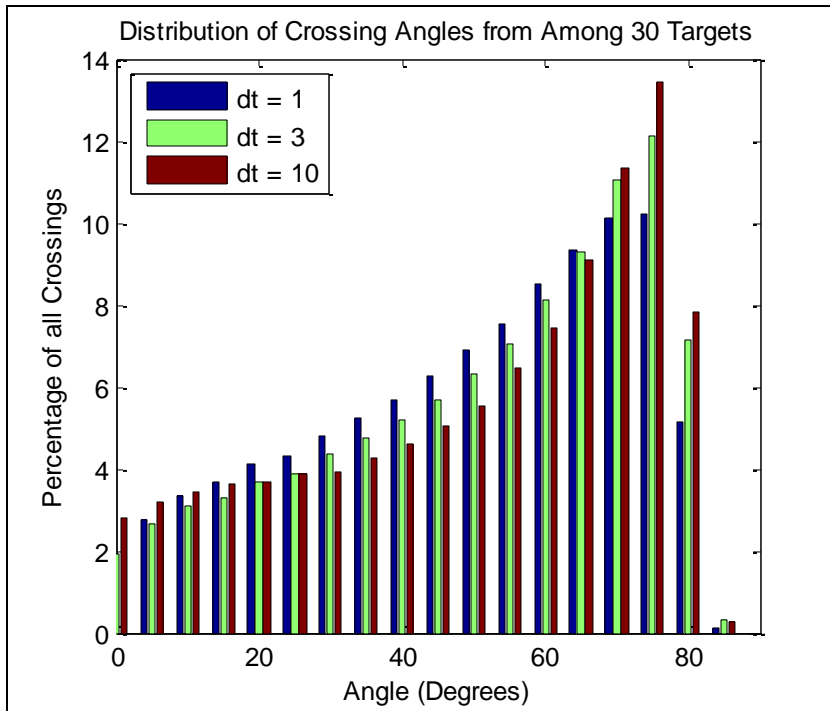
Figure 4.2.4 The distribution of crossing angles aggregated over the crossings from thirty objects ejected at time delays of one, three, and ten seconds.
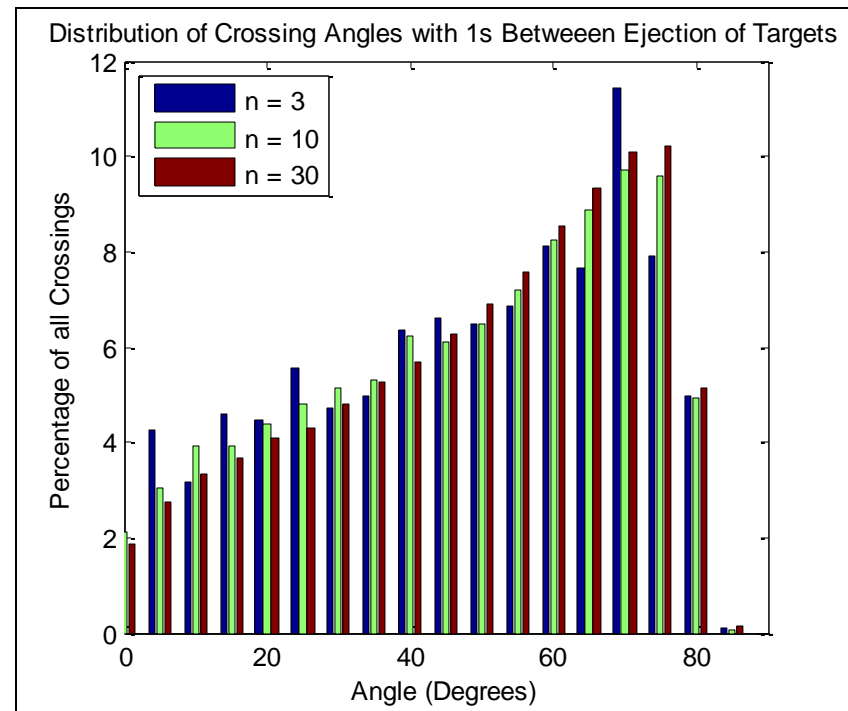
Figure 4.2.5 The distribution of crossing angles aggregated from objects ejected at one second intervals for three, ten and thirty objects.

The distribution of crossing angles is roughly triangular over the [0°,90°] range with a peak at 75°. About one quarter of all crossings have crossing angles below 25°. As the time between object ejections increases, the distribution of crossing angles shifts slightly to the right.

When the time delay between object ejections is one second, the number of objects ejected does not substantially change the distribution of the crossing angle as shown in Figure 4.2.5.

As can be seen by the previously non-existent spikes in the distribution, decreasing the number of objects ejected increases the variability of the crossing angle probabilities, but not the shape of the crossing angle distribution itself.

4.2.2.4 Time to First Crossing

In tandem with crossing angle, the track time up to the crossing is essential for determining which type of crossing has occurred. The time between ejection and an object's track's first crossing was aggregated over 1,000 scenarios for thirty ejected objects. The median time to first crossing is broken down by position in the ejection order and by time delay in Figure 4.2.6. The vertical bars mark the 25th and 75th quartiles to provide a sense of range.
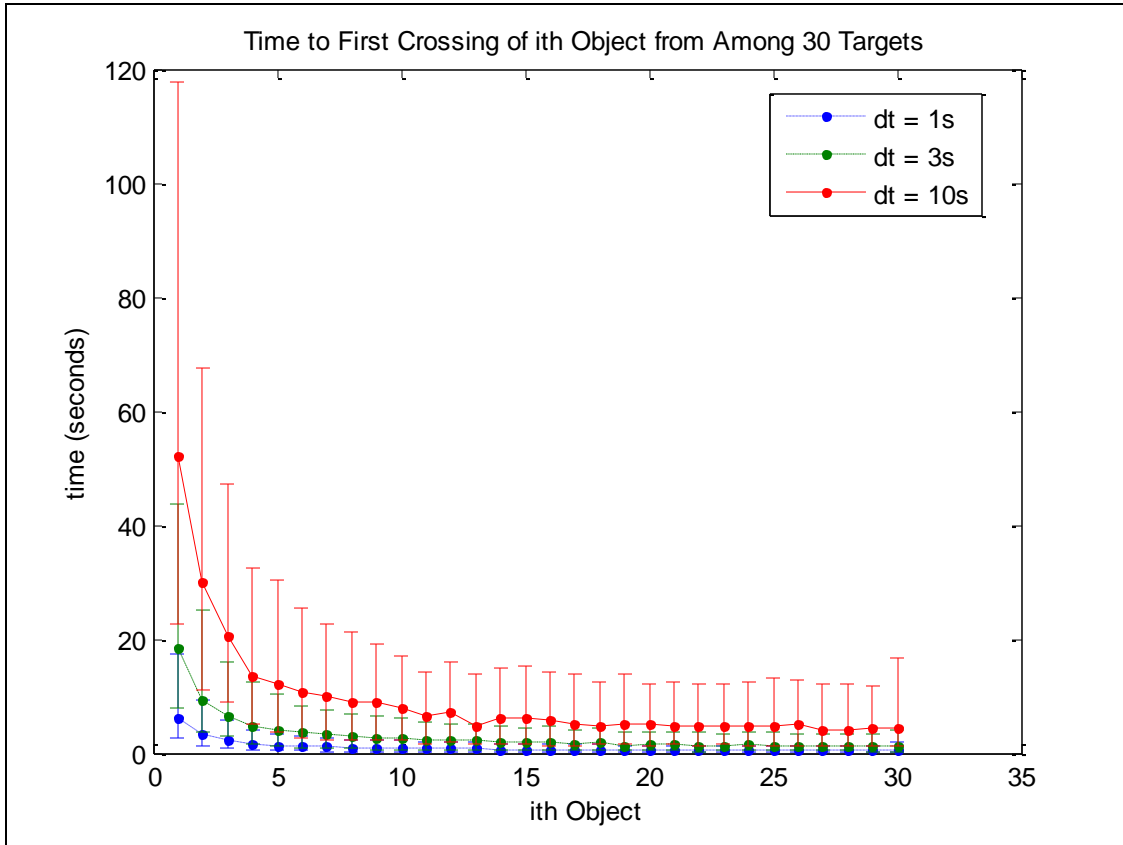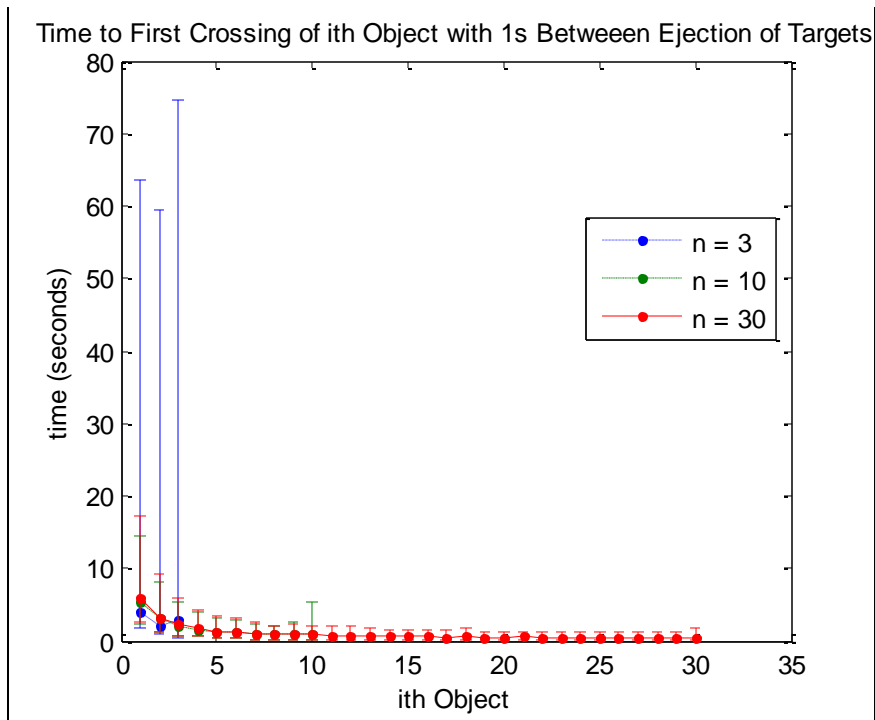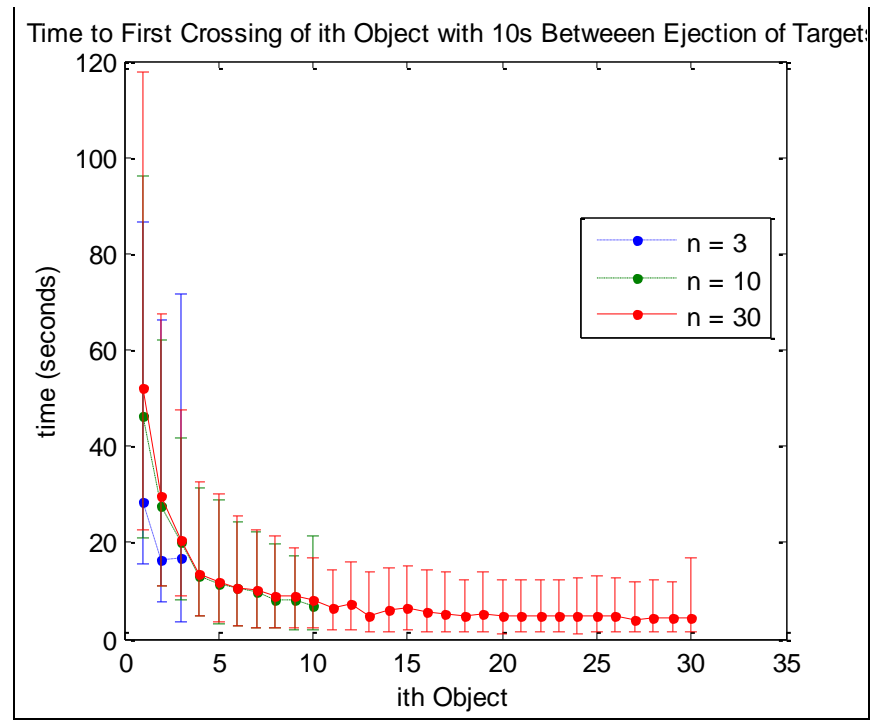
Figure 4.2.6 The median time between ejection and the first crossing of the *i^th* object is plotted for the three time delays ("dt") investigated: one, three, and ten seconds between target ejections.

Objects ejected with larger time delays between ejections had uniformly longer times between ejection and first crossing. Overall, time to first crossing decreases sharply and generally monotonically for each subsequent object. The 25th and 75th quartiles follow similar paths.

Looking at the data across another dimension, Figure 4.2.7 expands on the one second time delay curve adding to it curves for crossings made with three and ten ejected objects as well.

Figure 4.2.7 The median time between ejection and the first crossing of the ith object is plotted for the three different numbers of objects ejected: three, ten, and thirty.

Figure 4.2.8 The median time between ejection and the first crossing of the ith object with a time delay of ten seconds between ejections is plotted for three, ten, and thirty ejected objects.

Times between ejection and first crossing are similar across all set sizes. Overall, time to first crossing decreases gradually and monotonically for each subsequent object. For larger n there also appears to be a slight decrease in the time to the first crossing, though the variability of the data is large in this area.

Taking a slightly different slice of the data along the same dimension, Figure 4.2.8 shows the same three curves as before except the time delay between object ejections is now ten seconds instead of one.

The trends are essentially the same as before only there is a marked increase in the heights of the curves. Times between ejection and first crossing are again similar across all set sizes, with a slight decrease for n = 3. With an increase in time between ejections, average time to first crossings increases across all set sizes.
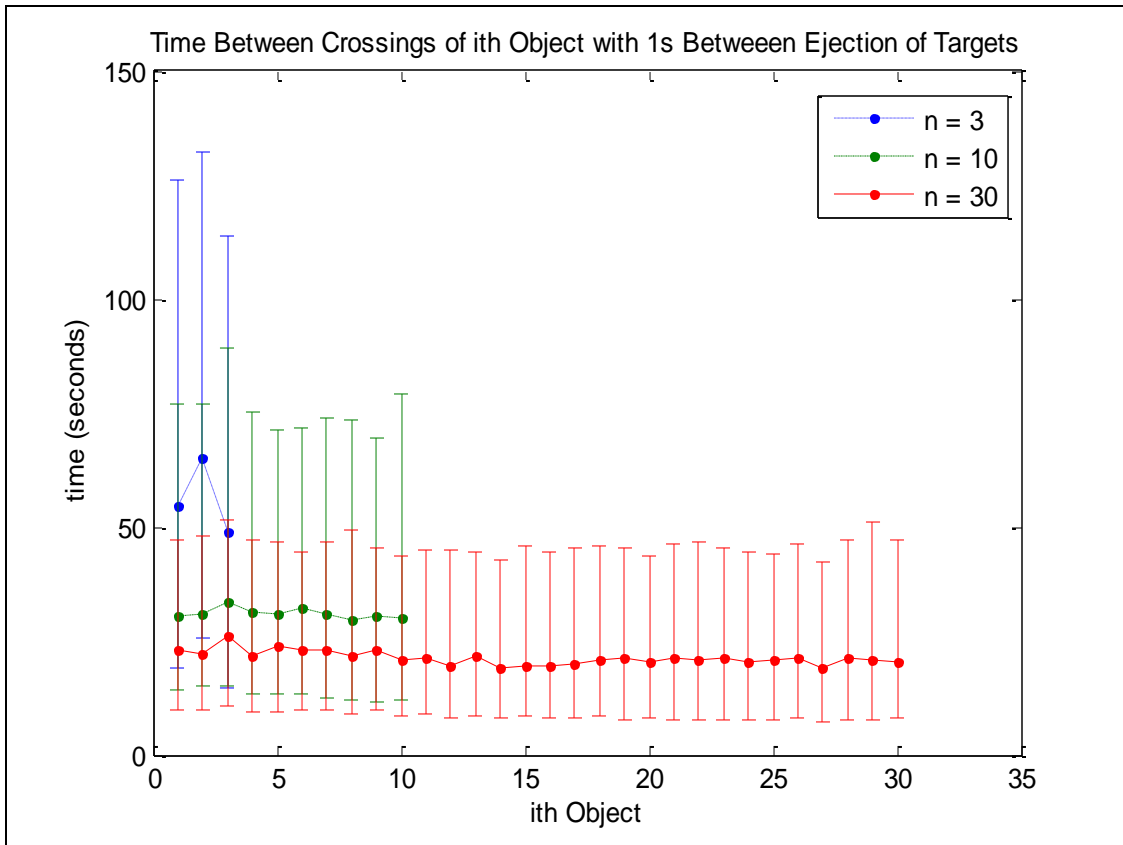
4.2.2.5 Time Between Crossing

Following a track's first crossing, many more can result, thus making tracking more difficult. In order to better understand these subsequent crossings, the average time between crossings was also analyzed. The shape of this curve, as shown in Figure 4.2.9, is markedly different from Figure 4.2.6, demonstrating why both measures were needed. Both figures aggregate data about crossing times for thirty objects grouped by the three time delays used.
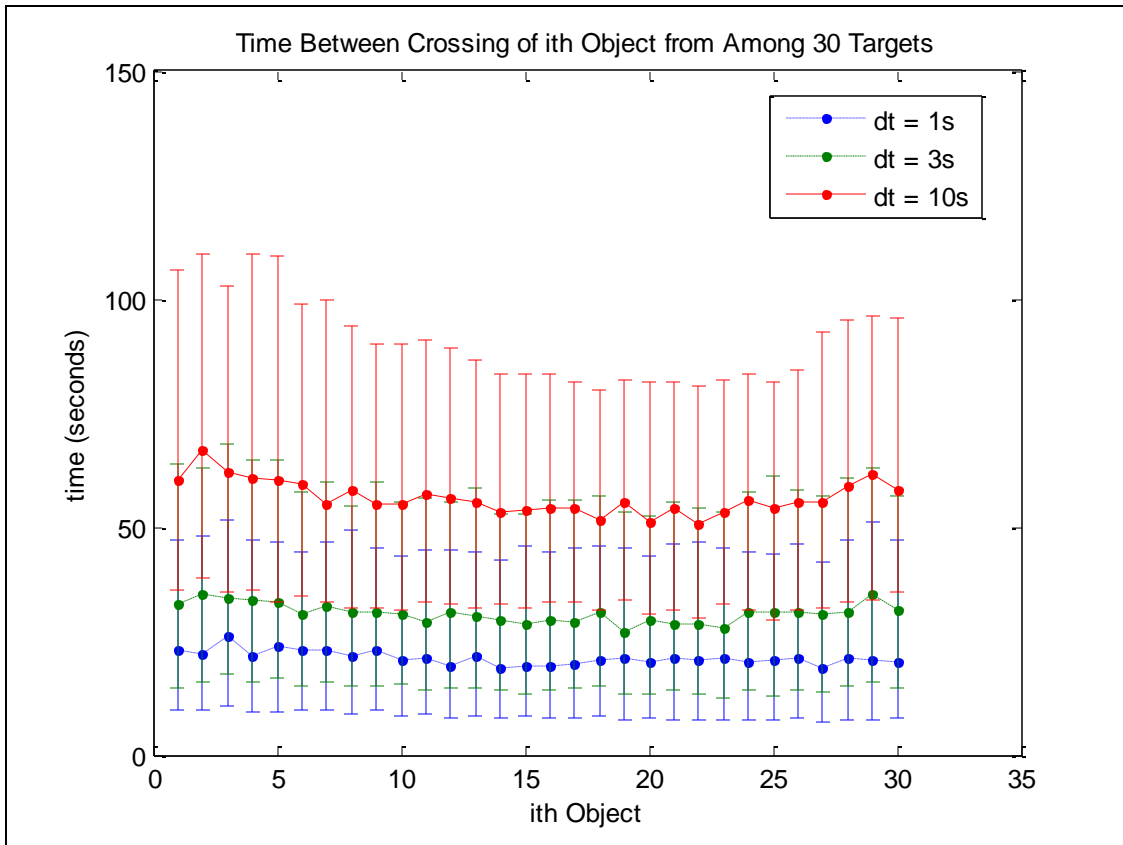
Figure 4.2.9 Plots the median of the average time between crossings for the ith object along with error bars for the 25th and 75th quartiles. Three curves represent time delays between ejection of one, three, and ten seconds.

In contrast to Figure 4.2.6, the average time between crossings curve is flat across all thirty objects for a given time delay. However, a smaller delay led to a substantial decrease in average time between crossings.

Figure 4.2.10 Plots the median of the average time between crossings for the ith object along with error bars for the 25th and 75th quartiles. Three curves represent three sets of objects of size three, ten and thirty, which were simulated as being ejected one every second.

Again, looking at the data grouped by number of objects ejected and aggregating the data for a time delay of one second Figure 4.2.10 plots the time between crossings for the three object set sizes. Smaller set sizes lead to higher average times between crossings. The difference is modest between ten and thirty objects, but the average time between crossings more than doubles between thirty and three objects. The effect of the number of objects ejected is actually convoluted with time delay. Since the time between crossings curves are flat, their means have been plotted in Figure 4.2.10.
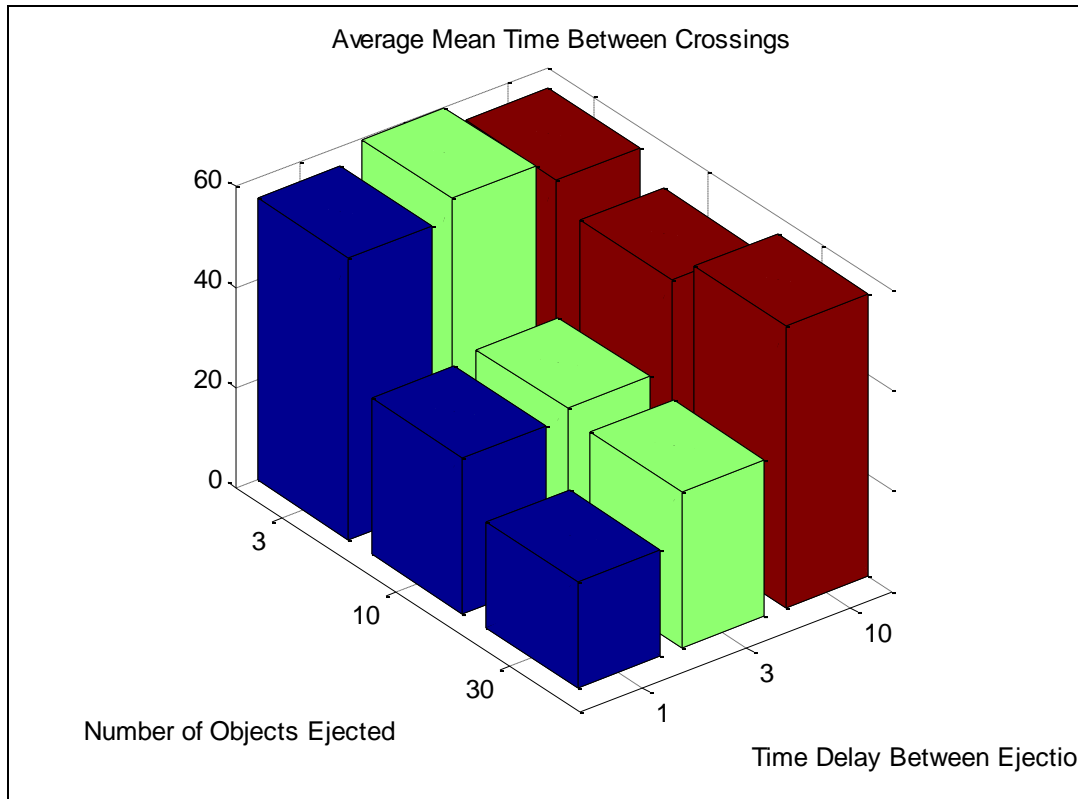
Figure 4.2.11 Plots the average mean time between crossings for the ith object. Each bar represents a particular time delay and number of objects ejected.

As shown in Figure 4.2.9, an increase in time delay between ejections increases the average time between crossings. In Figure 4.2.10, it was shown that larger sets of objects lead to lower average times between crossings. When these effects are combined, an interesting dynamic arises: for a given number of objects ejected, increasing the time delay increases the average time between crossings for all of the objects. When only three objects were ejected, the time between crossings was about the same for a one second time delay as for a ten second time delay: about fifty seconds. When the time delay between ejections is increased for the largest group of objects, the average time between crossings more than doubled from 25 to 60 seconds.

4.2.2.6 Evolution of Crossings over Time

For individual crossings, analysis of crossing angle and time before crossing are important. To better understand the task of tracking a group of objects, information about how the total number of crossings evolves over time was also aggregated. The frequency of crossing

times, starting at time $t = 0$, for thirty objects ejected at a variety of time delays between ejections is plotted in Figure 4.2.12.
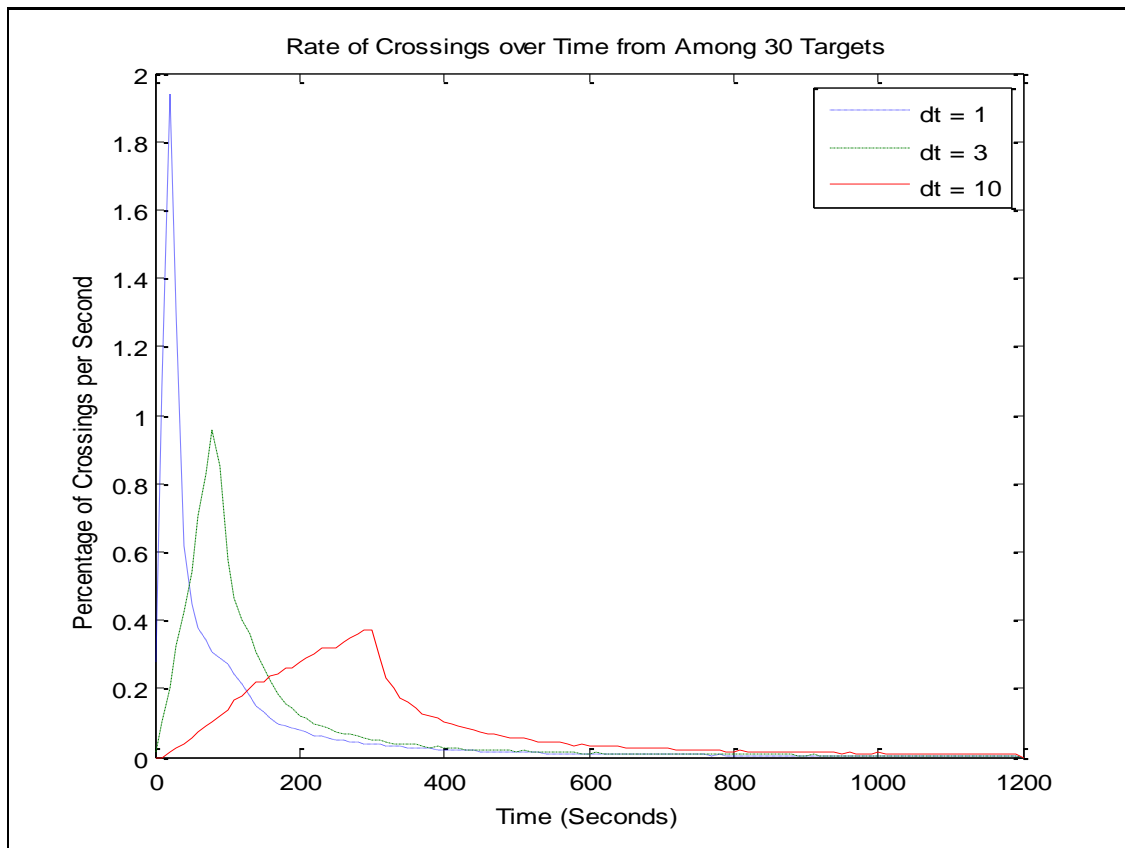
Figure 4.2.12 The frequency of crossings for each ten second period was averaged and plotted for thirty objects ejected every one, three, and ten seconds.

As the time delay increases, crossing times skew to the right, to later periods of time. This shift also decreases the density of the crossings, or number of crossings per second, by spreading them out over a longer period of time.

Similarly, when the time delay between object ejections is held constant at ten seconds and the number of objects ejected is varied, crossing times skew to the right as shown in Figure 4.2.13.
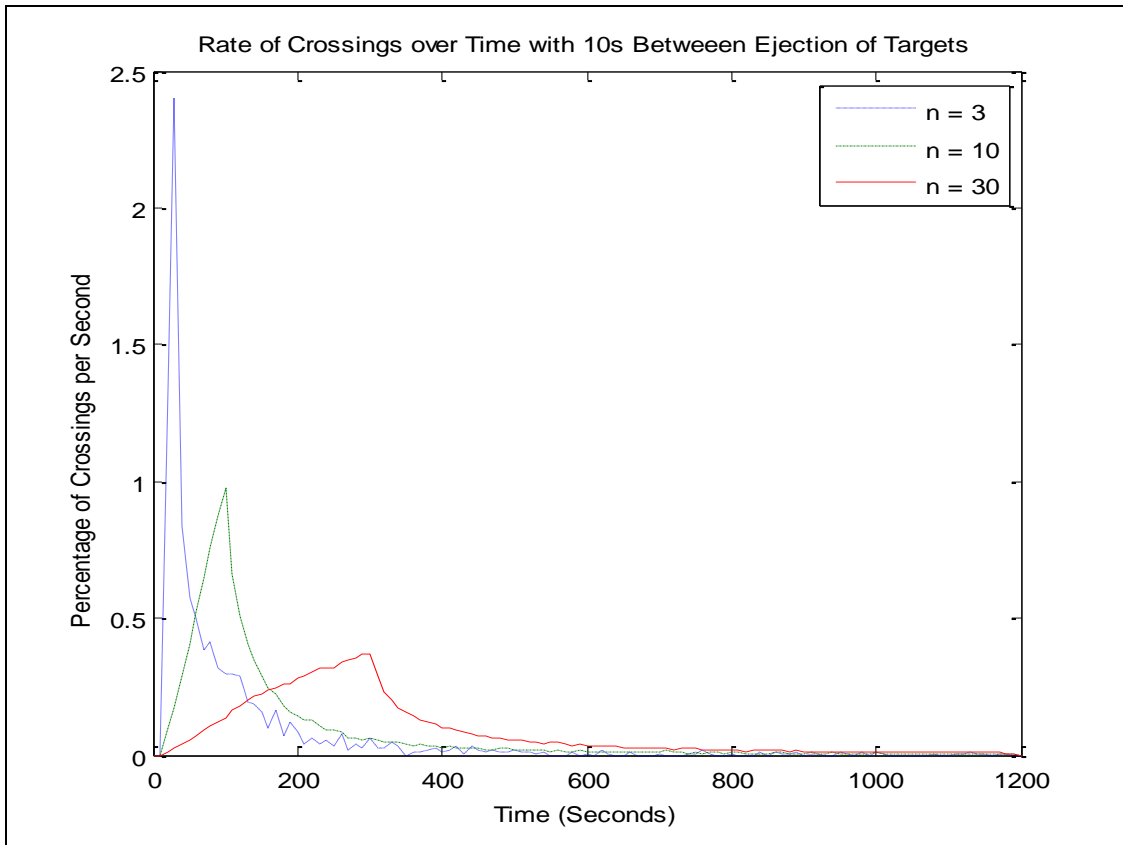
Figure 4.2.13 The frequency of crossings for each ten second period was averaged and plotted for three, ten and thirty objects ejected every ten seconds.

Increases in the number of objects ejected lead to an almost identical skew of the crossing times to later periods. Similarly, this effect decreased the density of the crossings.

4.3 Track Crossing Discussion

4.3.1 Starbursts

As was shown in section 4.1.2, a simple algorithm allows for the perfect association of targets to tracks when a starburst occurs. If measurement error is large, there may be confusion as to whether the targets separating from an original target do so at the same instant, or over time. Otherwise, the full track of each target can be discerned. Thus, if one is certain a starburst has occurred, crossings can be resolved with 100% accuracy without further analysis.

4.3.2 Periodic Ejections

4.3.2.1 Crossings-Free Tracks

While tracking the periodic ejection of objects from an original object, few tracks will not experience a single crossing, making the corresponding targets relatively easy to track, while other tracks may experience many crossings, making them more difficult to track. The probability of a crossing-free track is most dependent on the number of objects ejected simply because the ejection of more objects results in more tracks and therefore more crossings, as can easily be seen in Figure 4.2.1.

Two other factors are better shown by Figure 4.2.2: the time delay between object ejections and object's position in ejection early on had a substantially higher probability of having crossing-free tracks likely because they had a head start on moving away from the soon-to-be-ejected objects. Objects toward the end also had slightly higher probabilities of having crossing-free tracks, though, less so than the objects ejected earlier. This occurred because, by the time the latter objects are ejected, the earlier ones have already dispersed. This effect becomes more slightly pronounced with a larger time delay between ejections, causing objects ejected both earlier and later to have higher probabilities of having crossing-free tracks because the earlier objects have more time to get away from the group, and latter objects are being ejected into a group of already dispersed objects.

4.3.2.2 Even Crossings

Despite the effects of the number of objects and the time delay between ejections, most targets' tracks have crossings where they intersect with another target's track. Without measurement error, two tracks would have to be located at the same distance from the radar at the same time while travelling at the same radial velocity in order to create an even crossing. In real life, as modeled in our simulations, there is measurement error. One of the goals of this project was to understand even crossings in terms of crossing angle and time between crossings. Unfortunately, the largest measurement error used in our simulations was 10m, while the first even crossing would only appear at an error of 19m. Thus, despite the occurrence of more than half a million crossings, there were no even crossings at any of the radar measurement error levels used in our simulation. While more complicated scenarios, such as multiple starbursting

targets might result in more even crossings, if our simulation is realistic, we conclude even crossings are exceedingly rare based on our scenarios. Because of the dearth of these even crossings, the distribution of crossing angles and the time between crossings is only presented, and valid, for odd crossings.

4.3.2.3 Crossing Angle Distribution

Because no even crossings were found, the crossing angle distribution was not analyzed by crossing type, and was aggregated from all of the simulations. The distribution's shift toward 90°, caused by an increase in time between ejections of light objects is explained by the fact that this longer ejection time gave objects more time to separate before the crossing. This resulted in slightly larger crossing angles, as can be seen in Figure 4.2.4. In contrast to the subtle effect of the time delay, the number of objects ejected seemed to have no effect on the distribution of the crossing angle. As can be seen in Figure 4.2.5, the distribution is much less smooth for $n = 3$ than for $n = 30$. This variability was most likely caused by the total number of crossings. The maximum number of intersections of n lines grows with the square of n. Extension of this principle leads to the conclusion that since any pair of target tracks can cross up to two times, target crossings similarly grow with the square of the number of objects. Thus, the unevenness seen in the $n = 3$ distribution was probably caused by the substantial difference in total crossings because the largest number of crossings caused by tracking thirty objects is on the order of 100 times larger than the number caused by tracking three.

4.3.2.4 Time to First Crossing

As work in the Track Crossing Discrimination section will show, the next most significant factor in successfully distinguishing crossings is the amount of crossing-free track time before the crossing. As clearly shown in Figure 4.2.6, the later an object is ejected, the sooner its first crossing occurs because it is ejected into an ever-growing set of nearby objects. As this set grows, the time between ejection and first crossing goes down. Juxtaposing Figure 4.2.7 and Figure 4.2.8, the linear relationship between time delay and time to first crossing can be observed. In the latter figure, the time delay between ejections is ten times that in the former figure. Similarly, the times to first crossing are ten times larger in the latter figure than the first, because the longer time delay has caused previously ejected objects to move further away from

the original object. Thus, objects which are subsequently ejected take more time before their tracks intersect those of objects ejected earlier. In both figures, it is clear that the number of objects ejected does not have a substantial impact on the time to the first crossing. The exception to this observation is the $n = 3$ curve which is lower than the other two in both figures because a large number of these scenarios contain no crossings (as was observed earlier). Thus, crossings either occur early or not at all in these scenarios because there are so few objects that if their tracks do not cross initially, the objects may move too far apart to make any crossings possible.

4.3.2.5 Time Between Crossings

Beyond the first crossing, objects must be tracked through subsequent crossings as well. As justified by the stark change in shape between Figure 4.2.6 and Figure 4.2.9, the separation of first and subsequent crossings was useful because it may take an object's track some amount of time to get to the first crossing, but then subsequent crossings occur once it is within the cloud of other objects, until, finally, the cloud disperses. Unsurprisingly, the time between crossings scales with the amount of time between ejections. This phenomenon is similar to what occurred with time to first crossing in Figure 4.2.6; objects are farther away and so it takes longer for a newly ejected object's track to begin crossing the tracks of other objects. In this case, a similar effect results in the target's tracks being father apart because of the larger time delay, and, thus, it takes longer for other targets' tracks to cross.

Curiously, the effect of increasing the time delay between target separations is not independent of the number of objects ejected. For fewer objects, a change in the time delay between ejections did not have such a large effect as for thirty objects because the time between crossings was already fairly large. For three objects, an average time between crossings of fifty seconds means that one can expect that many crossings will occur before 200 seconds because any one object's track can only have four crossings (this maximum is reached if there are two crossings with each of the other two object's tracks). Thus, if all crossings end in this short period of time, then increasing the time delay between ejections only has the effect of delaying the time to the first crossing. When the number of objects ejected is large, an increase in the time delay serves to disperse the entire cloud of objects. By moving them farther apart from each other, the time between crossings is likewise increased.

4.3.2.6 Rate of Crossings

By considering the number of crossings that occur within a given amount of time as opposed to the amount of time between crossings, the frequency of crossings can be understood. As Figure 4.2.12 and Figure 4.2.13 demonstrate, increases in the time between ejections and the number of objects ejected both serve to skew the frequency of crossings to later times and result in a decrease in crossing density. In both figures, the peak frequency of crossings occurs at the time of the last object's ejection. Thus, objects being ejected could be considered as "forcing" the number of crossings to increase with each ejection. The frequency of crossings seems to grow linearly in this phase as objects are ejected one after another. After this forcing is complete, the number of crossings trails off, because the objects disperse and their tracks move apart.

4.3.2.7 Summary

In summary, though our scenarios did not find any even crossings, we found the statistics of odd crossings to depend on the time between ejections and the number of objects ejected in a variety of ways. As expected, time to first crossing, and mean time between crossings decreased as the number of objects ejected increased and as they were ejected more rapidly. Interestingly, increasing the time delay had a much stronger effect when there were more objects ejected. Overall, the frequency of crossings was found to grow linearly over time until all objects have been ejected into a rapidly dispersing cloud. As this cloud disperses the probability of crossings tapers off accordingly. Another interesting result was that increasing the time delay between ejections shifted the distribution of crossing angles toward 90°, where crossings are easier to distinguish.

The model, based on a single scatterer, discrete target ejecting objects which do not affect its own trajectory, is a simplified one. The choices for input parameters including this initial object's velocity, and position, as well as the distribution of ejected target velocities may not reflect reality. Though our simulation yields a very low probability of even crossings, the scenarios which bring about even crossings may be more likely in real life. Despite these limitations, many useful statistics were ascertained about odd crossings.

5   Track Crossing Discrimination

Although starbursts and periodic separations rarely resulted in even crossings on Range Time plots in our simulations, other separating scenarios may result in more frequent even crossings. The probability of successfully identifying individual crossings as even or odd was the second focus of the project. The radar returns were first examined using only Range Time plots. Then we studied the effectiveness of applying statistical tests to these data to estimate whether crossings were even or odd. It was then examined how well Range Doppler could discriminate cases for which Range Time discrimination does not provide a definitive answer. Figure 5.4.3.1 displays how the series of simulations were tested and analyzed. Fifty thousand simulations were generated and evaluated with Range Time tests only, with possible outcomes of either even or odd, in order to analyze how well Range Time discrimination performs on its own. Another 500 simulations were generated and evaluated with Range Time tests, with possible outcomes of even, odd, or uncertain. The uncertain cases were then re-analyzed by Range Doppler tests, with possible outcomes of even, odd, or uncertain.
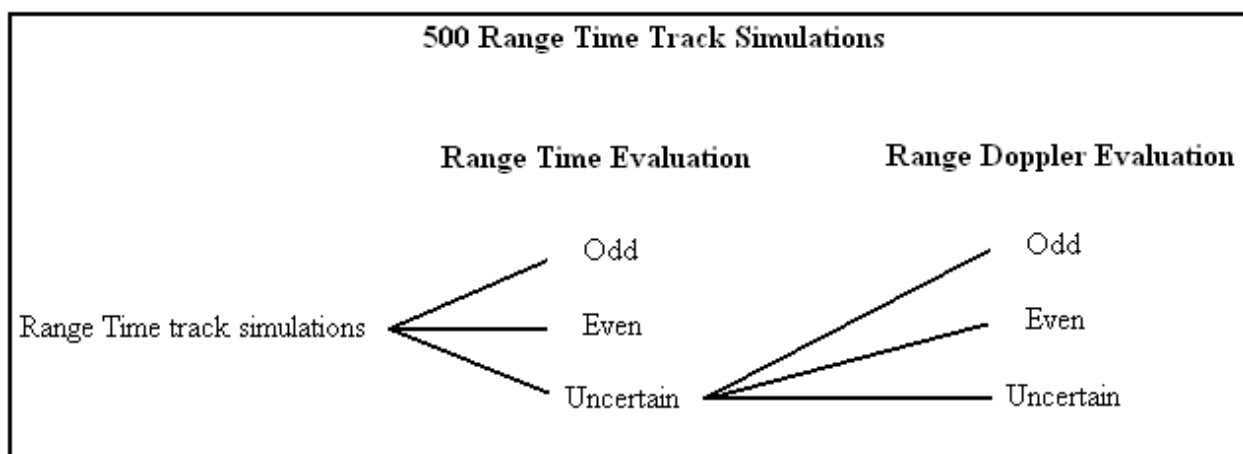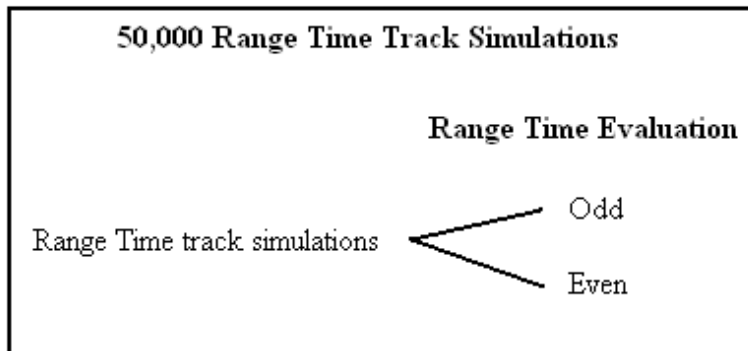
**Figure 5.4.3.1 – A diagram showing the simulations that were run and how they were evaluated.**

5.1 Range Time Plots

5.1.1 Range Time Plots of Point Scatterer Targets

A major challenge with Range Time plots is tracking targets as they approach each other in range. The assumption was made that without measurement error, or noise, the tracks generated by point scatterers' trajectories can be approximated by either lines or parabolas over the short duration of our observation [Weiner, 2008]. Two sets of tracks, without measurement error, are shown in Figure 5.1.1 and Figure 5.1.2, representing the two different types of crossings. Because the pulse repetition frequency is so high, the tracks appear as lines, even though they consist of discrete dots drawn closely together.
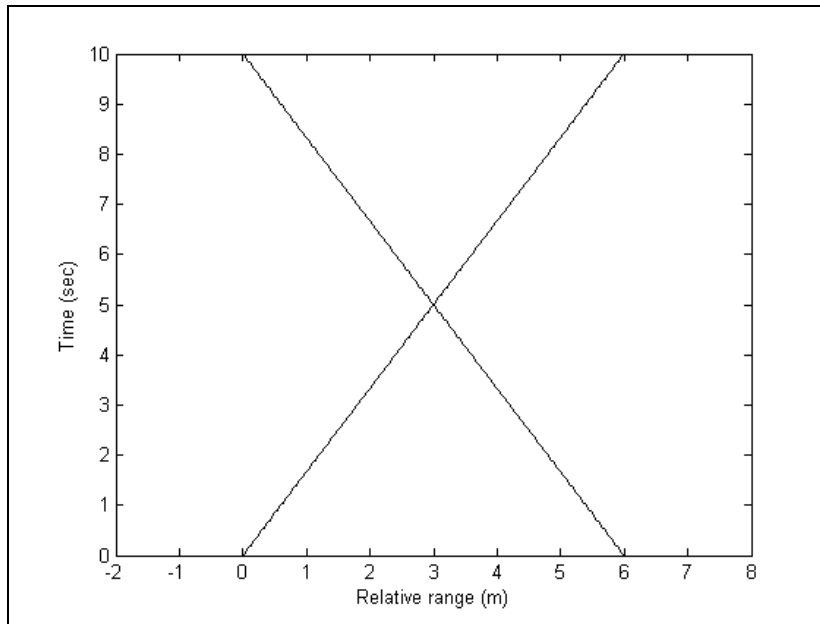
Figure 5.1.1 – A Range Time plot without measurement error of two point scatterer targets whose tracks form an odd crossing by crossing straight through each other.
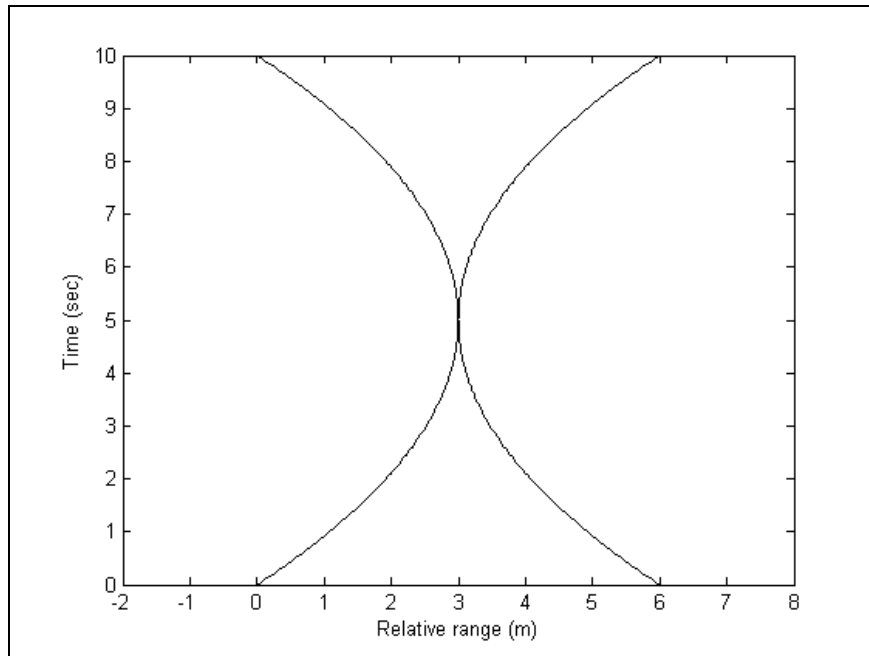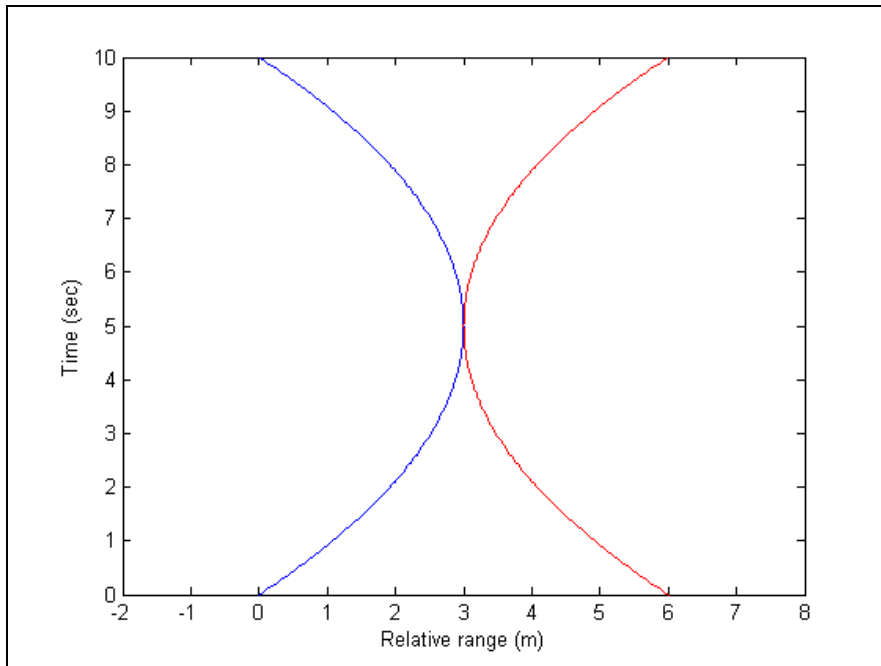

Figure 5.1.2 – A Range Time plot without measurement error of two point scatterer targets whose tracks form an even crossing by becoming very close and then diverging.

From the shape of the tracks, and the assumption that tracks are either lines or parabolas, it is clear that the crossing in Figure 5.1.1 is odd and that the crossing in Figure 5.1.2 is even. With this knowledge, one could color code the tracks of these plots in order to indicate which track is associated with which target, as in Figure 5.1.3 and Figure 5.1.4.
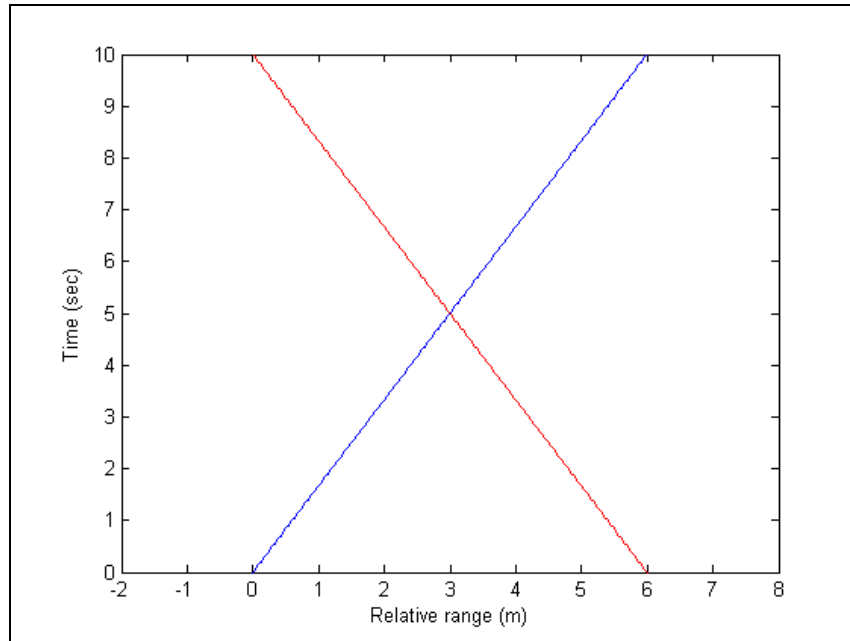
Figure 5.1.3 – A Range Time plot without measurement error of two point scatterer targets, Target A (blue) and Target B (red), whose tracks create an odd cross.

Figure 5.1.4 – A Range Time plot without measurement error of two point scatterer targets, Target A (blue) and Target B (red), whose tracks create an even cross.

Without measurement error, it is trivial to determine which track belongs to which target at every point in time. In reality, though, each measurement of range has error. For time t, denote the range of a target by r_t, the measurement error by e_t, and the measurement by m_t. It is assumed that $m_t = r_t + e_t$, and that each error is from an independent Gaussian distribution with mean zero and variance σ^2. Once noise is added to our model, the plot in Figure 5.1.3 might look like the plot in Figure 5.1.5, and the plot in Figure 5.1.4 might look like the plot in Figure 5.1.6.
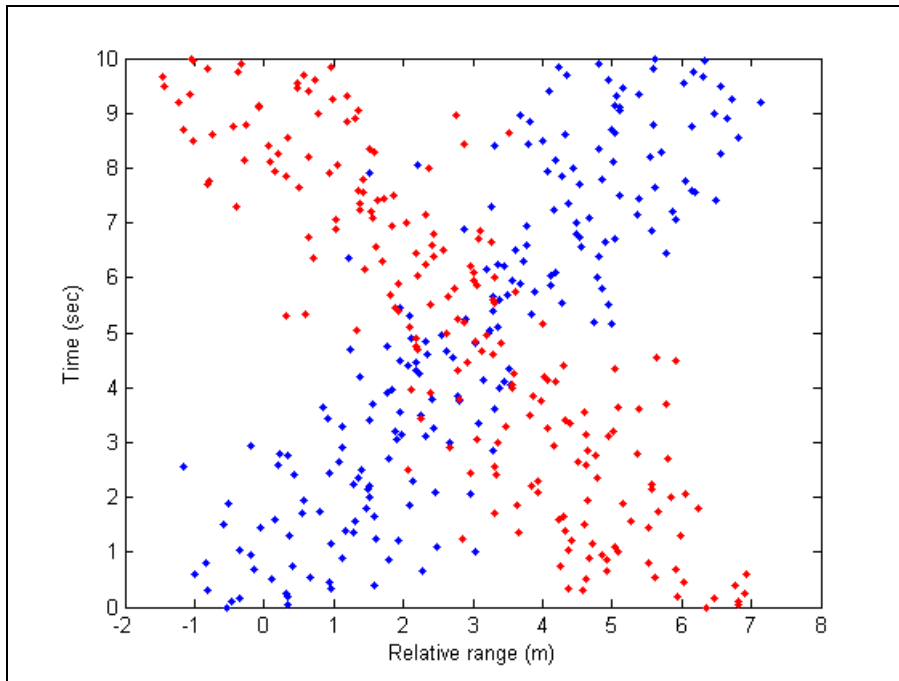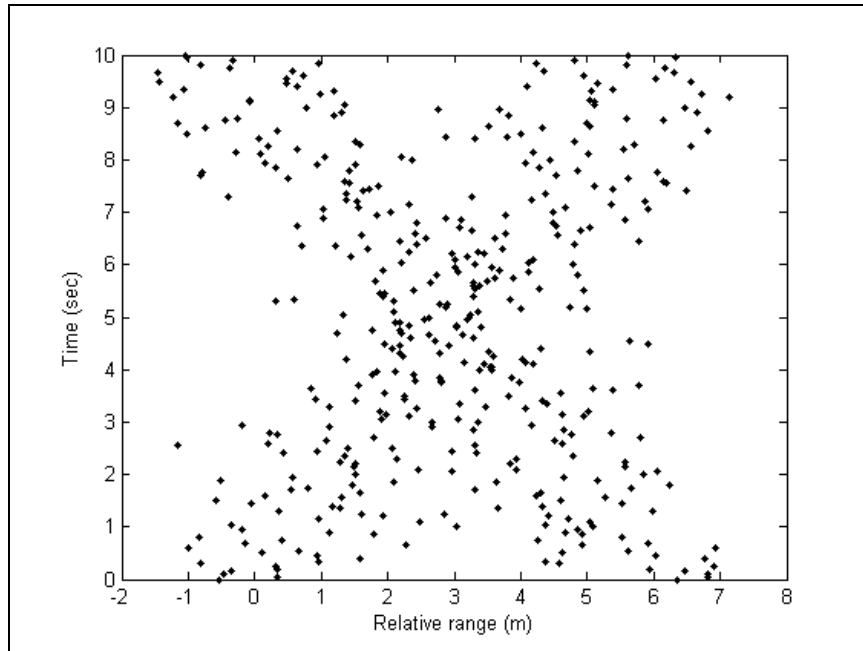
Figure 5.1.5 – A Range Time plot with measurement error of two point scatterer targets, Target A (blue) and Target B (red), whose tracks create an odd cross.
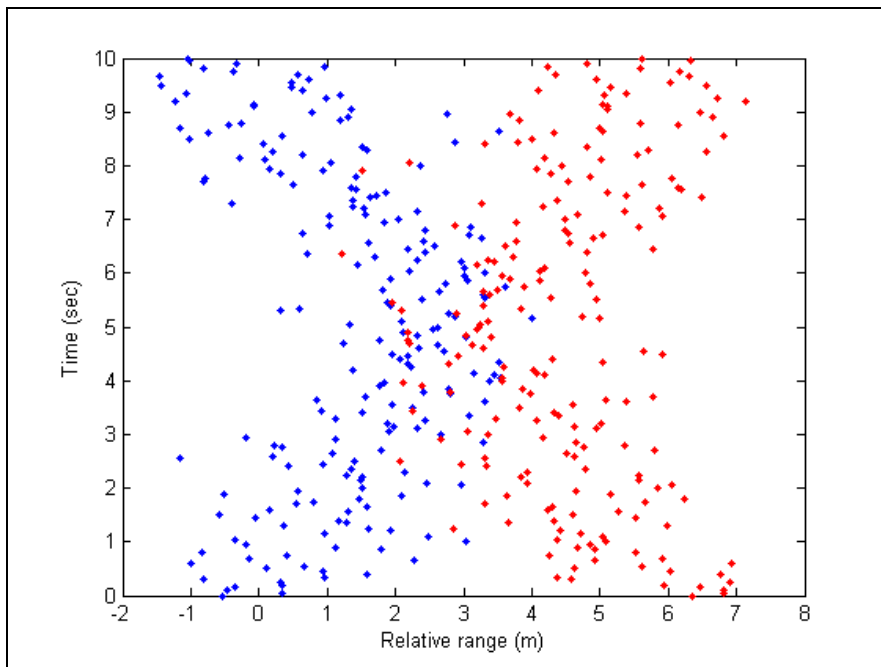
Figure 5.1.6 – A Range Time plot with measurement error of two point scatterer targets, Target A (blue) and Target B (red), whose tracks create an even cross.

If the points in the previous two figures are not color coded, one would see a plot like that in Figure 5.1.7.


Figure 5.1.7 – A Range Time plot with measurement error of two point scatterer targets, Target A and Target B, whose tracks could create either an odd or an even cross

Given only the data in this plot, as is the case for actual radar data, it is not immediately obvious whether the crossing is even or odd. Thus, when radar measurement error is factored in, it is no longer a trivial task to determine whether a given crossing is even or odd.

5.1.2 Testing Point Scatterers' Tracks for Curvature

Because of this measurement noise, it is sometimes unclear which track belongs to which target after the crossing. To determine whether the crossing is even or odd, a method for estimating whether the tracks before the crossing are linear or curved was developed. Over short periods of time, linear tracks usually lead to odd crossings, and curved tracks usually lead to even crossings [Weiner 2008]. Thus, a test was constructed to evaluate the curvature of the

tracks. The crossings of tracks that were significantly linear were estimated to be odd, and the crossings of tracks that were significantly curved were estimated to be even. Figure 5.1.8 illustrates a Range Time plot in which two curved tracks meet at $t = t_{cross}$. With measurement error, a situation similar to Figure 5.1.8 might result from two odd crossings that are close in time and range. The values m_0, $m_{tcross/2}$, and m_{tcross} denote the measurements of range at times $t = 0$, tcross/2, and tcross, respectively.
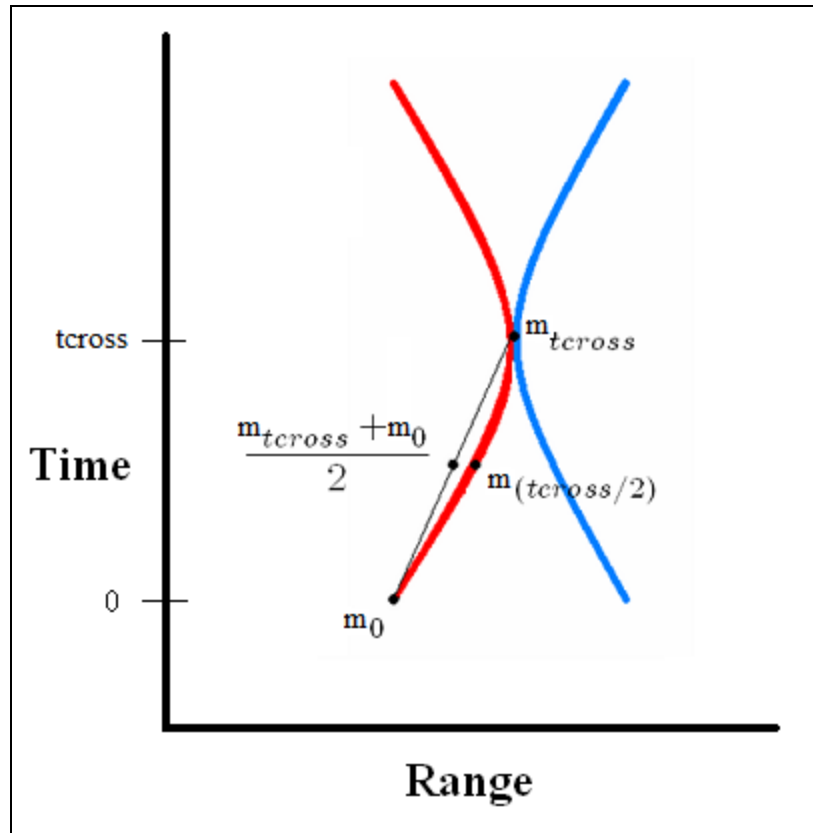
Figure 5.1.8 – A Range Time plot in which two curved tracks meet at time tcross.

In order to estimate whether a single track was curved or linear, it was established whether the mean of m_0 and m_{tcross} was significantly different from $m_{tcross/2}$. If the track were linear and the cross odd, then m_0, $m_{tcross/2}$, and m_{tcross} would all lie on a line, and the mean of m_0 and m_{tcross} would equal to $m_{tcross/2}$. But if $m_{tcross/2}$ is significantly different from the mean of m_0 and m_{tcross}, then it is likely that the track is not linear, and that the cross could be even.

The measurement error's variance, σ^2, was assumed to be known. Then, the average of m_0 and m_{tcross} denoted by $\overline{m}$, has a variance of $\sigma^2/2$. Additionally, $m_{tcross/2}$ has variance σ^2.

Because $\bar{m}$ and $m_{tcross/2}$ are independent, the variance of $\bar{m}$ - $m_{tcross/2}$ is $\sigma^2/2 + \sigma^2$. Then,

$\dfrac{\bar{m} - m_{tcross/2}}{\sigma\sqrt{1/2+1}}$ follows a standard normal distribution if there was no curvature in the track. This

information allowed us to reject the null hypothesis that $\bar{m} - m_{tcross/2} = 0$, that is, that the track

was linear. If the value of $\dfrac{\bar{m} - m_{tcross/2}}{\sigma\sqrt{1/2+1}}$ was greater than 1.65, then the track was estimated to be

curved. Otherwise, it was estimated to be linear. The pre-crossing portions of both tracks were subjected to this test, and if both were not curved, the crossing was identified as odd. If either one was determined to be curved, then the crossing was identified as even.

5.1.3 Range Time Plots of Dumbbell Targets

When this model was extended to include dumbbell targets instead of single point scatterers, the tumbling of the targets created helixes in three-dimensional space. One end of the dumbbell tumbles around the other, as would occur with the target's center of gravity located at the stationary end, while the end that does not tumble travels at a constant velocity. These trajectories, when mapped onto two-dimensional Range Time plots without measurement error, result in plots similar to those in Figure 5.1.9 and Figure 5.1.10.
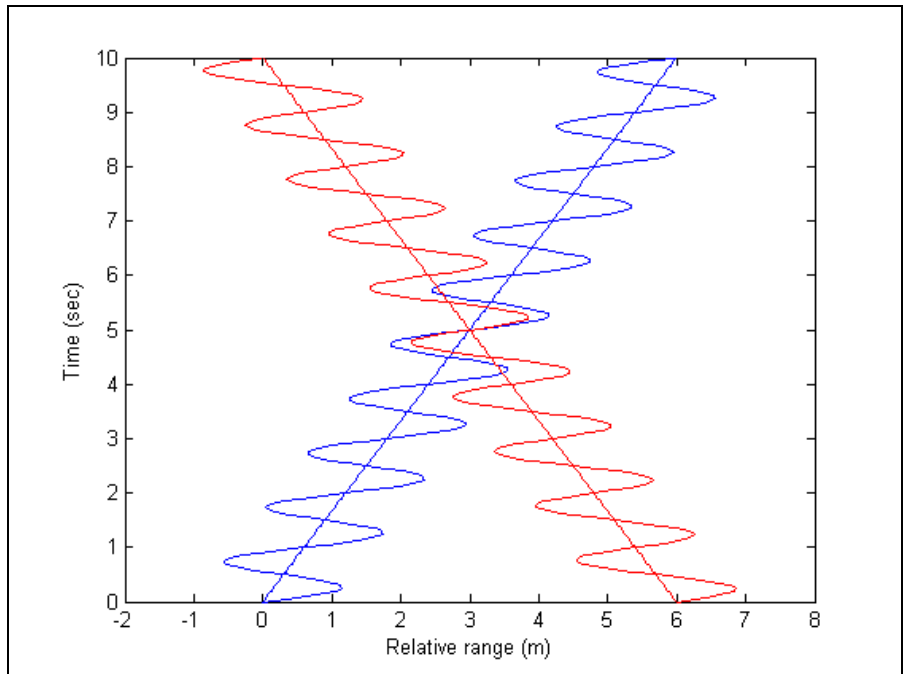
Figure 5.1.9 – A Range Time plot without measurement error of two dumbbell targets, Target A (blue) and Target B (red), whose tracks create an odd cross.
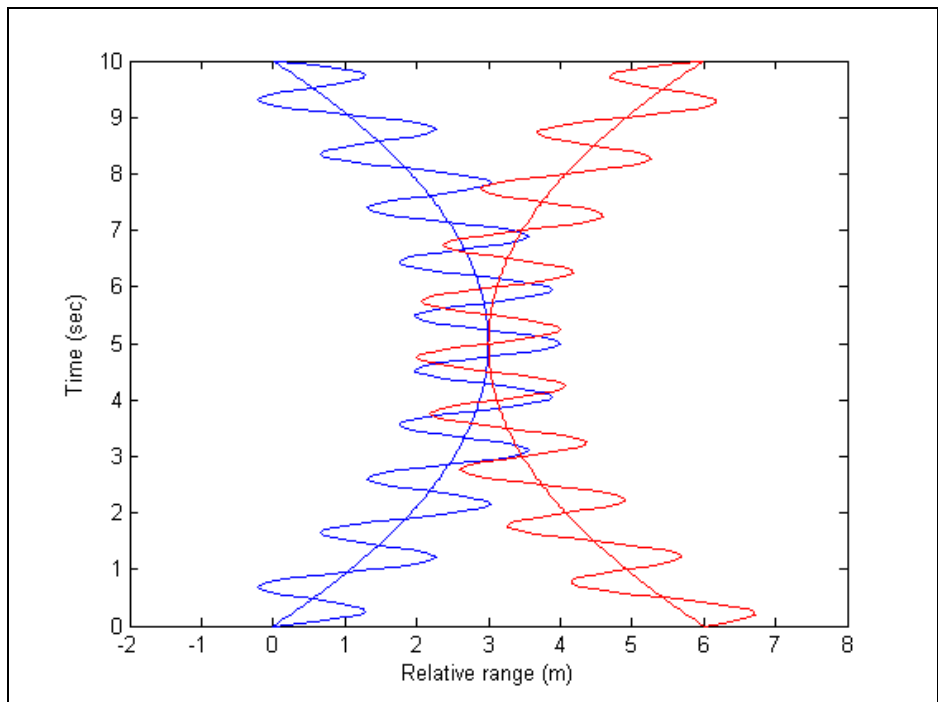

Figure 5.1.10 – A Range Time plot without measurement error of two dumbbell targets, Target A (blue) and Target B (red), whose tracks create an even cross.

Notice that the tracks are approximately sine waves added to either a parabola or a line, from the tumbling end, and a line or parabola drawn through the sine wave, from the non-tumbling end. But again, because of measurement error, the type of crossing may not be immediately clear, without the a priori knowledge of the coloring of the tracks shown in the figure.

### 5.1.4 Testing Tracks of Dumbbell Targets for Curvature

Figure 5.1.11 shows the portion of a track of a dumbbell target before a cross with another target's track. Once again, to estimate whether the crossing is even or odd, it must be estimated whether the track is linear or curved. If the crossing is even, the peaks and troughs of the oscillations should roughly form a parabola. If the crossing is odd, the peaks and troughs of the oscillations should roughly form a line. The following section describes the technique used for finding these peaks and troughs.
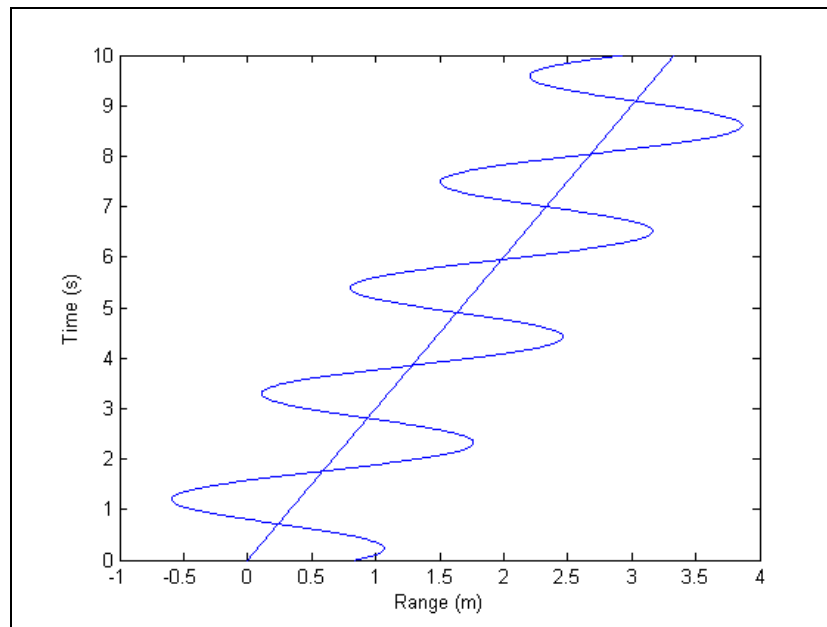
Figure 5.1.11 – The portion of a track of a dumbbell target before a cross with another target's track.

The same test that was used for point scatterers was used again to make an initial rough estimate of whether the tracks are linear or curved. This initial estimate was used to decide whether a line, if the tracks were roughly linear, or a quadratic, if the tracks are roughly curved,

should be interpolated through the data. If this line or quadratic is subtracted from the data, roughly a sine wave and the straight line at range = 0 should remain, as in Figure 5.1.12.
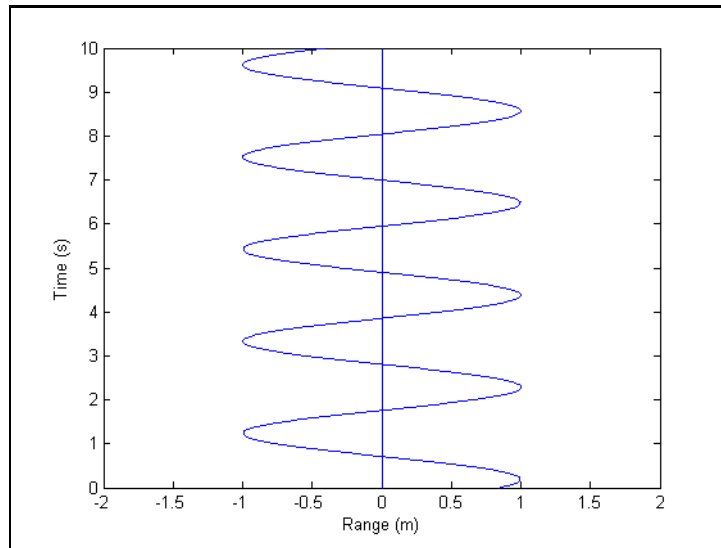
Figure 5.1.12 – The portion of a track of a dumbbell target, minus an interpolated line through the track.

The frequency and period of tumble was estimated with a plot of the Fourier transform of the adjusted data from a Range Time plot's track, with range and time as the dependent and independent variables, respectively. The spectral representation which arises from the Fourier transform of the signal was used to identify the spectral peak of the signal which signified the frequency of the target's oscillation. After this period was determined, the Range Time plot's time axis was divided into vertical pieces, each with the length of the estimated period, as shown in Figure 5.1.13.
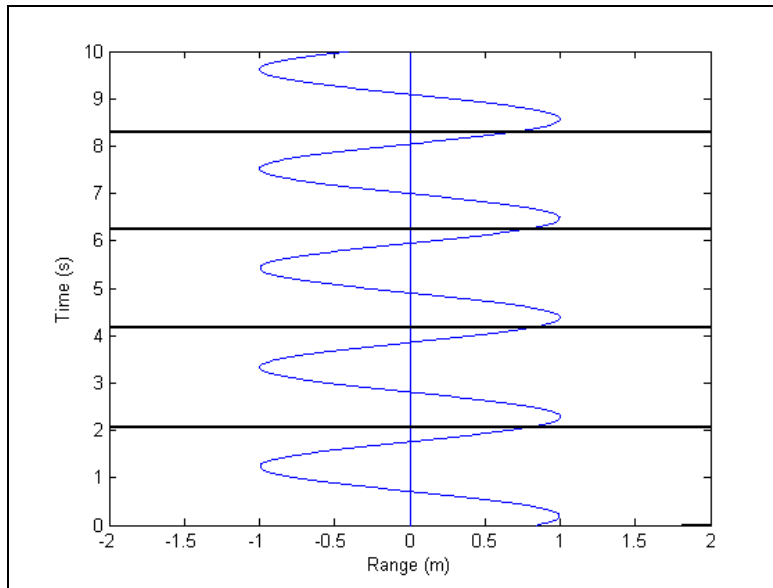
Figure 5.1.13 – The portion of a track caused by a dumbbell target, minus an interpolated line through the track, with the time axis divided into portions each the length of the estimated period of oscillation.

In each segment of the graph, the minimum range and maximum range should correspond to the peak and trough of the sine wave, as in Figure 5.1.14.
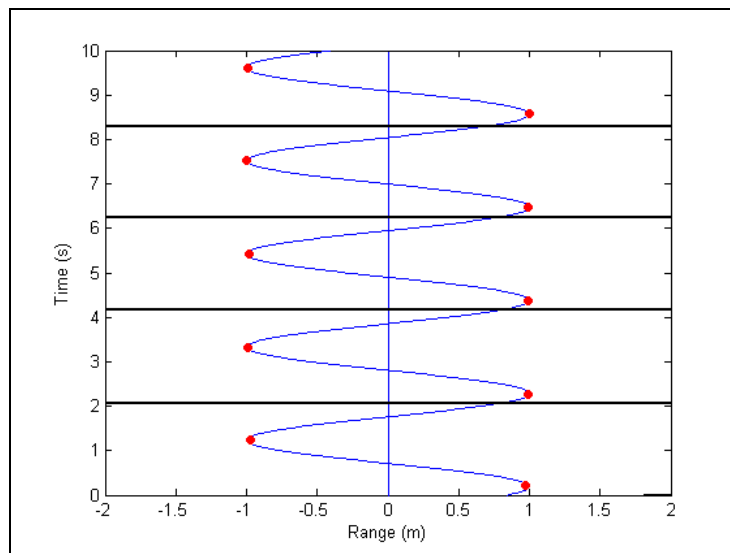
Figure 5.1.14 – The portion of a track of a dumbbell target, minus an interpolated line through the track, with the time axis divided into portions each the length of the estimated period of oscillation and containing a local minimum and maximum.

The times at which these extrema occurred were recorded, and the corresponding ranges were found on the original Range Time plot, as demonstrated in Figure 5.1.15.
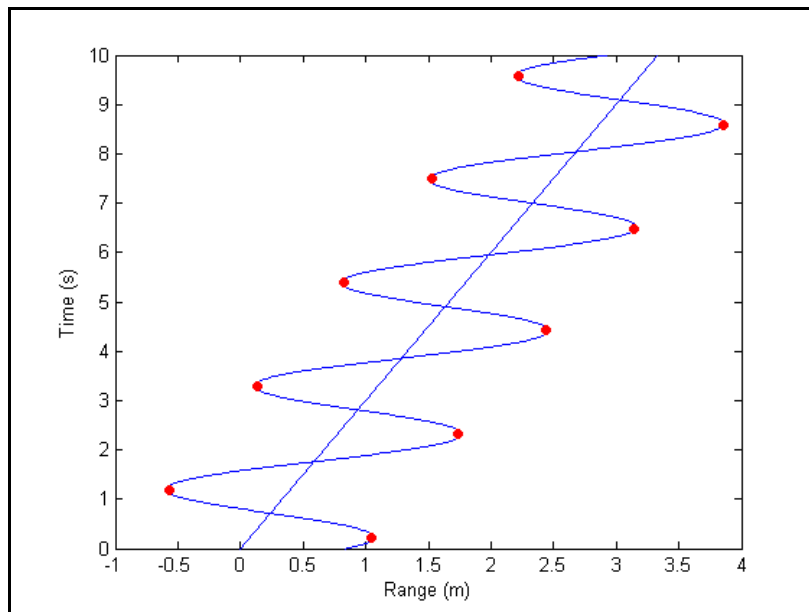
Figure 5.1.15 – The portion of a track of a dumbbell target in blue, with the estimated peaks and troughs in red.

If these points roughly formed a line, the crossing was identified as odd. Similarly, if these points formed a curve, the crossing was declared even. If there were at least three of each, the points representing the minimum ranges and the points representing the maximum ranges were tested for curvature and linearity. The test used the minima from the leftmost track and the maxima from the rightmost track. If either of the tracks was determined to be curved, the crossing was declared even.

When there were fewer than three extrema to test, the last resort was to average the measurements of the two scatterers from the first target at each time before the crossing. The same was done for the two scatterers from the second target. These averages were treated as the measurement of a point scatterer, and subjected to the previously described test for curvature of tracks for point scatterers.

5.1.5 Generating Simulations

To generate simulated Range Time plots of the dumbbell-shaped targets, several parameters were considered, namely: the amount of time tracked, the angle between the crossing tracks, the targets' rate of tumble and angle between the radar line of sight (RLOS) and the targets' z-inertial axis. It was assumed that without measurement error, Range Time plots look similar to either Figure 5.1.9 or Figure 5.1.10. It was also assumed that the variance of measurement error is 0.1 m^2, that the prf is 100 Hz, and that each target's body length is 2 m. The target's rate of tumble determines the frequency of the sine wave. The angle between the RLOS and targets' z-inertial axes was used to approximate the amplitude of the sine wave with the formula:

Amplitude = Target body length * cos(RLOS-z-inertial angle)

When the radar was facing the same direction as the target's velocity, none of the tumble is in the direction of the radar, and the amplitude of the oscillation is zero. When the RLOS was perpendicular to the target's z-inertial axis, all of the oscillation from the tumble was either towards or away from the radar, and the amplitude of the oscillation was at a maximum.

For each of the parameters, there was a distribution of values from which independent random values were selected to generate simulations. The following distributions for the parameters were used, where U(a,b) denotes a uniform distribution of values between a and b:

Time (sec): U(5,25)
Crossing Angle (deg): U(0,67.5)
Rate of tumble (Hz): U(0.01, 0.33)
RLOS-z-inertial angle (rad): U(0, 2π)

Fifty thousand tests were run to determine how well Range Time discrimination performs on its own. Another five hundred simulations and tests were run to determine what combinations of these parameters give poor probabilities of successfully determining whether the crossings are even or odd when used in combination with Range Doppler discrimination.

5.1.6 Passing cases to Range Doppler Discrimination

Every simulation was analyzed through Range Time discrimination. As a test of curvature, the value of $\dfrac{\overline{m} - m_{tcross/2}}{\sigma\sqrt{1/2+1}}$ for each track wascalculated, for each track before the crossing. For each simulation, if either of these two values fell between -0.5 and 1.7, Range Time discrimination was deemed inconclusive. Range Time discrimination used in this way was most effective for identifying crossings that are obviously even. When this threshold was used, only about 2% of the simulations were incorrectly identified as odd or even. The threshold was selected to be wide enough to contain almost all incorrect identifications, so that very little incorrect identifications "leaked" through. The simulations that fell within this threshold were then forwarded to Range Doppler discrimination to be re-analyzed. The simulations that fell outside this threshold were said to be "certain," and the identification that the Range Time test produced was used.

5.2 Range Doppler Methodology

Similar to the Range Time algorithm that tested for curvature to classify a single crossing, the purpose of the Range Doppler tracking experiment was to test the ability to classify a single crossing by means of human-in-the-loop discrimination. A Range Doppler target tracking simulation was used to increase the probability of correctly tracking multiple targets whose tracks formed either an even or odd crossing on a Range Time plot. Range Doppler plots were created and visually discriminated in a blinded test to decide which of the two situations was occurring. The motivating hypothesis was that target tracks that had an ambiguous crossing on a Range Time plot may be discernable when viewed on a Range Doppler plot, thus resulting in an increased probability of correct track association through the crossing. The difference in plots was due to the different observables used to plot radar representations.

The quality of Range Doppler tracking was tested and evaluated using a Monte Carlo simulation. The targets, which were modeled as cones, each consisted of two scatterers, one on the base and one at the tip, as shown in Figure 5.2.1. Each scenario used data generated for both scatterers on each conic target. The targets in the Range Doppler tracking were simulated as such in order to incorporate the spin of a three dimensional body into the model, because spin has a large effect on a target's Doppler spectrum. The distance that separates the base scatterer from

the centroid, about which the body spins, causes the scatterer's radial velocity and Doppler frequency to modulate. The scatterers were simulated as discrete points without shadowing.

Parameters for the angles of precession θ, rates of precession ω_p, velocities and ranges of the targets were taken from ballistic scenarios which led to uncertain results from Range Time discrimination. Three unique rates of spin, 0 Hz, 0.5Hz, and 1Hz were used to analyze this parameter's effect on Range Doppler discrimination. An upper bound of 1 Hz spin was set because this rate of spin was used in the Firefly Experiments [Schultz et al., 1993], actual Doppler identification experiments done by Lincoln Laboratory.
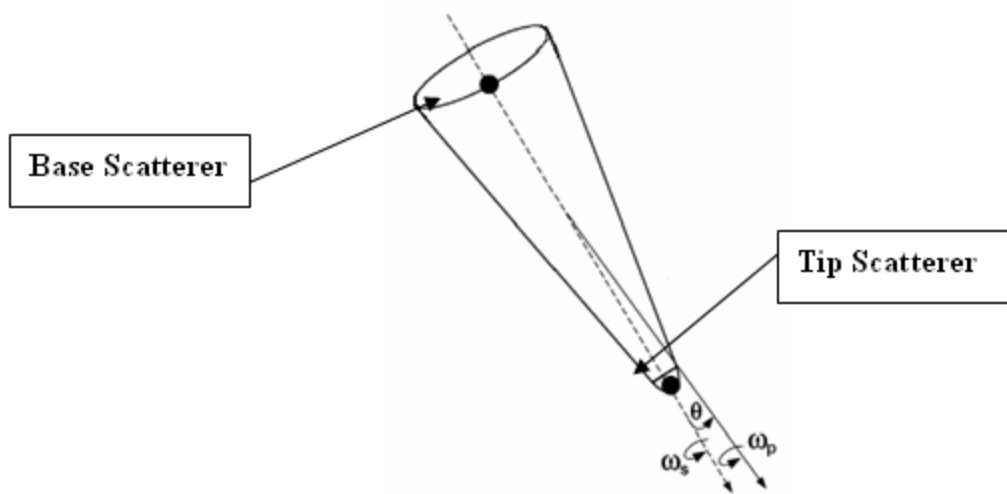

Figure 5.2.1 - Conical target identifying the two scatterers, angle of precession θ, rate of precession ωp, and rate of spin ωs.

The simulation generated and stored the location of each scatterer as a function of time. Once all the positions of scatterers were stored, they were plotted in chronological order, for both targets, on a Range Doppler plot. The program calculated the range from the origin of the radar and target velocity based on the range rate of the target. In these measurements the theoretical usage of the Doppler frequency shift was paramount; using Doppler shift meant a measurement error with a standard deviation on the scale of 10's of cm/s was used as opposed to an order of m/s which would have accompanied a range rate based calculation. Measurement error was simulated by adding this uncorrelated Gaussian noise to both the range and radial velocity measurements.

The noisy tracks were plotted for the two targets and then subjected to blinded visual discrimination. After the operator observed real time movies of the tracking scenarios, he noted that the ability to classify the crossing scenario did not degrade when the data was viewed as a single plot These singular Range Doppler outputs plotted the targets' tracks in their entirety over the observation time interval in one frame, similar to the Doppler plots presented later in Figure 5.2.6.

Much of the foundation for the visual track association was in the physical principles due to the ballistic trajectory of the objects being viewed. Two specific cases, even and odd crossings, were passed to the Range Doppler plotting simulation for evaluation. The goal was to see if the two unique physical situations could be identified by the limitations placed on them by physics. One case was when the targets' tracks on a Range Time plot were parabolic, coming very close and then diverging. An example of such an even crossing is shown in Figure 5.2.2a along with the Range Doppler representation in Figure 5.2.2b of such a situation.
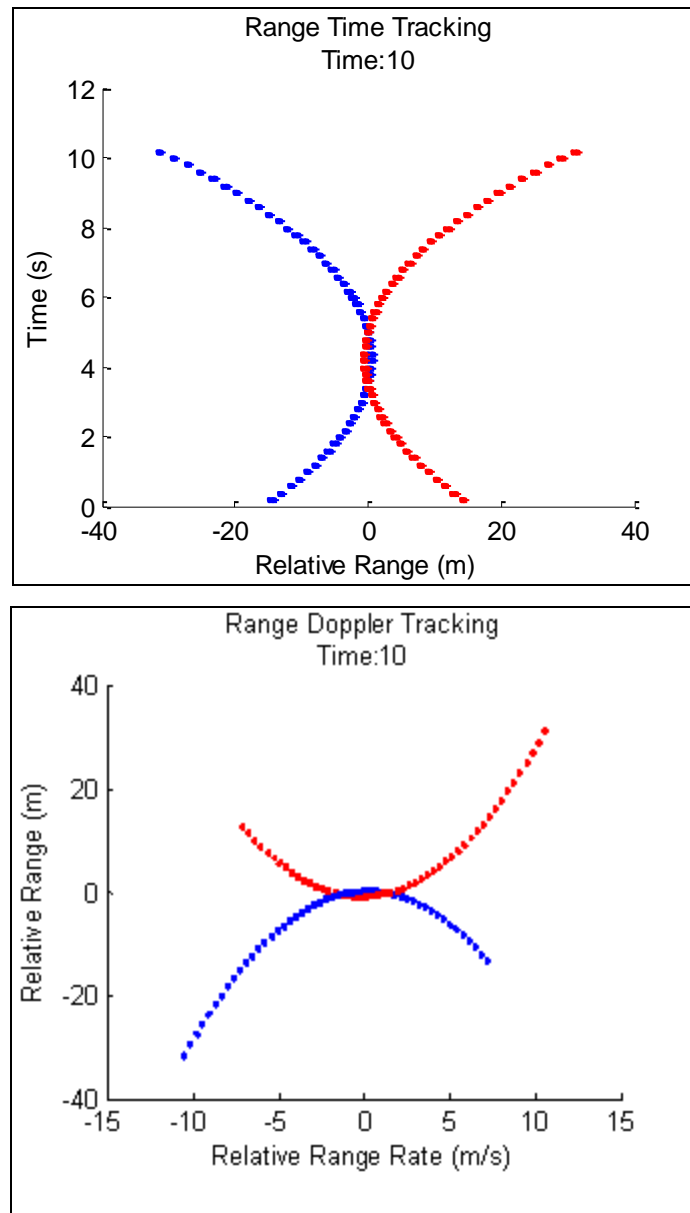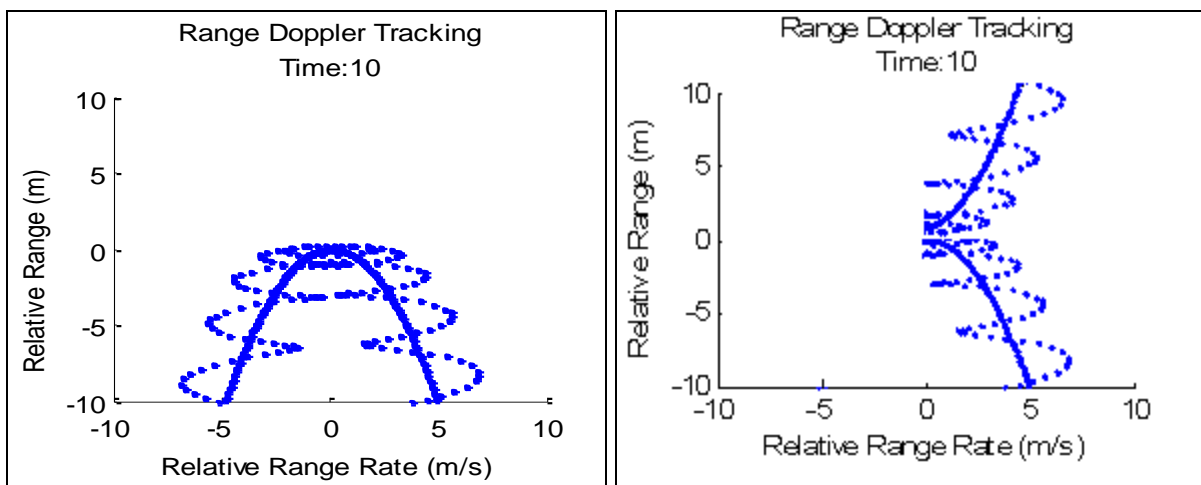
Figure 5.2.2

a.) (top) – Parabolic Range Time plot, red track is for first target, blue track is for second target, scatterers are not subject to precession or spin for clarity.

b.) (bottom) - The equivalent Range Doppler representation for Figure A, red track is for first target, blue track is for second target, scatterers are not subject to precession or spin for clarity (blue target moves from right to left, red target moves from left to right).

As before, the representations in Figure 5.2.2 are idealizations; the simulated radar data was not color coded and much noisier than the tracks shown. The Range Doppler plot illustrated

by Figure 5.2.2 could only represent an even cross which, for whatever reason, might not have been evident on a Range Time plot. Consider just the blue track which has been isolated and shown again, with spin this time, on a Range Doppler plot in Figure 5.2.3a. Here, as the track approaches a zero Doppler frequency shift, from either direction, the approach represents a slowing of the target's relative velocity towards or from the radar. Because the trajectories being modeled are of objects moving at constant velocities through space, there was only one possible outcome of this slowing: a continuation through the zero Doppler frequency shift accompanied by a symmetrical reversal of the velocity. Only a linear trajectory with a sharp deviation could have allowed anything else, such as the plot on the right in Figure 5.2.3

Figure 5.2.3

a.) (left) - A possible Range Doppler of a target with a linear trajectory in the project, the oscillating line was the base scatterer, subject to a spin, and the stationary line was the tip scatterer, not subjected to precession.

b.) (right) - An impossible representation of a linear trajectory (on right), though a similar graph could be attained due to precession of the tip of the cone.

A simplified example that could lead to the plot in 5.2.3a is shown in Figure 5.2.4 with the corresponding Range Doppler plot in 5.2.4b. The plot on the left is a two dimensional depiction with the actual target track in red and the radar symbol representing the location of the radar. Three points in time are illustrated in both plots: t1 when the target has a positive range rate and is approaching the radar, t2 when the target is moving parallel to the radar and has a zero range rate, and t3 when the target has a negative range rate and is receding from the radar.
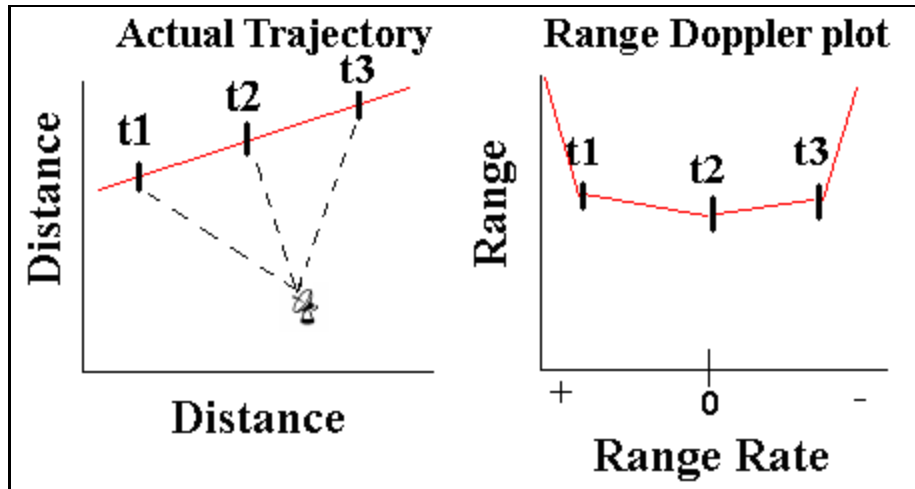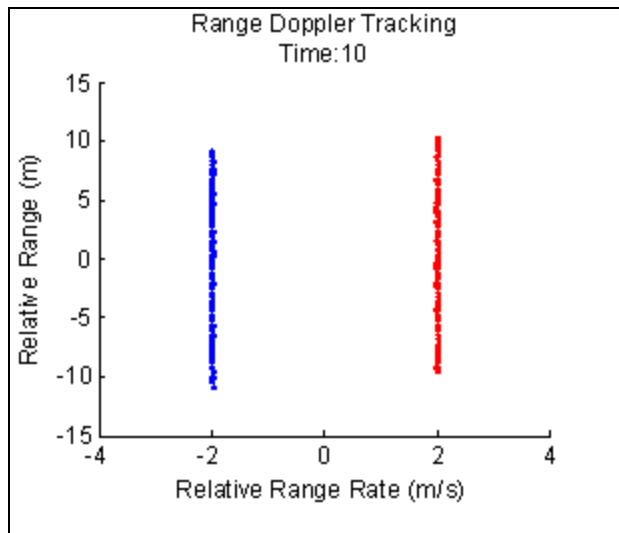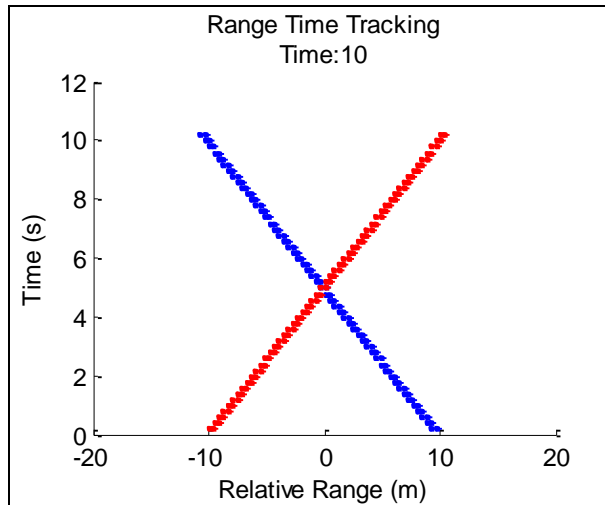
Figure 5.2.4

a.) (left) - Two dimensional plot of a continuous target track from a target moving past a radar, sampled at three discrete times t1, t2 and t3.

b.) (right) - The corresponding Range Doppler plot for a.

Figure 5.2.4 shows an idealized target represented as a single scatterer, with a continuous track. The addition of multiple scatterers, noise, and precession characteristics all sampled at discrete times would complicate the simulated Range Doppler plots.

A second situation which was evaluated was an odd cross of two targets' tracks on a Range Time plot. In this case their tracks were separated in a Range Doppler plot by a Doppler frequency proportional to the difference in their relative velocities.
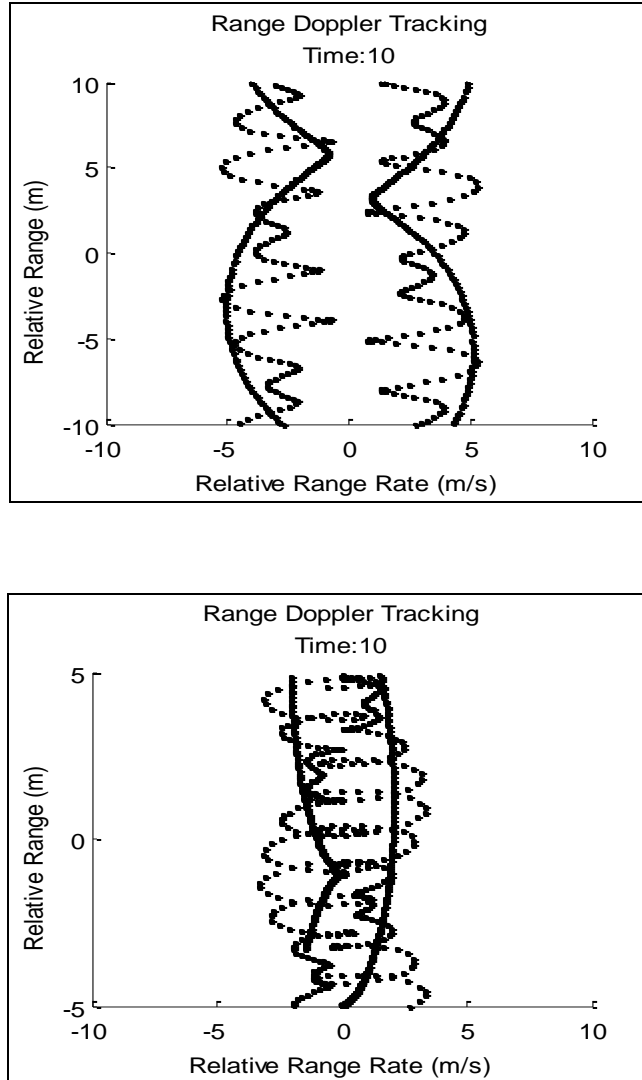
Figure 5.2.5

a.) (top) - A track crossing on a Range Time plot, red track is for first target, blue track is for second target.

b.) (bottom) - The corresponding Range Doppler plot for a.), red track is for first target, blue track is for second target (blue target is moving down, red target moving up).

As with the first case examined, the ability to correctly associate target tracks was subject to precession dynamics, multiple scatterers and noise which created a more diffuse track. The magnitude of the difference between the relative velocities of the targets also governed the probability of track association. Two targets closely aligned in relative velocity were drawn close

on a Range Doppler plot making them indistinguishable, while targets with very different relative velocities were drawn far apart and become easily discernable.
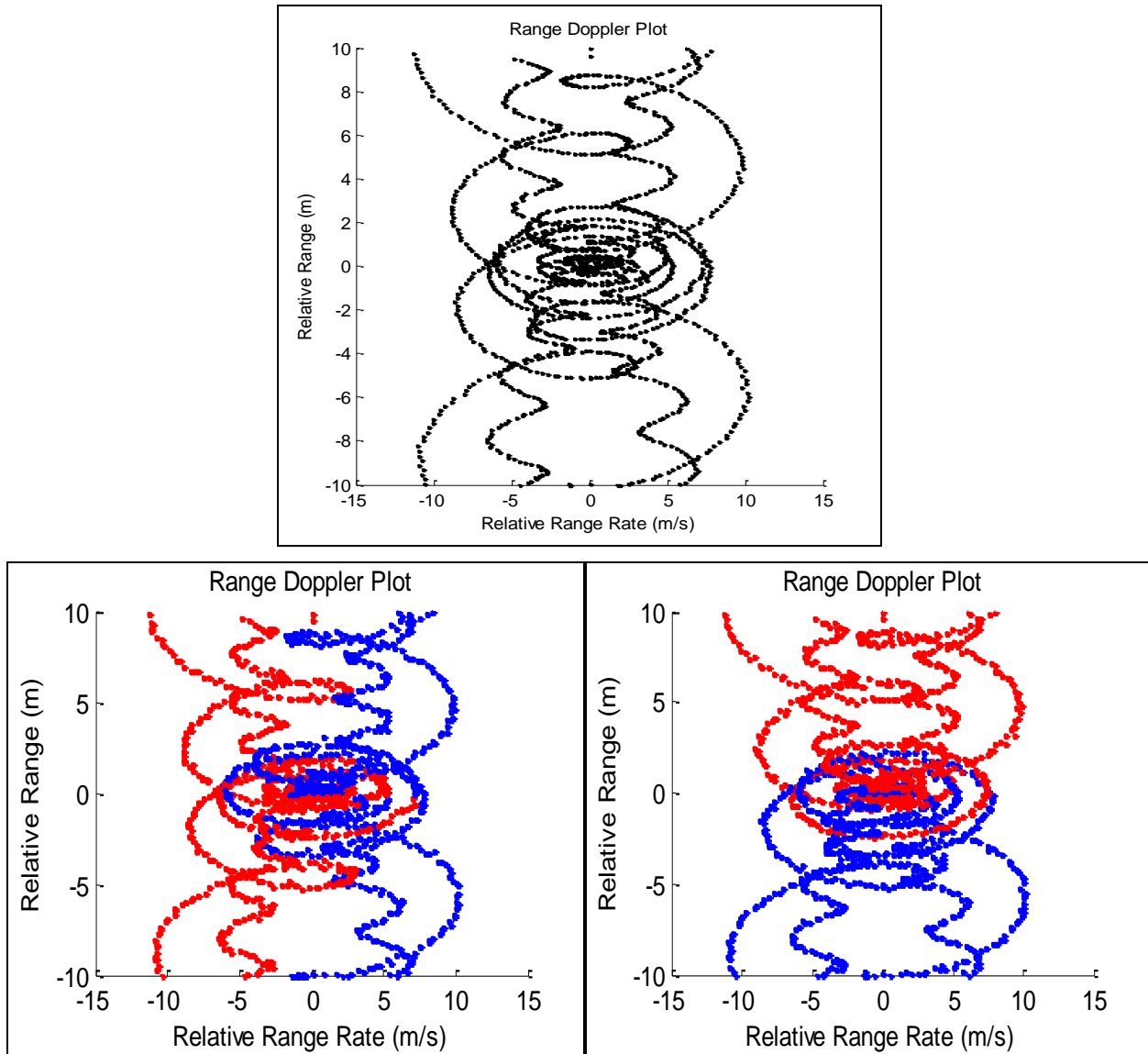

Figure 5.2.6

a.) (top) - Range Doppler plot of two target tracks, distinguishable because of their difference in velocities is significant.

b.) (bottom) - Range Doppler plot of two target tracks, indistinguishable because their difference in velocities is not significant.

In some cases it was impossible to decipher which of the two cases, shown in Figure 5.2.7b and Figure 5.2.7c, actually occurred, resulting in a loss of correct target track association.

Keep in mind that the two colored track options which uniquely identify individual tracks were not available for comparison in the simulated plots, only the single color as shown in Figure 5.2.7a.
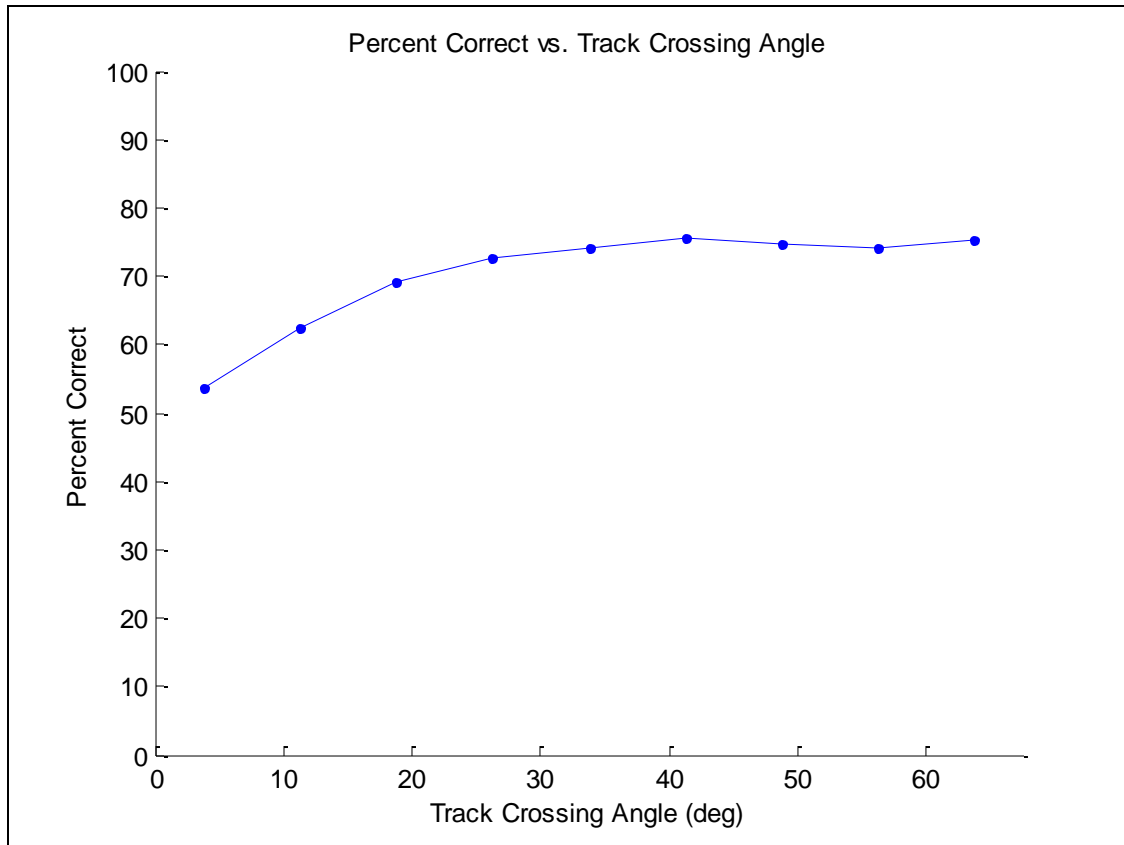

Figure 5.2.7

a.) (top) - A Range Doppler plot of two target tracks either crossing in range or nearly doing so along a parabolic path.

b.)(bottom left) - Figure A with the two tracks colored in a manner which represents two targets' tracks crossing in range.

c.)(bottom right) - Figure A with the two tracks colored in a manner which represents two targets approaching then diverging along parabolic tracks.

The pivotal concept of the plot is that when tracking began, the a priori information about target trajectory was not known; it was only used to generate the simulated measurements. It was unknown which of the two previously described cases was being illustrated in the plot; therefore for this method to be useful it must have been clear in the Range Doppler plot which situation occurred. The purpose of the simulation is to find the probability that the correct situation can be identified.

The operator making the blinded assignment gave one of three responses for each scenario that was plotted. One response from the operator was "uncertain," which meant there was not enough information contained within the Range Doppler plot to determine, with certainty, whether the crossing was even or odd. The Range Doppler plot could also be classified as either even or odd, depending on the operator's conclusion about the type of crossing first seen on the Range Time plot. The "uncertain" cases could be subjected to further discrimination in reality, so the focus was on whether or not the even or odd classification was correct. After all situations were assessed, the operator's responses were checked against the actual situation. Whether they were incorrect or correct was recorded to be examined later, to look for a dependence of correctness on specific parameters.

5.3 Range Time Results

Fifty thousand of the previously described simulations of Range Time plots were generated and tested. Two outcomes of each test were possible: even or odd. Figure 5.3.1 shows the percent of these 50,000 simulations that were correct with track crossing angles across the previously described range with intervals 7.5 degrees wide.
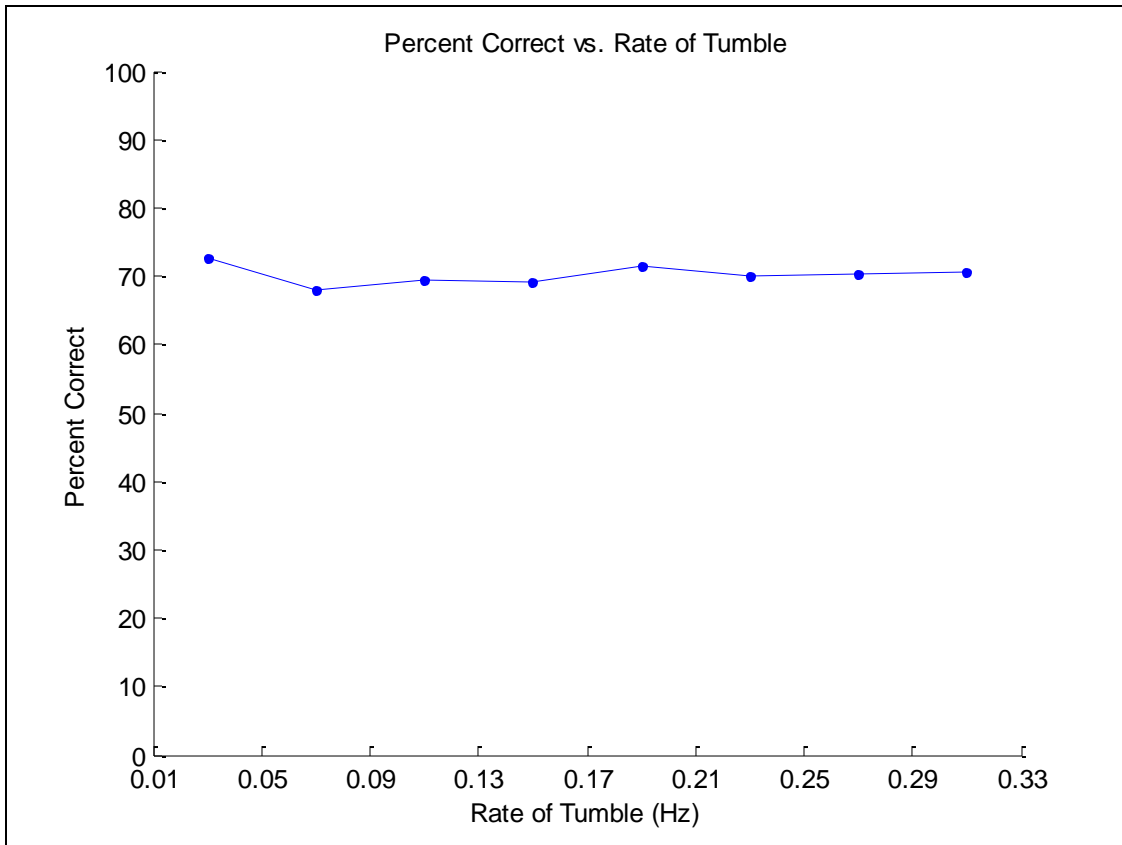
Figure 5.3.1 - From 50,000 simulations, the percentage of simulations that tests (with the possible outcomes of either odd or even) correctly identified vs. track crossing angle.

Figure 5.3.2 displays the percent of these 50,000 simulations that were correct with amounts of track time between five and six seconds, six and seven seconds, seven and eight seconds, etc.
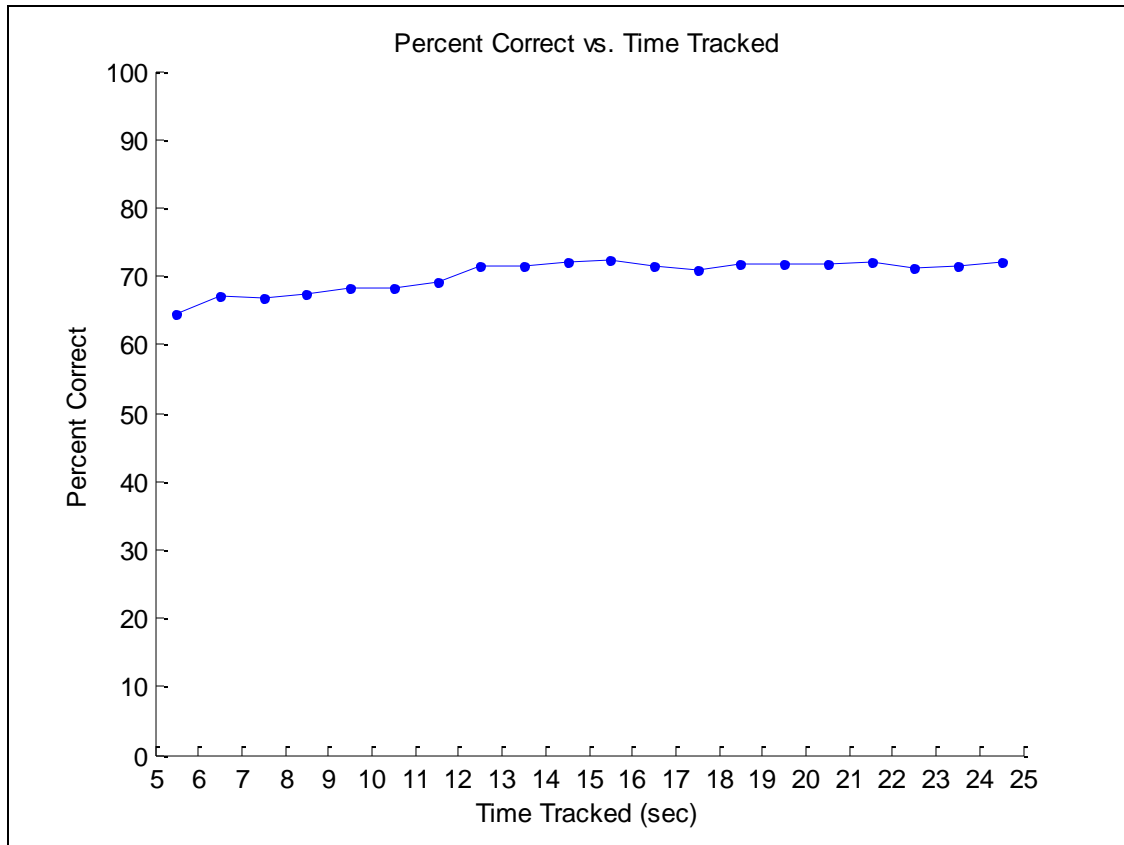
Figure 5.3.2 – From 50,000 simulations, the percentage of simulations that tests (with the possible outcomes of either odd or even) correctly identified vs. amount of time the targets were tracked.

Figure 5.3.3 displays the percent of these 50,000 simulations that were correct with rates of tumble between 0.01 and 0.05 Hz, 0.05 and 0.09 Hz, 0.09 and 0.13 Hz, etc.

Figure 5.3.3 – From 50,000 simulations, the percentage of simulations that tests (with the possible outcomes of either odd or even) correctly identified vs. rate of tumble.

Figure 5.3.4 displays the percent of these 50,000 simulations that were correct with angles between RLOS and z-inertial axes between 0 and 60 degrees, 60 and 120 degrees, 120 and 180 degrees, etc.
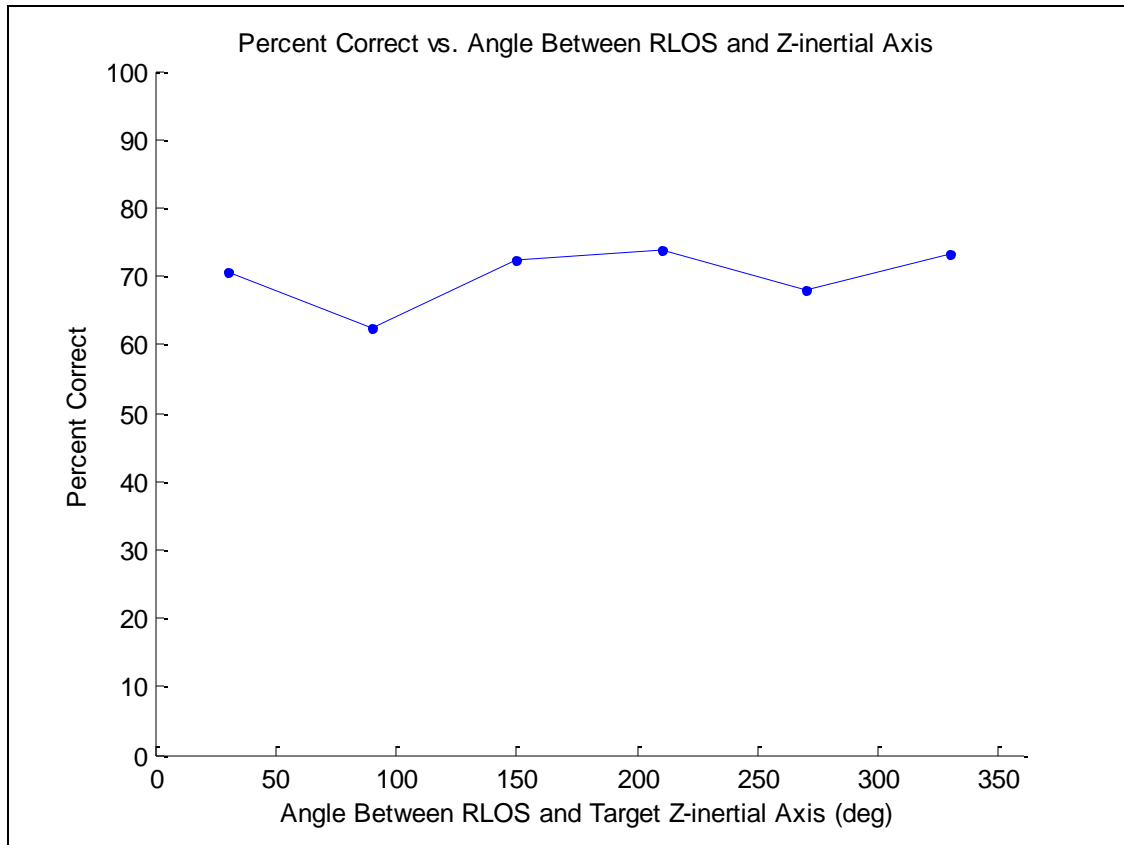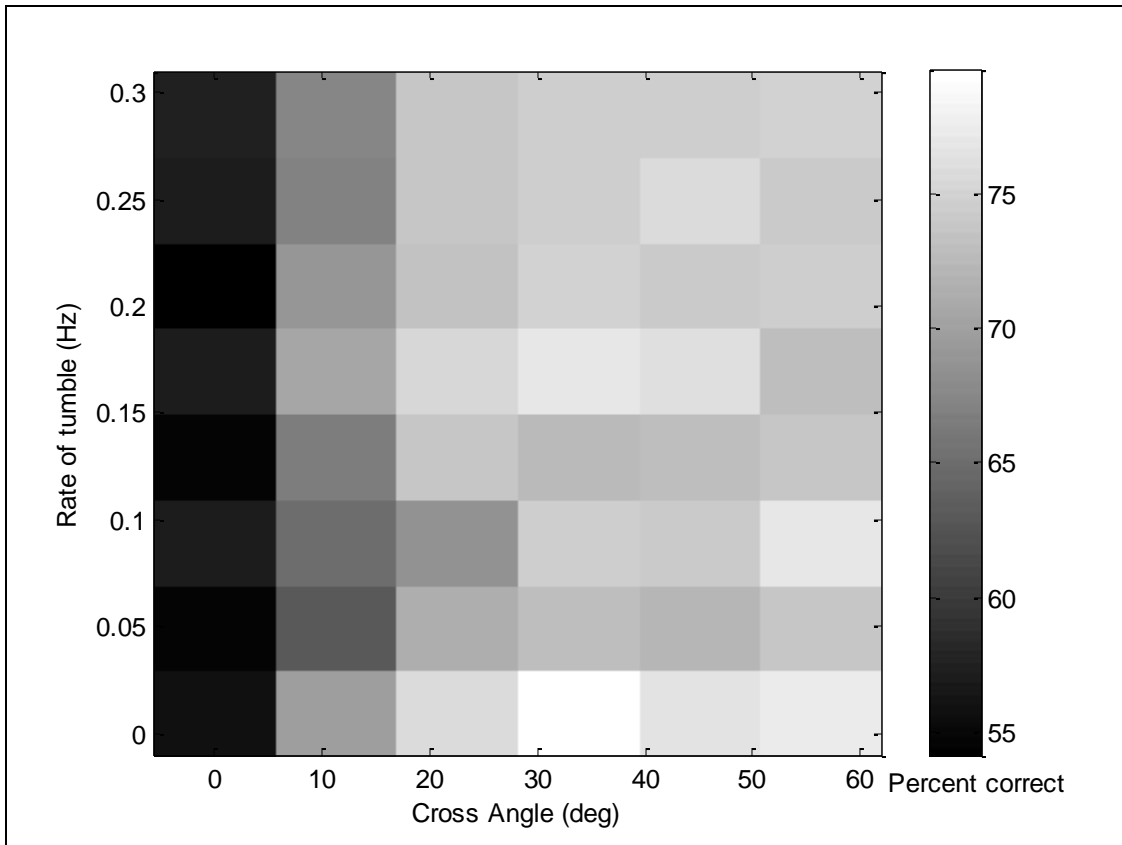
Figure 5.3.4 – From 50,000 simulations, the percentage of simulations that tests (with the possible outcomes of either odd or even) correctly identified vs. the angle between the RLOS and a target's z-inertial axis.

From Figs 5.3.2 through 5.3.4, it looks like none of those variables alone has a significant influence on the decision performance. Consequently, we looked at variables two-at-a-time to see if there were any important correlations. Figure 5.3.5, Figure 5.3.6, and Figure 5.3.7 show the contour plots of the percentage correct vs. cross angle and angle between RLOS and z-inertial axes, vs. cross angle and rate of tumble, and vs. cross angle and amount of time tracked, respectively.
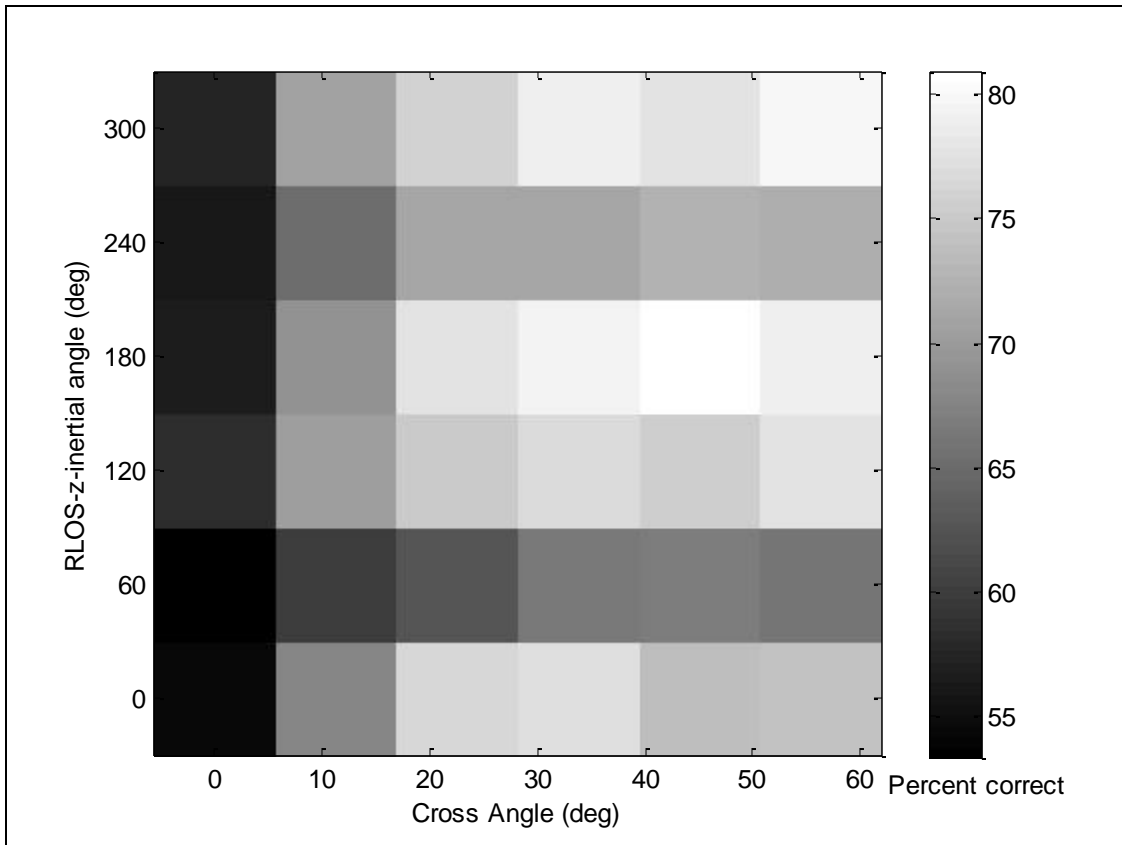
Figure 5.3.5 – From 50,000 simulations, the percentage of simulations that tests (with the possible outcomes of either odd or even) correctly identified vs. the track crossing angle and the angle between the RLOS and a target's z-inertial axis.

Figure 5.3.6 – From 50,000 simulations, the percentage of simulations that tests (with the possible outcomes of either odd or even) correctly identified vs. the track crossing angle and the rate of tumble.
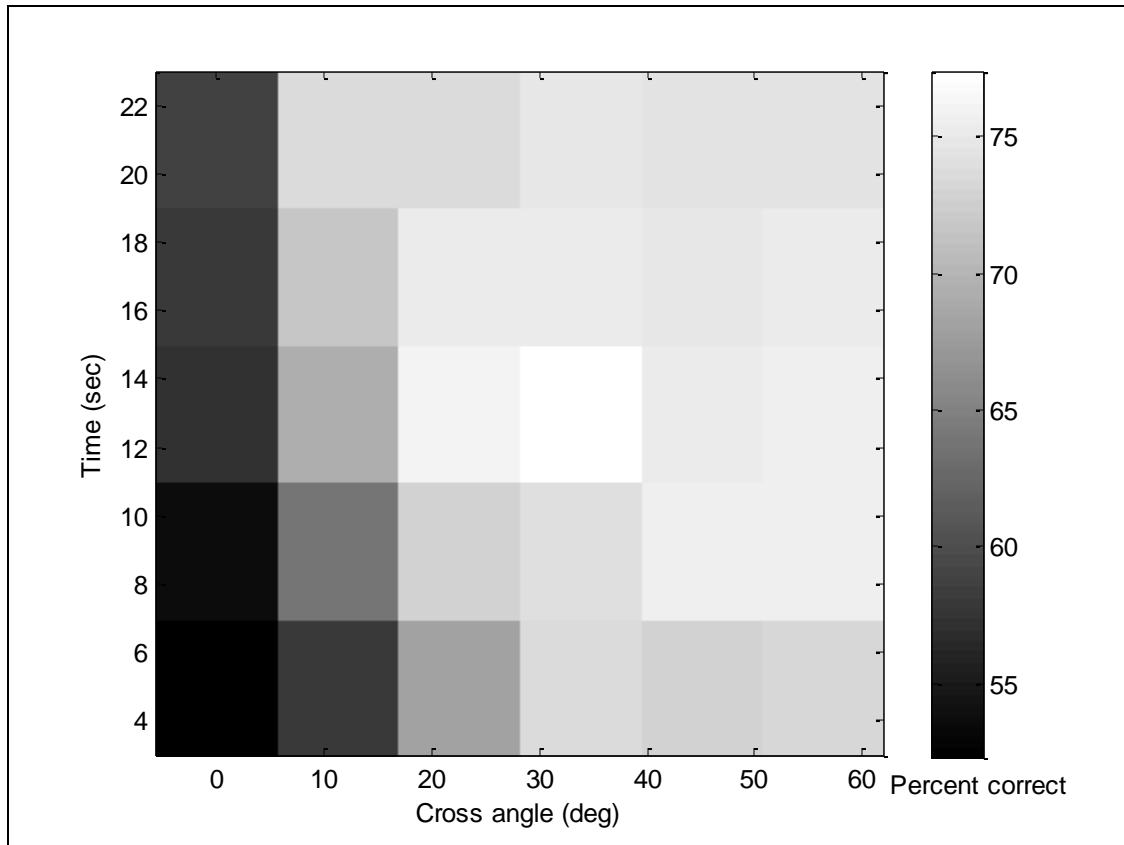
Figure 5.3.7 – From 50,000 simulations, the percentage of simulations that tests (with the possible outcomes of either odd or even) correctly identified vs. the track crossing angle and the amount of time the targets were tracked.

Another five hundred simulations were run and tested, with three possible outcomes: even, odd, or uncertain. The table below displays how many of those 500 tests were identified in five different categories – an actual odd cross that the test identified correctly, an actual odd cross that the test identified incorrectly, an actual even cross that the test identified correctly, an actual even cross that the test identified incorrectly, and a cross whose p-value fell into the range of "uncertainty." The uncertain category was deliberately allowed to be high because we knew the Range Doppler option was available for reevaluation.

Actual odd cross, test correct	Actual odd cross, test incorrect	Actual even cross, test correct	Actual even cross, test incorrect	Uncertain
9 (1.8%)	6 (1.2%)	88 (17.6%)	3 (0.6%)	394 (78.8%)

These 394 uncertain cases were re-analyzed using visual discrimination of a Range Doppler plot and, for different rates of spin, classified in the same manner.

|	Actual odd cross, test correct	Actual odd cross, test incorrect	Actual even cross, test correct	Actual even cross, test incorrect	Uncertain
Spin: 0 Hz	191(48.5%)	6 (1.5%)	152 (38.6%)	5 (1.3%)	40(10.2%)
Spin: 0.5 Hz	179 (45.4%)	4 (1.0%)	147 (37.3%)	12 (3.0%)	52(13.2%)
Spin: 1 Hz	187	3 (0.8%)	147 (37.3%)	5 (1.3%)	52(13.2%)

5.4 Range Doppler Results

The following resulting data are presented as percentages of correct discrimination of the cases that were assigned by the operator. The percentages correct are comprised of 1038 scenarios assigned either even or odd, excluding the 144 cases classified as uncertain. Every scenario tested by the Range Doppler method, whether classified as odd, even or uncertain, was previously tested by the Range Time algorithm and classified as uncertain. These percentages were functions of the various parameters previously described. The percentage correct is the vertical component in the graphs and the different parameters are broken into finite bins on the horizontal axes. Each parameter is presented as a unique line for each of the spin rates the test was run at, 0 Hz, 0.5 Hz, and 1 Hz. Again, we will start by plotting the performance as a function of the variables one-at-a-time. Figure 5.4.1 shows percentages of correctly discriminated Range Doppler cases as a function of the tracks' crossing angle on a Range Time plot. This angle is measured in degrees between the two tracks. The percentage is of 1038 scenarios classified by range Doppler as either even or odd and evaluated as correct or incorrect. All scenarios were previously classified as uncertain by the Range Time algorithm. This percentage did not include scenarios classified as uncertain by Range Doppler.
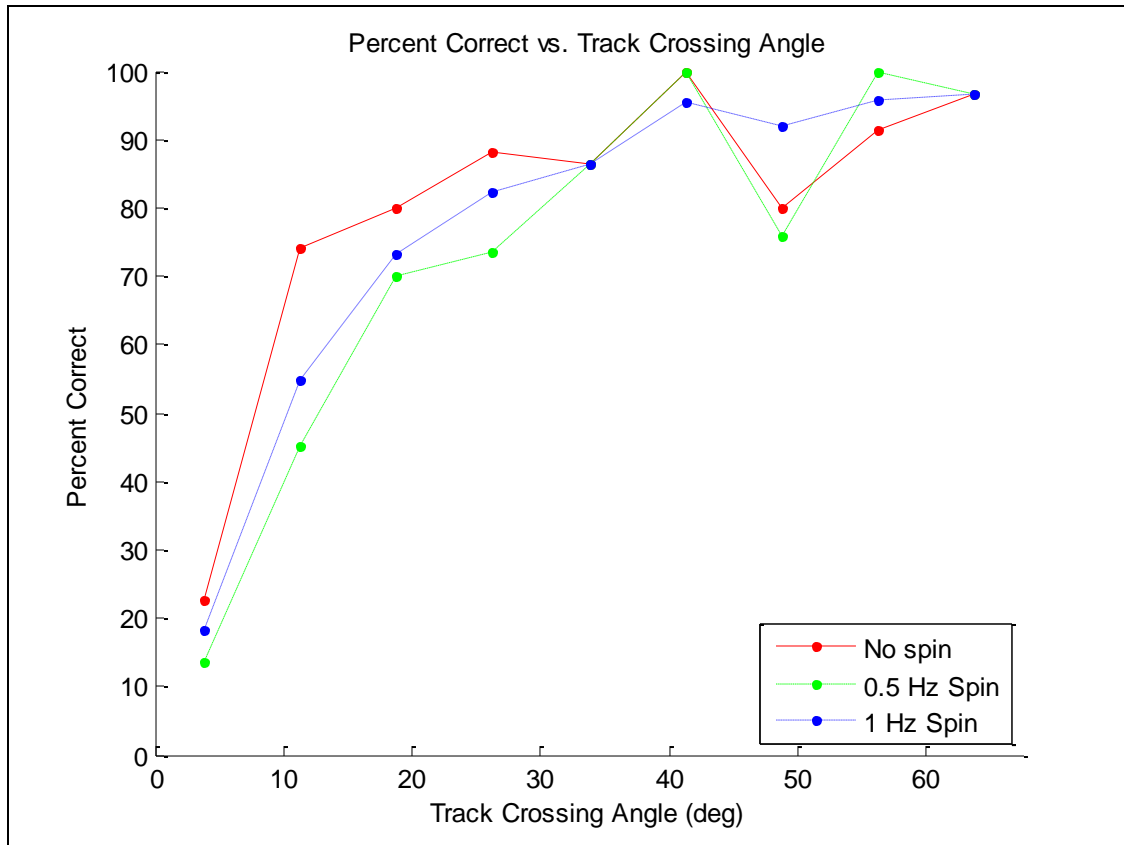
Figure 5.4.1 - Chart of accuracy of predictions as a function of the angle, in degrees, at which the two target tracks cross. The red line is for cases with no spin. The green line is for cases with 0.5 Hz spin. The blue line is for cases with 1 Hz spin.

Figure 5.4.2 displays the percentage of correctly discriminated Range Doppler cases as a function of the angle, in degrees, between the radar line of sight and the z inertial axis of the first target. The percentage is of 1038 scenarios classified by range Doppler as either even or odd and evaluated as correct or incorrect. All scenarios were previously classified as uncertain by the Range Time algorithm. This percentage does not include scenarios classified as uncertain by Range Doppler.
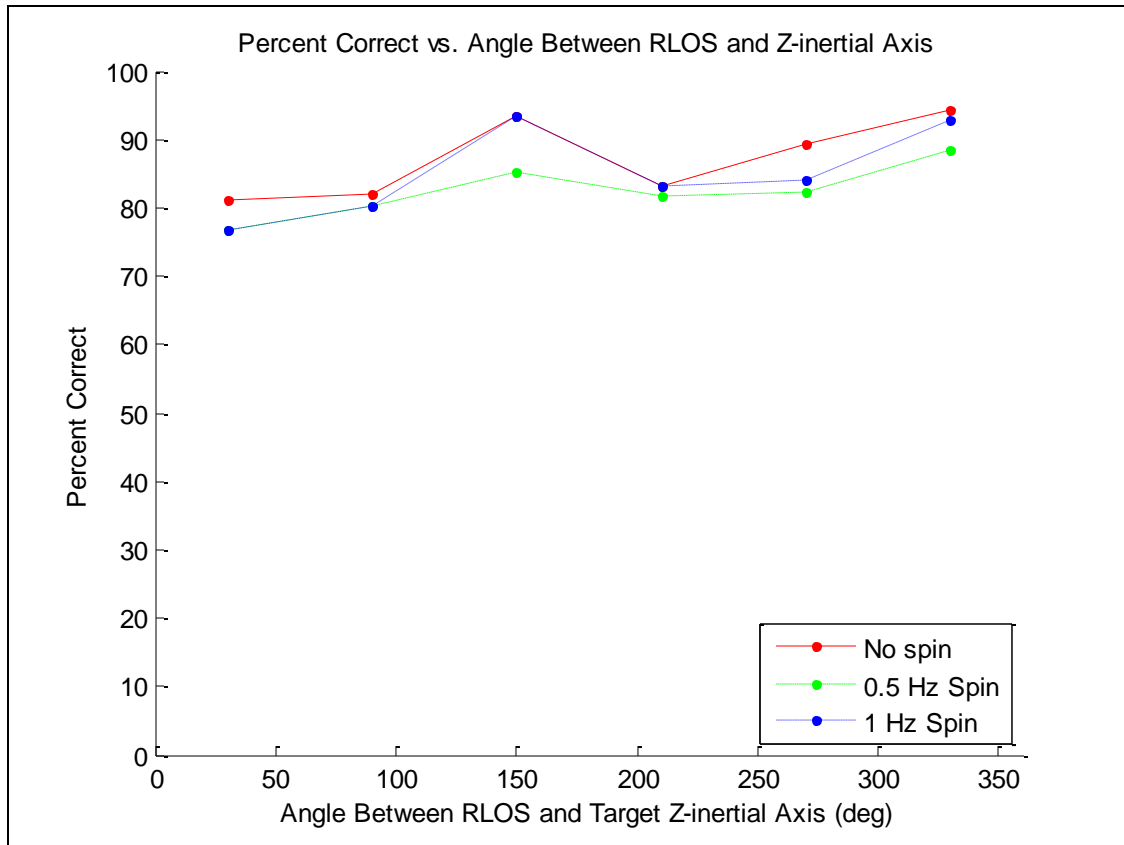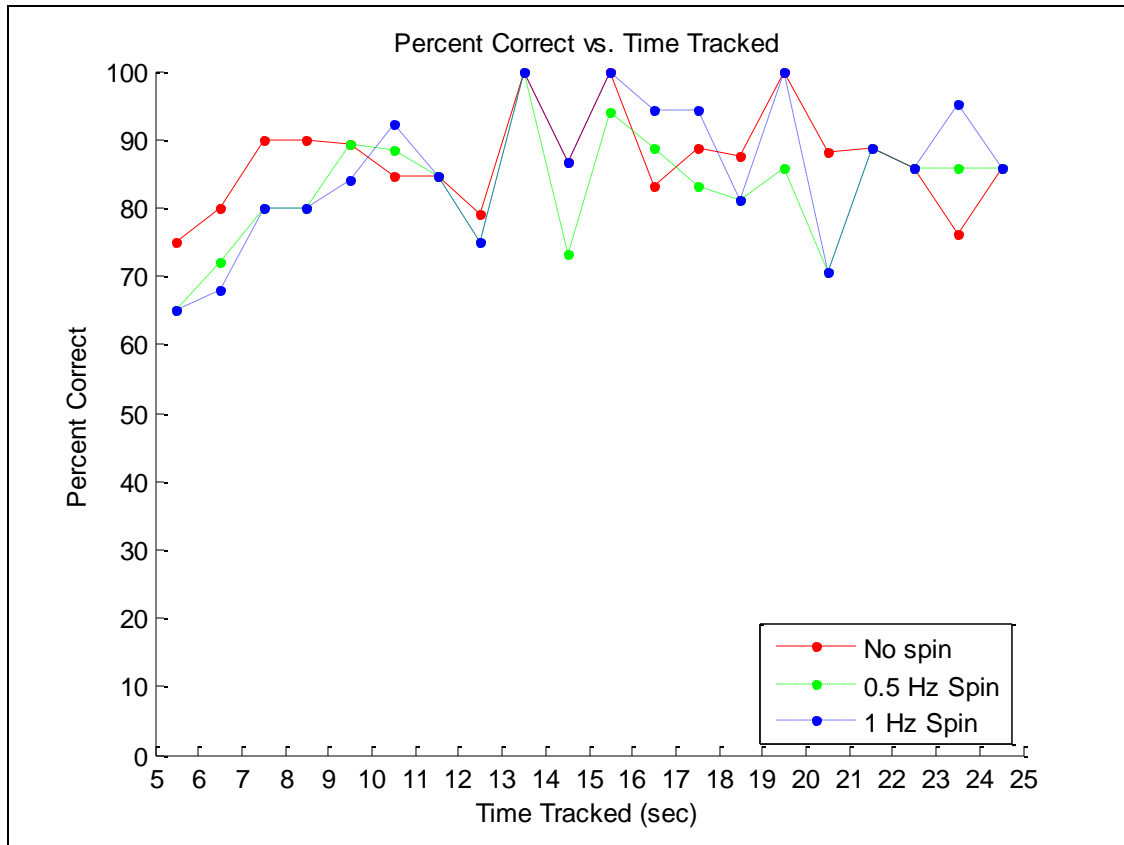
Figure 5.4.2 - Chart of accuracy of predictions as a function of the angle, in degrees, between the radar line of sight and the z inertial axis of the first target. The red line is for cases with no spin. The green line is for cases with 0.5 Hz spin. The blue line is for cases with 1 Hz spin.

Figure 5.4.3 shows the percentage of correctly discriminated Range Doppler cases as a function of the track time. The percentage is of 1038 scenarios classified by range Doppler as either even or odd and evaluated as correct or incorrect. All scenarios were previously classified as uncertain by the Range Time algorithm. This percentage does not include scenarios classified as uncertain by Range Doppler.

Figure 5.4.3 - Chart of accuracy of predictions as a function of the track time. The red line is for cases with no spin. The green line is for cases with 0.5 Hz spin. The blue line is for cases with 1 Hz spin.

The last graph is the percentage of correctly discriminated Range Doppler cases plotted as a function of the rate of the first target's tumble in Hz. The percentage is of 1038 scenarios classified by range Doppler as either even or odd and evaluated as correct or incorrect. All scenarios were previously classified as uncertain by the Range Time algorithm. This percentage does not include scenarios classified as uncertain by Range Doppler.
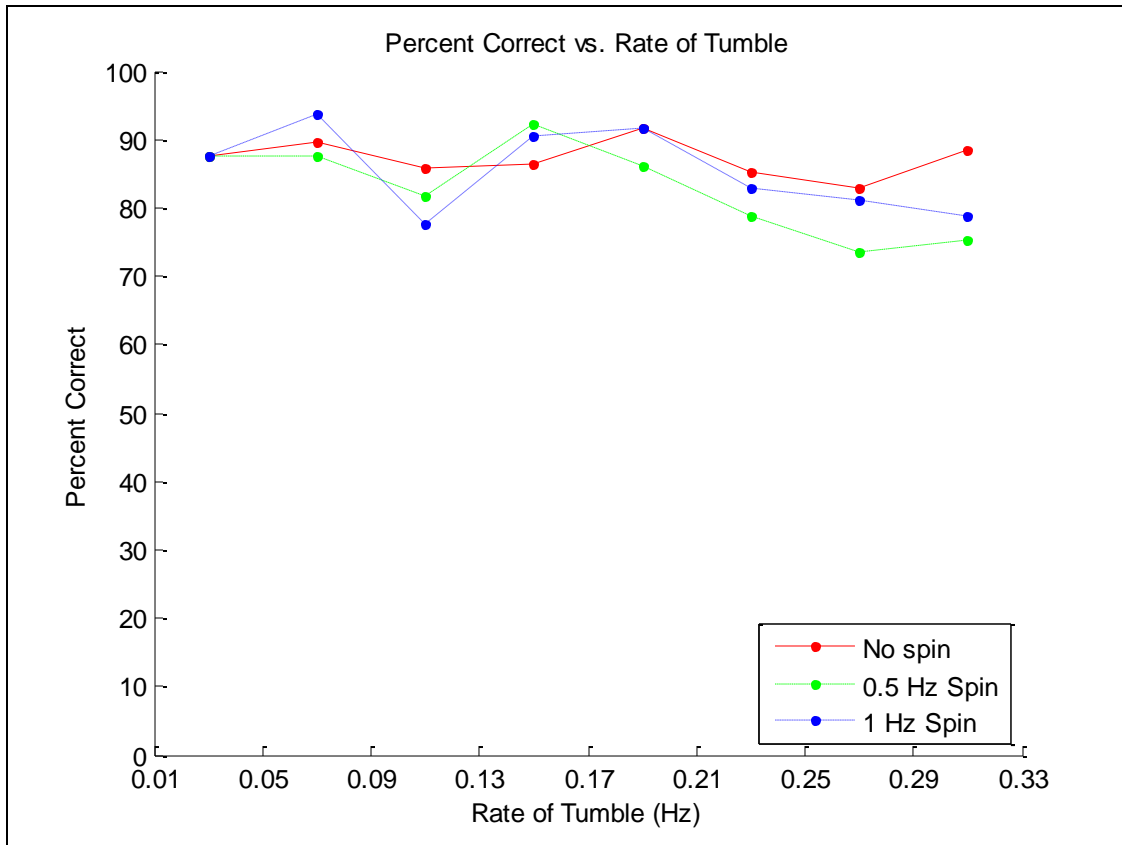
Figure 5.4.4 - Chart of accuracy of predictions as a function of the rate of the first target's tumble in Hz. The red line is for cases with no spin. The green line is for cases with 0.5 Hz spin. The blue line is for cases with 1 Hz spin.

5.5 Range Time Discussion

When only the test for the data from Range Time plots, with possible outcomes of either even or odd, was applied to 50,000 simulations, roughly 70.2% of the simulations were correctly identified. In addition, several patterns emerged. The percentage of successfully identified Range Time plots increased as track time and track crossing angle increased. At track times between five and ten seconds, 64.5% of simulations were correctly identified, but at track times between 20 and 25 seconds, 72.1% were correctly identified. When track crossing angles increased from between 0 to 5.625 degrees to between 61.875 to 67.5 degrees, percentages correct increased from 50.5% to 72.5%, respectively. As the lengths of the tracks increased over time, more and more data were available to be processed, resulting in more successful tests. As the angle between the crossing tracks increased, the curvature of the tracks in even crossings became more pronounced, allowing the tests to more accurately identify the crossings as even or odd.

Most of the 500 simulations in the previous section, whose tests resulted in outcomes of even, odd, or uncertain, were declared "uncertain" in Range-Time space because the selected threshold for uncertain cases was wide. Rather than select a narrower threshold that would classify less simulations as uncertain but allow more incorrect identifications be classified as certain, a threshold was selected that was conservative in allowing very few incorrect identifications to "leak" through. Out of the 500 simulations that were run, only 1.8% were both identified incorrectly and identified as being certain.

5.6 Range Doppler Discussion

Range Doppler discrimination was applied with three different rates of spin to the 394 cases that Range Time discrimination classified as uncertain. Overall, roughly 84.9% of these 1182 simulations were correctly identified as even or odd. The cases without spin had the highest percentage of correct predictions. Though the 0 Hz spin cases outperformed cases with spin, every scenario shared a dependence on the angle of track crossing.

Figure 5.4.1 shows the percentages of correct predictions, for the cases that were evaluated, plotted as functions of tracks' crossing angles on a Range Time plot for all three spin rates. Correct discrimination improved drastically from 10% at small crossing angles to better than 90% at angles greater than 30˚. The angle at which the two tracks cross each other on a Range Time plot is related to the relative range rate of the targets. A bigger crossing angle equates to a larger difference in the velocities of the two targets. The difference in velocities created a spatial separation horizontally between the two tracks of an odd crossing in Range Doppler, making odd crossings easier to identify. With even crossings, the crossing angle correlated to the shallowness of the parabola. Larger crossing angles leading to shallower parabolic tracks were easier to distinguish from a precession characteristic and identify. The angle of crossing was the most influential parameter in the performance of tests for Range Doppler plots. Also, there was a higher dependency in the performance of tests for Range Doppler plots on crossing angle than in tests for Range Time plots.

There was not much correlation between decision accuracy and the different angles of the radar line of sight and target orientation in Range Doppler. There just may have been too few cases evaluated to fully explore the dependence. The Range Doppler simulation of a conical

target resulted in unique scatterings from different angles. Evaluating a greater number of scenarios could lead to a dependence.

The target track time had a 90% correct threshold on observation periods of 11 seconds or longer independent of spin rate. The 0 Hz spin performed the best in the sub-threshold range having 75% accuracy in the 5 second bin, the lower bound of track time, and quickly recovered to 90% correct by 7 seconds. Targets with spin were 10% less accurate at five seconds and set the optimum thresholds at 11 seconds improving slower than the cases without spin. Better performance over longer viewing periods is due to tracks becoming more evident over precession characteristics, random noise in the return, and further track dispersal in cases with spin. Tracking duration, angle of crossing, and percent correct are presented in the three dimensional chart in Figure 5.6.1. The lower left corner of the chart is the area of interest. This portion of the chart shows the negative relationship between a short track time and low cross angle. In these cases the targets were not tracked long enough to get a clear picture before they crossed in range, making accuracy of identification low.
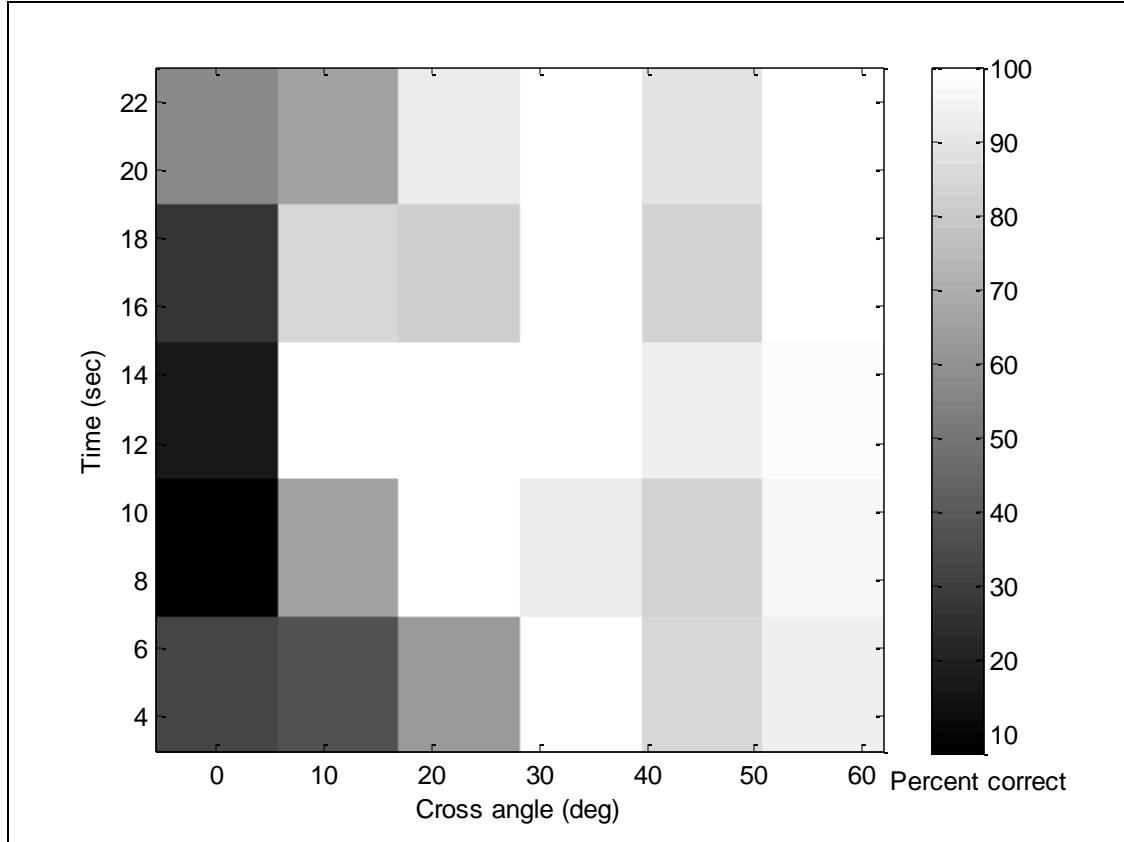
Figure 5.6.1 - Three dimensional chart of accuracy of predictions as functions of the angle, in degrees, at which the two target tracks cross and track time. This chart is for results of all three rates spin combined.

The cases without spin showed no dependence on the parameter of rate of tumble. These 0 Hz spin cases were independent because no matter how fast the tip of the cone rotated about the center of the body, the scatterer on the body only fluctuated proportional to the distance to the body center of gravity, about 40 cm. This small fluctuation meant that in cases without spin the base scatterer left a relatively linear track, easily identified. In Figure 5.4.4 a threshold can be noted in the 0.135 Hz - 0.17 Hz bin for the 0.5 Hz and 1 Hz spin cases. Cases with these two rates of spin experience a linear degradation at rates of tumble faster than 0.17 Hz. Degradation in the classification of these tracks was due to the dispersal of the returns, faster rates of tumble created a wider Doppler spectrum causing more overlap in the tracks. It is believed that increasing the range of simulated tumble frequencies to include higher rates may further

emphasize this linear degradation. Figure 5.6.2 shows a gradient chart of angle of crossing and rate of tumble with percentage correct as the third dimension.. The half of the chart for rates of spin greater than 0.15 Hz can be identified as being less favorable by counting the white and black squares in that half and noting that there are more black and less white than for the region defined by rates of spin less than 0.15Hz.. An area of interest in Figure 5.6.2 is the top right corner of the chart. Even over the most favorable interval of crossing angle, greater than 40˚, there is still a 10% to 20% decrease in the percentage of correct assignments due to the higher rate of tumble.
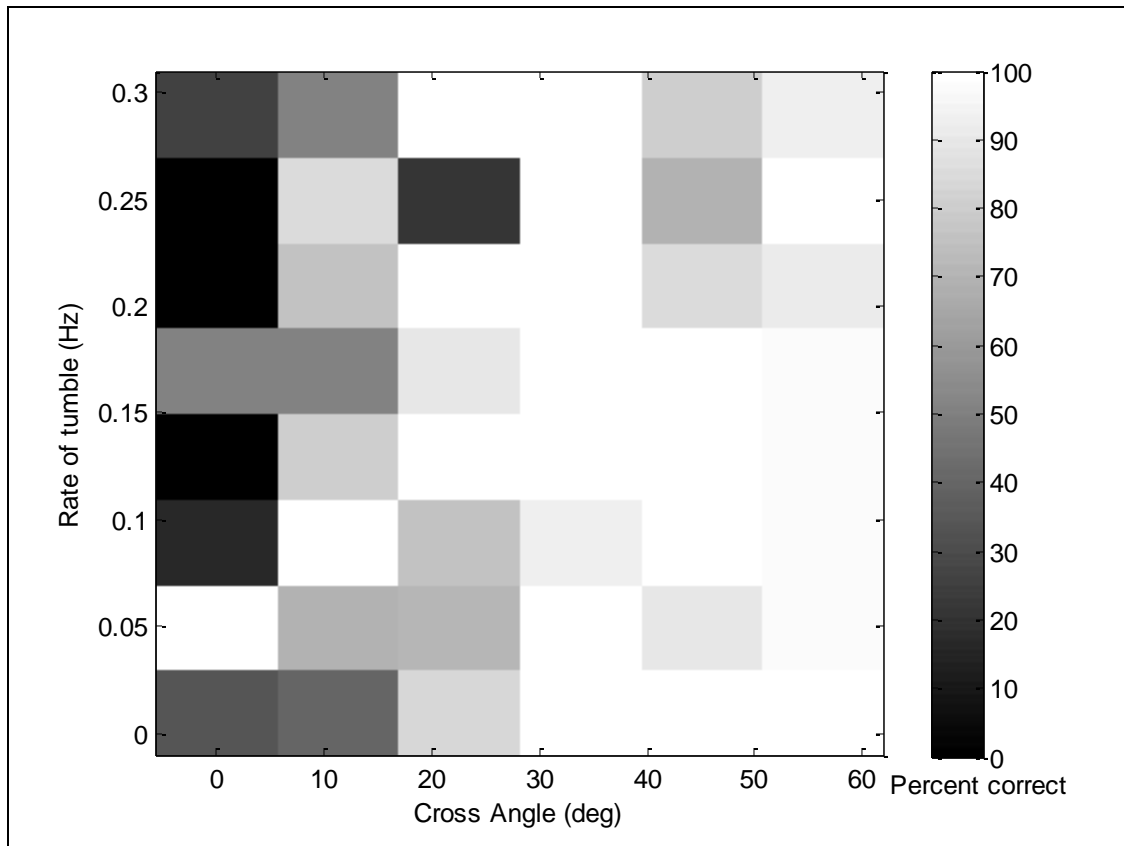
Figure 5.6.2 - Three dimensional chart of accuracy of predictions as functions of the angle, in degrees, at which the two target tracks cross and frequency of the first target. This chart is for results of 0.5 Hz and 1 Hz rates spin combined.

5.7 Range Time and Range Doppler Discussion

From these results, it is evident that, given the stated models, assumptions, and methods, the combination of Range Time and Range Doppler discrimination performed better than Range

Time discrimination by itself. Range Time discrimination alone successfully identified about 70.2% of its simulations, and Range Time and Range Doppler discrimination combined successfully identified about 86.2% of simulations.

6 Conclusion

When radar is used to track objects on ballistic midcourse trajectories, the representative Range Time tracks may contain many crossings. Ascertaining information about how these crossings occur and resolving whether these crossings are odd or even is essential to correctly associating track segments to targets and thus preserving a priori information. In this project, we mathematically analyzed various scenarios and the Range Time crossings which resulted. Crossing times in periodic ejection scenarios were mathematically derived, though crossing distribution and various other statistics were derived from Monte Carlo simulations. Individual odd and even crossings were also generated with Monte Carlo simulations in order to determine the effectiveness of Range Time discrimination of crossing type and assess the benefit afforded by sensor fusion via the addition of Range Doppler discrimination.

The mathematics of starbursts proved that objects which split up into many targets, at some instant, can be tracked perfectly. Tracks can be associated with targets, even if multiple tracks cross at the same point because all crossings are odd. In fact, the presence of radar measurement error cannot introduce even crossings either.

For objects which separate targets periodically, two crossing times could occur, and thus even and odd crossings were possible. The result of Monte Carlo simulation was to gain a better understanding about how the distribution of crossing angles and crossing times are affected by the number of objects ejected, the time delay between ejections, and a given object's position in the order of ejections. Overall, the pieces coalesce into a general framework of the situation: immediately after an object is ejected, the probability there will be a crossing is low, though this steadily increases until all objects have been ejected into a dispersing cloud, and then finally, the probability of a crossing decays to zero. The absence of even crossings suggests that this type of crossing is indeed a rarity, though this may have simply been a consequence of the chosen simulation parameters and model.

For individual crossings on a Range Time plot, a test for evenness and oddness was devised. The assumption was made that if the tracks before the crossing were approximately linear, then the crossing was odd. Similarly, if the tracks before the crossing were curved, then the crossing was assumed to be even. By testing 50,000 simulations of Range Time plots, it was determined that roughly 70% were successfully identified as even or odd by this test. Another

500 tests were run, and those which the test for curvature could not identify with certainty were passed to Range Doppler discrimination. These 394 "uncertain" cases were visually analyzed by a human to blindly distinguish between those which would have created an odd cross and those which would have created an even cross on a Range Time plot.

The 394 "uncertain" cases were visually assessed by the Range Doppler operator for each of three spin rates of 0 Hz, 0.5 Hz and 1 Hz. The operator relied on principles that were governed by the linear trajectories of the targets to visually discriminate between even and odd crossings. For the 1,182 simulations run, an encouraging 85% were correctly identified. The most positively influential parameters were longer tracking time and a larger difference between the relative velocities of the targets.

By itself, Range Time discrimination successfully identified 70.2% of the simulations it tested, and combined Range Time and Range Doppler discrimination successfully identified 86.2% of the simulations they tested. Overall, given the models, assumptions, and methods used, there was a significant increase in the number of crossings that could successfully be identified as even or odd.

References

- Kachelmeyer, A.L. <u>IMAGING TECHNIQUES FOR RANGE DOPPLER LADAR</u>. Massachusetts Institute of Technology. Lincoln Laboratory. 1991

- Levanon, Nadav. <u>Radar Principles</u>. New York: Wiley, 1988. 1-3.

- Petruccelli, Joseph et.al. <u>Applied Statistics for Engineers and Scientists</u>. Englewood Cliffs: Prentice Hall, 1999. 741-742.

- Shultz, Kenneth I., et al. <u>Range Doppler Laser Radar for Midcourse Discrimination: The Firefly Experiments</u>. Massachusetts Institute of Technology. Lincoln Laboratory. 1993

- Skolnik, Merril I. <u>INTRODUCTION TO RADAR SYSTEMS</u>. New York: McGraw-Hill, 2001. 1-5, 14-19, 210-211, 246-247, 252, 301.

- Toomay, J.C. <u>Radar principles for the non-specialist</u>. New York: Nostrand, 1989. 1-8, 59-61, 86-93.

- Weiner, Stephen. Private conversations.

- Werrel, Kenneth P. <u>Hitting a Bullet with a Bullet</u>. College of Aerospace Doctrine, Research and Education. Air University. Research Paper 2000.